

BIOMECHANICAL ANALYSIS OF THE CORNEA
TO IMPROVE POST SURGICAL OUTCOMES
THROUGH FINITE ELEMENT
ANALYSIS

by

SALMAN NASIR KHAN

Presented to the Faculty of the Graduate School of
The University of Texas at Arlington in Partial Fulfillment
of the Requirements
for the Degree of

DOCTOR OF PHILOSOPHY

THE UNIVERSITY OF TEXAS AT ARLINGTON

May 2015

Copyright © by Salman Nasir Khan 2015

All Rights Reserved



*To My Beloved Mother and
The Memory of My Father*

Acknowledgements

I would like to express my deepest gratitude to everyone who contributed and helped me complete this research work. I am thankful to my dissertation advisor Dr. P. S. Shiakolas for his intellectual contribution and moral support. His thoughtful guidance and technical support helped me complete this dissertation. Moreover, I want to thank the members of my dissertation committee Dr. Lawrence (UTA), Dr. Aswath (UTA), Dr. Eberhart (UTSW), Dr. Welch (UTSW) and Dr. Petroll (UTSW) for their guidance and feedback.

I will like to acknowledge the contribution of my family. My mother and my brother have been my motivation and inspiration throughout my life in fact they are the ones who persuaded me to join graduate school in the first place. My mother holds a special place in my life, I believe I owe everything good that I achieve in my life to her. It is her guidance and values that have made me the person that I am today. Besides my mother, I would like to acknowledge the contribution of my wife, who has always believed in me and has stuck with me through thick and thin. The contribution of these lovely and caring women has been immense during my time at UT Arlington.

Lastly, I would like to acknowledge the contribution of my friends, classmates and lab members. Conducting research, taking courses and performing projects with them during these last few years have given me memories worth a lifetime.

April 15, 2015

Abstract

BIOMECHANICAL ANALYSIS OF THE CORNEA
TO IMPROVE SURGICAL OUTCOMES
THROUGH FINITE ELEMENT
ANALYSIS

Salman N. Khan, PhD

The University of Texas at Arlington, 2015

Supervising Professor: P. S. Shiakolas

Vision deterioration is a major healthcare concern. It is estimated that one in three persons develops some form of vision reducing eye disease by the age of 65 and these numbers are expected to increase. Deterioration in visual acuity is due to ocular diseases that change the shape or clarity of the cornea. Health/shape of the cornea is extremely important as it determines the refractive power of the eye.

This work studies ocular surgeries from a mechanical/structural engineering perspective. It begins by discussing laser in-situ keratomileusis (LASIK) surgery and explains the role of lasers in modifying the corneal shape to improve visual acuity. Besides LASIK, this work studies a refractive surgery involving intrastromal corneal ring (ICR) implants by developing a computationally efficient finite element (FE) model for the cornea and the implant. The results of the FE analysis qualitatively agree with published clinical studies and experimental data.

The effects of ICR dimensions and surgical conditions on the postoperative visual acuity are studied. The results indicate that smaller diameter and larger thickness

ICRs lead to pronounced myopic rectification and that 40-75% deep corneal pockets yield stable results and smaller diameter corneal pockets lead to pronounced myopic rectification.

The second part of this research studies the Descemet's stripping automated endothelial keratoplasty (DSAEK) surgery by understanding the limitations of this procedure and the allograft delivering devices currently used to improve surgical outcomes. A FE model was developed to analyze the stress distribution generated on the allograft during popular DSAEK allograft configurations and the results were correlated with endothelial cell (EC) health. The results of the FE analysis reveal high stress region areas for forceps, taco and double coil configurations. The obtained stress distribution results were in qualitative agreement with published experimental EC loss data. The FE modeling procedures were used for the design of a novel new inserter, binocular inserter, that has the potential to improve DSAEK surgical outcomes especially in patients with shallow anterior chambers (ACs). The inserter prototype conceptual design analysis, the allograft tip shape analysis and allograft finite element analysis results indicate that the binocular inserter should improve DSAEK surgery results by: increasing inserter tip space utilization, reducing surgical and mechanical trauma, utilizing AC maintainer, improve recovery time and size of incision, protecting against incision compression pressure issues, and modulating the location and magnitude of stresses on the allograft to facilitate natural allograft unfolding especially in constrained ACs.

Table of Contents

Acknowledgements	iv
Abstract	v
List of Illustrations	xii
List of Tables	xvi
Chapter 1 Introduction	1
Ocular Biomechanics	1
Ocular Conditions and Rectification Surgeries	2
Aims and Scope	2
Intrastromal Corneal Rings	3
Descemet's Stripping Automated Endothelial Keratoplasty	4
Binocular Corneal Inserter	5
Chapter 2 The Human Eye	7
Anatomy Of the Human Eye	7
Structure of cornea	8
Epithelial Layer	8
The Bowman's Membrane	9
The Stroma	9
Transverse Mechanical Strength of stroma	13
Descemet's Membrane	13
The Endothelium	14
Limbus	15
Sclera	16
Methods Used for Material Characterization of the Cornea	17

Chapter 3 An Overview On Performance Characteristics Of Laser In-Situ Keratomileusis (LASIK) And Identification Of Challenges.....	19
Introduction	19
Refractive Errors	21
Laser In-Situ Keratomileusis - LASIK.....	22
Flap Creation In LASIK.....	24
Comparison Of Femtosecond Lasers With Mechanical Microkeratomes	25
Modes Of Laser Tissue Interaction.....	26
Lasers Used In LASIK	28
Femtosecond Laser	28
Mechanism Of Tissue Ablation Under Effect Of A Femtosecond Laser	29
Why Femtosecond Lasers Are Suitable For Ophthalmic Applications	30
Excimer Laser	30
Why Excimer Lasers Are Suitable For Ophthalmic Applications	31
Impact Of Femtosecond Lasers On LASIK	32
Thin Flap Or Sub Bowman LASIK	32
Flap Cut Profile.....	32
Stromal Bed Quality	32
Flap Centration	33
Post LASIK Complications	33
Epithelial In-Growth.....	33
Early Flap Displacement After LASIK	34
Night Glare And Halos	35
Epithelial Erosion	35
Dry Eye.....	36

Conclusions	37
Chapter 4 Application Of Finite Element Analysis To Study The Mechanical Behavior Of Cornea Due To Implantation Of An Intrastromal Corneal Ring	39
Introduction	39
Optics of the eye and refractive ailments	41
Materials and Methods	42
Structure of cornea	42
Material Properties Selection	43
Finite Element Modeling	44
Modeling Methodology	44
FE Model Assumptions	45
FE Model Development and Simplifications	45
Advantages and Limitations of Simplified Eye Model	49
Intrastromal Corneal Rings (ICRs)	54
Results.....	56
Discussion.....	57
ICR implant thickness effects.....	57
ICR implant diameter effect	58
ICR implantation depth effect.....	60
Smaller diameter corneal pocket effect	61
Sensitivity Analysis of the ICR implantation surgery control parameters	62
Conclusions	64
Chapter 5 Descemet's Stripping Automated Endothelial Keratoplasty (DSAEK) Allograft Insertion Devices: A Review.....	66
Introduction	66

Endothelial allograft insertion devices.....	70
Endothelial glides	71
Busin Glide.....	71
Macaluso inserter	72
Tan Endoglide	73
Endothelial allograft injectors	75
Neusidl corneal inserter.....	75
Endoinjector	77
Endoserter	78
Discussion and Conclusions	79
 Chapter 6 Finite Element Analysis of Descemet's Stripping Automated Endothelial Keratoplasty (DSAEK) Surgery Allograft to Predict Endothelial	
Cell Loss.....	84
Introduction	84
Materials and Methods	86
Corneal Endothelium and its function	87
Causes of death of endothelial cells	88
Endothelial cell death due to external stimuli.....	89
Allograft Folding Configurations	91
Finite Element Modeling Methodology	92
FE Model Assumptions	92
FE Model Development.....	92
Results and Discussion	98
Conclusions	104

Chapter 7 Design of a Novel Allograft Insertion Device for Descemet's Stripping Automated Endothelial Keratoplasty (DSAEK) Surgery	105
Introduction	105
Materials and Methods	106
Allograft Folding Configurations	108
Proposed Allograft Inserter Design.....	109
Operation of the Proposed Binocular Inserter Design	110
Binocular Inserter Construction	111
Allograft Tip Shape Analysis	112
Finite Element Modeling	114
Results and Discussion	116
Conclusions	118
Chapter 8 Summary, Conclusions and Recommendations for Future Research	120
Recommendations for Future Research	122
Appendix A Allograft Tip Space Utilization Analysis.....	124
References.....	128
Biographical Information.....	157

List of Illustrations

Figure 2-1: Anatomy of a human eye [7]	7
Figure 2-2: Corneal layers [9]	9
Figure 2-3: Schematic representation of the corneal stroma where lamellae layers are stacked at an angle to each other. The collagen fibrils that comprise the lamellae sheets are also approximately parallel to each other and are embedded in an extra-fibrillar matrix linked by proteoglycan molecules [17]	10
Figure 2-4: Preferential orientation of collagen fibrils in posterior stroma. Fibrils have an ordered limbal-to-limbal arrangement, running preferentially in the inferior--superior and medial--lateral meridians, interweaving circumferentially with scleral collagen fibrils at the limbus [19]	12
Figure 2-5: Optical polarization figure demonstrating the interweaving of the collagen lamellae in one third anterior stromal portion of the cornea, whereas the posterior two thirds demonstrate planar organization of the lamellae. The arrow in the figure signifies the anterior stromal surface [22].....	13
Figure 2-6: SEM of corneal endothelial layer [28]	15
Figure 2-7: This figure shows the limbus where solid lines demarcate the pathologist's limbus whereas the dotted lines demarcate the histologist's limbus [31]	16
Figure 2-8: Figure representing the interlacing of collagen lamellae in the corneal stroma and sclera [22].....	17
Figure 3-1: Refractive errors in a human eye [49]	22
Figure 3-2: Steps for LASIK procedure [50]	23
Figure 3-3: Laser tissue interaction [70]	27
Figure 3-4: Flap configurations [115]	37

Figure 4-1: (a) Radius of corneal curvature increases which leads to a flatter cornea (b) Corneal curvature remains constant however the location of cornea is closer to retina (decrease in axial length of eyeball)	42
Figure 4-2: Stress strain material properties of the porcine cornea [156]	44
Figure 4-3: Full eye model with axisymmetric modeling assumption	47
Figure 4-4: Applied loadings and BCs for the full eye axisymmetric model	47
Figure 4-5: Full eye model displacement results.....	47
Figure 4-6: Simplified cornea model showing angle of inclined roller supports	48
Figure 4-7: Dimensions of simplified FE cornea model	49
Figure 4-8: Corneal apical deformation and intraocular pressure for various angle supports and their comparison with experimental results	49
Figure 4-9: Corneal apical deformation vs intraocular pressure for full eye model, simplified cornea model and experimental results	51
Figure 4-10: Nodal positions and displacement equations highlighting the topography of the cornea (Not to scale)	51
Figure 4-11: Radius of corneal curvature as a function of IOP.....	53
Figure 4-12: FE model displacement results for full eye and simplified cornea models with respective undeformed wireframes at an IOP of 12 kPa	53
Figure 4-13: FEM model of cornea segment with pocket and ICR implant	55
Figure 4-14: FEM model with loading and boundary conditions (BCs)	56
Figure 4-15: Representative FE model displacement results in meters of cornea segment with 5 mm diameter Myoring with $(0.5 \times 0.3) \text{ mm}^2$ cross section.....	57
Figure 4-16: Change in corneal apical deformation (before and after ICR implantation) as function of ICR thickness	58

Figure 4-17: Change in corneal apical deformation (before and after ICR implantation) as function of ICR diameter.....	59
Figure 4-18: Change in corneal apical deformation (before and after ICR implantation) as function of ICR implantation depth	60
Figure 4-19: Change in corneal apical deformation (=5 mm value - smaller corneal pocket diameter value) as function of corneal pocket diameter	62
Figure 4-20: (A) Apical deformation as function of ICR diameter and ICR thickness (B) Apical deformation as function of ICR implantation depth and corneal pocket diameter ..	63
Figure 5-1: Full thickness penetrating keratoplasty (PK) [175]	67
Figure 5-2: Partial thickness endothelial keratoplasty (EK) [176]	67
Figure 5-3: Types of partial thickness keratoplasty procedures [173]	68
Figure 5-4: Busin Glide inserter [205]	72
Figure 5-5: Macaluso endothelial inserter [211]	73
Figure 5-6: Tan Endoglide [202]	75
Figure 5-7: Neusidl Injector [214]	76
Figure 5-8: Endoinjector [217].....	78
Figure 5-9: Endoserter [219]	79
Figure 6-1: Stress strain material properties of the porcine cornea [156]	87
Figure 6-2: Cross sectional views of the three dominant folding configurations	91
Figure 6-3: Meshing of the allograft in the FE model.....	94
Figure 6-4: Modeling of the symmetrical plane boundary condition	95
Figure 6-5: Modeling of the symmetrical plane BC fixed in horizontal plane and free in vertical plane	95
Figure 6-6: Loading sequence for 'Forceps' configuration	97
Figure 6-7: Loading sequence for 'Taco' configuration	97

Figure 6-8: Loading sequence for 'Double Coil' configuration	98
Figure 6-9: Undeformed allograft	99
Figure 6-10: Deformed shape of the constrained symmetry plane that clearly experiences a downward pull.....	99
Figure 6-11: FE model results.....	102
Figure 6-12: EC loss clinical experimental results.....	103
Figure 7-1: Stress strain material properties of the porcine cornea [156]	108
Figure 7-2: Cross sectional view of prevalent DSAEK allograft folding configurations ..	109
Figure 7-3: (a) Cross sectional view of the Binocular Inserter tip with the allograft folding configuration (b) Preliminary CAD rendering of Binocular tip inserter	110
Figure 7-4: Preliminary inserter design manufactured using ABS via 3D printing technology	112
Figure 7-5: BCs and loading sequence for binocular configuration	116
Figure 7-6: (a) Side View of the allograft for the binocular configuration (b) von Mises stress level of allograft for the binocular configuration.....	118

List of Tables

Table 4-1: Summary of FE model apical deformation displacement results	57
Table 5-1: Characteristics of corneal inserters	83
Table 6-1: Summary of maximum stress magnitude in allograft configurations	101
Table 7-1: Summary of nomenclature for the inserter tip geometry analysis	113
Table 7-2: Summary of maximum diameter allograft carrying capability for the folding configurations	114

Chapter 1

Introduction

Closing your eyes and trying to perform the normal functions of daily life can be a daunting experience. Importance of vision in life cannot be emphasized enough. I first realized the importance of vision when I saw a visually impaired person for the first time in my hometown. I could not fathom life with impaired vision and that is where my fascination with the eyes began. However, I later realized that I am not alone in my fascination with the eyes. Humans throughout history have been attempting to understand the eye in an effort to find cures for ocular diseases. Yet, statistics reveal that even today one in three persons develops some form of visual impairment by the age of 65 and these numbers are expected to grow with increase in life expectancy [1]. These statistics reveal that there is still a need for better understanding of the human eye. So that ocular knowledge can be extended and better ophthalmic surgical procedures/devices can be developed which will help in the development of viable, adequate and sustainable solutions for vision related diseases.

Ocular Biomechanics

Physically, the eye appears to be a very simple biological system. But, even after advanced experimental and clinical studies, some ocular mechanisms are still unknown. In reality, the eye is an extremely intricate biomechanical system, where each part has to function properly and in synchronization for proper operation. The eye is a unique biomechanical system, in simplistic mechanical terms it can be considered as a pressurized spherical vessel whose shape is dependent on the intraocular pressure, tissue thickness and material properties. Changes in any one of these parameters can destabilize the system which leads to changes in the shape of the eye. Proper understanding of ocular biomechanics is therefore extremely important as it, can not only

help us understand ocular conditions, but also the gained knowledge can be leveraged to propose novel solutions for rectifying ocular conditions.

Ocular Conditions and Rectification Surgeries

Deterioration in visual acuity is witnessed due to various ocular diseases which change the shape and/or clarity of the eye and more importantly the cornea, which can be considered the window of the eye that allows light rays to come inside. The shape of the cornea holds great importance since it is the principal refractive element contributing almost 45 of the 60 diopters of ocular refractive power. It is responsible not only for transmitting light rays but also for maintaining mechanical/structural stability. The structure/shape of the cornea governs the amount of refraction for the incoming light rays which is why understanding the structure of the cornea holds so much importance.

Most ocular surgical procedures that aim to permanently improve visual acuity focus on changing shape of the cornea using surgical procedures such as laser assisted in-situ keratomileusis (LASIK), photo refractive keratotomy (PRK), radial keratotomy (RK) and intrastromal corneal ring (ICR) implantation. However, in severe cases full or partial corneal grafting is performed such as penetrating keratoplasty and Descemet's stripping automated endothelial keratoplasty (DSAEK). In all vision rectification surgical procedures, knowledge of corneal biomechanics is utilized to ensure that proper postsurgical corneal shape/clarity is acquired.

Aims and Scope

The presented study begins with an extensive review of the LASIK surgery, to highlight the role of lasers in the surgery and attempts to explain the postsurgical complications and the role of lasers in alleviating those complications. After studying LASIK, the presented work moves onto another upcoming refractive surgery that involves intrastromal corneal ring implantation. A finite element (FE) model was developed to

study the effects of ICR implantation on the corneal topography. Moreover, the analysis was extended to study the effect of changes in ICR cross section and surgical parameters. After discussing the refractive surgeries, the presented work moves onto a partial thickness corneal transplant surgery called DSAEK. It describes the advantages and limitations of the DSAEK surgery and the role of DSAEK allograft inserters in improving surgical outcomes. The knowledge gained from this review was utilized to develop a computationally efficient FE model to analyze the postsurgical corneal structure and propose a novel DSAEK inserter that should improve surgical outcomes especially for patients with shallow anterior chambers (ACs).

Intrastromal Corneal Rings

Intrastromal corneal rings are transparent PMMA implants used to rectify myopia. Myopia or shortsightedness is a visual impairment condition that is affecting more than 32 million Americans according to the American Academy of Ophthalmology, and this number is expected to increase even further with the increasing life expectancy in the United States [2]. Myopia occurs when light rays entering the cornea are focused in front of the retina due to high corneal curvature, short axial length of the eye, or high optical power of the natural lens. These reasons suggest that light refracting elements play a pivotal role in the determination of visual acuity, and since cornea is the principal refractive element in the eye contributing almost 75 percent of ocular refractive power, the shape of the cornea can be changed to increase or decrease the focal length of the converging light rays inside the eye. ICR implantation is a relatively new procedure that would benefit from FE analysis. The presented research strives to study the structure/shape of the cornea by developing a computationally efficient 3D axisymmetric FE model of the cornea. The results of the FE model were compared with published experimental results available in open literature to establish confidence in the modeling

procedures. Subsequently, a 360 degree ICR was introduced into the model and its effect on the corneal shape was studied. ICR is a circular implant inserted into the stromal layer of the cornea at a depth of approximately 300 to 350 μm in an effort to alleviate myopia by providing structural support to the cornea. The FE model results not only qualitatively agree with published clinical data but also provide a valuable insight into the surgery [3]. The knowledge gained from this analysis could be eventually utilized to formulate the design of customized implants for personalized vision care.

Descemet's Stripping Automated Endothelial Keratoplasty

The second surgery studied and analyzed in this work was DSAEK, a surgical procedure wherein the diseased endothelial layer of the patient's corneal tissue is replaced by a donor allograft to improve visual acuity. Endothelial layer corneal allograft surgery becomes necessary due to various ocular diseases which cause the cornea endothelial cell (EC) count to fall below ~ 500 cells/ mm^2 . Endothelial cells are extremely important to maintain proper corneal function since they act as small pumps that push the moisture out of the cornea into the AC. When the number of ECs falls below the minimum threshold they lose their pumping power and can no longer perform their function properly. Hence, the cornea loses its transparency due to excessive moisture and a transplant becomes necessary. In the US alone, almost 27 thousand endothelial keratoplasty procedures were performed in 2013 and this number is increasing every year due to the rise in average life expectancy [4]. The success of a DSAEK procedure depends on how the donor allograft is handled and inserted inside the anterior chamber (AC) of the patient's eye. Allograft insertion is an extremely important step, since any undue stresses imparted to the donor allograft during this step may lead to EC loss which in turn could reduce the success of the surgical procedure, as low EC count is the reason DSAEK procedure is performed in the first place [5]. The presented research aims to

utilize FE analysis techniques to study the effects of allograft deformation when popular insertion devices are employed for allograft delivery inside the AC. An extensive literature survey including patent literature was conducted focusing on structural analysis studies on the DSAEK surgery. To the best of our knowledge, no research studies are available in the open literature, that correlate EC loss with stress distribution utilizing FE modeling techniques. The presented study begins by developing a FE model for the cornea allograft. Once, the model is generated, a loading sequence was developed to deform the allograft geometry into the shape it takes during popular insertion techniques. Then, the generated stresses are evaluated. The quality of the developed FE models is verified by comparing the FE predicted high stress regions with the EC loss results observed in clinical studies available in open literature [6]. The acquired results qualitatively predict the high stress regions thus providing information about the expected EC loss locations. The FE modelling procedures presented in this research can be utilized to study existing insertion configurations and develop improved novel surgical devices to control the location of stress trauma on the donor allograft in an effort to decrease EC loss thereby improving the success of the DSAEK surgical procedure.

Binocular Corneal Inserter

The results of the FE analysis for DSAEK allografts were utilized to develop a novel corneal inserter in an effort to improve surgical outcomes especially for patients with shallow or constrained anterior chambers (ACs). The success of a DSAEK procedure in patients with shallow ACs depends on successful unfolding of the allograft inside the AC, amount of postsurgical EC loss and maintenance of pressure inside the AC. The factors which contribute to EC loss are mechanical trauma, surgical trauma and incision compression pressure (ICP). Natural allograft unfolding inside the AC depends on the location and magnitude of pre-existing stresses on the deformed allograft. AC

pressure maintenance depends on the incision length and the usage of an AC maintainer. Most of these factors depend on the inserter tip design, therefore a novel inserter design called the binocular inserter is presented in this work which aims to improve surgery results especially in constrained ACs. The inserter design/construction analysis, allograft tip shape analysis and allograft FE analysis results demonstrate that the binocular inserter should improve DSAEK surgery results by increasing inserter tip space utilization, reducing surgical and mechanical trauma, utilizing AC maintainer, protecting against ICP and modulating the location and magnitude of stresses on the allograft to facilitate natural allograft unfolding inside constrained ACs.

Chapter 2

The Human Eye

Anatomy Of the Human Eye

The human eye is a complex and intricate structure as presented in Figure 2-1, and understanding its anatomy and working are vital for better understanding of the issues discussed in this work [7]. This chapter provides a brief introduction to the basic anatomy of the human eye with the objective to familiarize the reader with some important aspects of ocular biomechanics that will serve as a basis for the justification of assumptions considered in the FE models developed and used in this work.

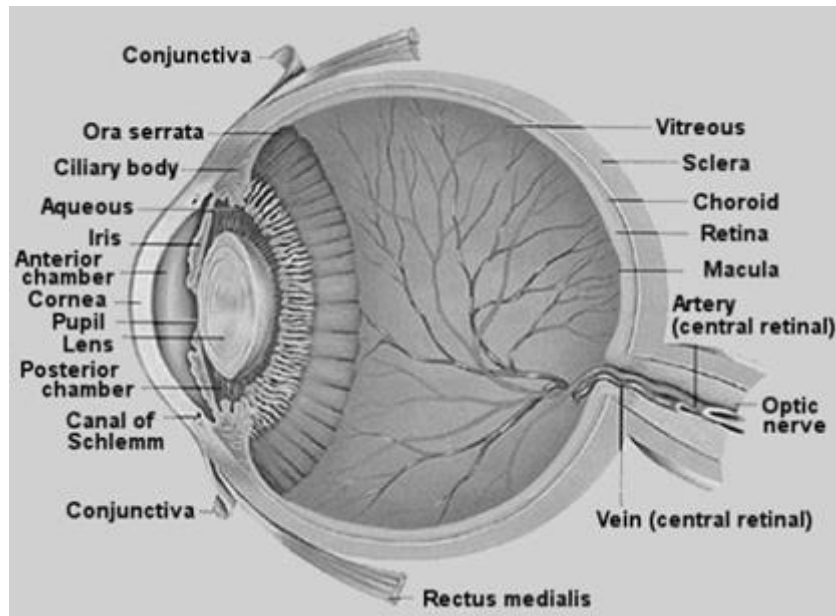


Figure 2-1: Anatomy of a human eye [7]

The eye is a roughly spherical pressurized vessel that is filled with a transparent viscous fluid known as vitreous humor, which maintains the pressure, hence the shape of the eye. The outer structure of the eye consists of the cornea, limbus and sclera. Light enters the eye through the cornea, where the incoming light rays undergo refraction. The,

refracted light rays reach the crystalline lens where they undergo further refraction before they focus onto the light sensitive retina. The retina then processes the image through the photosensitive cells that line the retina, and conveys the processed information to the brain via electrical impulses through the optic nerve. The crystalline lens inside the eye changes its shape due to various stimuli which in effect changes the focal length of the lens, thus enabling the eye to see near and distant objects with the same clarity. The ability of the human eye crystalline lens to change its focal length is rated by the term *accommodation* [8]. This ability is higher in adolescents who are able to accommodate 12 to 15 diopters, than middle age people (aged 40 to 50) who are able to accommodate 4 to 8 diopters.

Structure of cornea

The cornea primarily consists of five distinct layers, epithelium, Bowman's layer, stroma, Descemet's membrane and endothelium as presented in Figure 2-2 [9]. Each layer has a specific role and function that is vital for the satisfactory operation of the cornea.

Epithelial Layer

The epithelium is the outermost layer of the cornea that is lined with epithelial tissue and is about 5 to 7 cell layers thick [10]. The cells in the deepest epithelial layer are called basal cells after which follow 4 to 5 layers of stratified squamous epithelial cells, which are held together by tight junctions, to form an effective barrier against fluid loss and pathogen penetration [11]. Like most epithelia, the corneal epithelium continually sheds cells to the environment, a strategy which presumably impedes the progress of pathogens into the relatively immunologically deficient stromal tissue. Moreover, the layers of the epithelium are constantly undergoing mitosis [12]. Basal and wing cells migrate to the anterior of the cornea, while superficial squamous cells age and slough off

into the tear film. The epithelial corneal layer possesses numerous nerve endings making it one of the most sensitive tissues of the body which helps in the protection of the cornea.

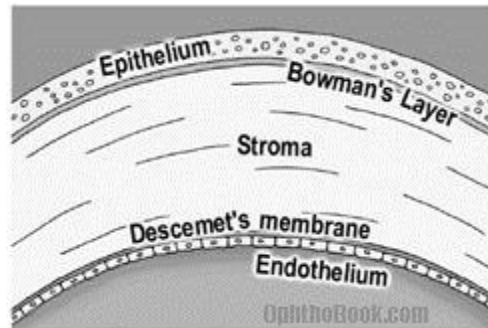


Figure 2-2: Corneal layers [9]

The Bowman's Membrane

Bowman's membrane (BM) is a non-regenerative corneal layer which is around 8 to 12 μm thick in normal adult humans. BM lies directly below the basement membrane of the epithelium and is composed of strong randomly oriented collagen fibrils [13]. It is suggested that BM acts as a physical barrier that protects the sub-epithelial cornea from direct traumatic contact with the corneal stroma. Hence, it is actively involved in stromal wound healing and the associated restoration of anterior corneal transparency [14].

The Stroma

The stroma is the central layer of the cornea that lies beneath the BM. The stroma is the thickest layer of the cornea (about 500 μm) that comprises around 90 percent of the cornea and dominates the mechanical response of the cornea to external physical inputs such as injury [15]. In terms of weight, the stroma is approximately composed of 78% water, 15% collagen and 7% non-collagenous proteins, proteoglycans and salts [16]. The stromal architecture can be understood in terms of parallel sheets

called lamellae. Each lamella has a number of in-plane collagen fibrils that run parallel to each other and held together by proteoglycans as shown in Figure 2-3 [17].

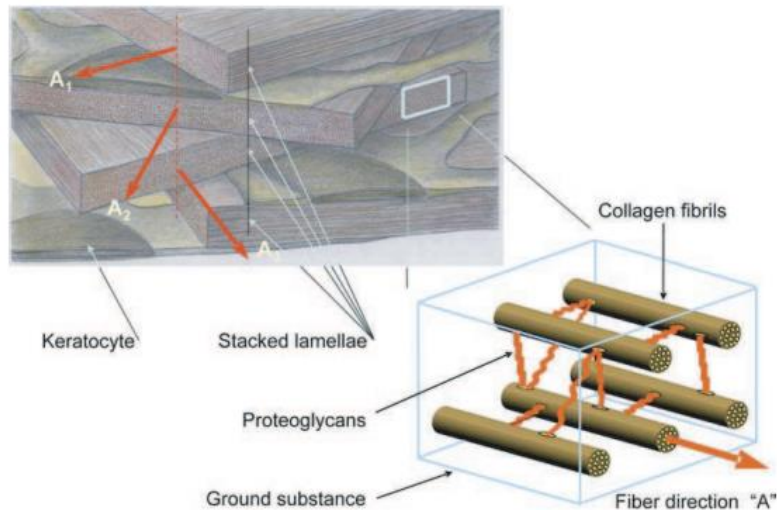


Figure 2-3: Schematic representation of the corneal stroma where lamellae layers are stacked at an angle to each other. The collagen fibrils that comprise the lamellae sheets are also approximately parallel to each other and are embedded in an extra-fibrillar matrix linked by proteoglycan molecules [17]

At the microscopic level, the corneal stroma appears as a dense, organized, avascular and comparatively acellular tissue. In appearance, the stroma is transparent and this transparency depends on the orderly packing of the collagen fibrils in each lamella that stack on top of each other to form the stromal layer. Collagen fibrils are narrow in diameter and closely packed in a regular array [18]. Collagen fibrils that comprise the stroma are type I, III, VI and XII, and it appears that the average diameter of the fibrils is approximately 31 nm. The arrangement of the fibrils follows a definite pattern, as there is a significant increase in collagen fibril spacing from the central cornea (about 57 nm) to the periphery (about 62 nm), followed by an even larger increase at the limbus [19].

The collagen fibrils in the stroma play an important role on the macroscopic scale in reference to the corneal shape and mechanical strength. Biomechanically, the collagen fibrils provide tensile load resistance [20]. The stromal fibrils are organized into three hundred to five hundred flat bundles/sheets, or lamellae, which run uninterrupted from limbus to limbus like thin belts up to 0.2 mm broad and about 1 to 2 μm thick. Fibrils within a given lamella run approximately parallel to each other as shown in Figure 2-3. X-ray scattering has demonstrated (Figure 2-4), that the majority of the collagen fibrils in the central stroma adopt a preferred orientation in the inferior-superior and nasal-temporal directions [19]. Previous studies have also demonstrated that fibril distribution directions vary from one cornea to the other, while some corneas favor one direction more out of the two favored fibril directions [19]. These fibril alignment orientations have a correlation with the direction of forces exerted by rectus muscles, with more collagen fibrils aligned in the direction of the force applied by the muscles. When the fibrils approach the limbus another transition in the preference of fibril directions is witnessed. The fibrils leave their preferred orthogonal direction to a circular directional preference as shown in Figure 2-4. The cornea is stiffest in this region due to the direction and close packing of the collagen fibrils [21].

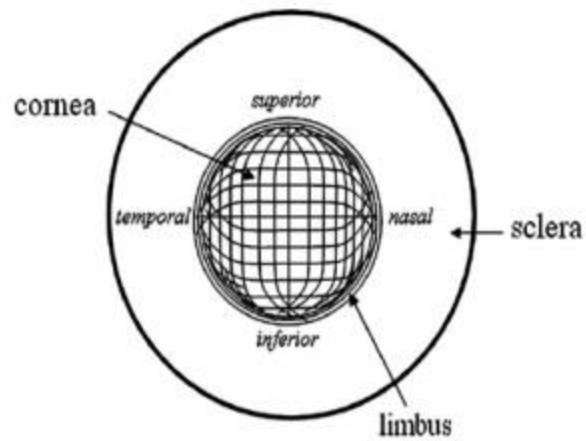


Figure 2-4: Preferential orientation of collagen fibrils in posterior stroma. Fibrils have an ordered limbal-to-limbal arrangement, running preferentially in the inferior--superior and medial--lateral meridians, interweaving circumferentially with scleral collagen fibrils at the limbus [19]

Parallel fibrils form a lamella and lamellar sheets in the corneal stroma are arranged parallel to the plane of the cornea. However, adjacent lamellae alternate in direction by 90 degrees with inferior-superior and nasal-temporal as the principal directions. Other factors that add variation to the stromal architecture include lamellar size variation as a function of stromal depth. The anterior stromal lamellae (0.5-30 μm wide and 0.2-1.2 μm thick) being generally smaller in size as compared to posterior stromal lamellae (100-200 μm wide and 1.0-2.5 μm thick). Lamellae and fibrils are held together by a substance called the proteoglycan matrix, commonly known as ground substance. Proteoglycan is a gel-like substance, consisting predominantly of water. It is proposed that the proteoglycan composition of the cornea is associated with the maintenance of a proper stromal ultrastructure. Proteoglycans also provide an internal swelling pressure of nearly 60 mmHg [20].

Transverse Mechanical Strength of stroma

Mechanical properties of the cornea in the transverse direction vary from the in-plane direction. The corneal stroma can be divided into three parts, an anterior third and a posterior two thirds. Previous studies show striking variations in the lamellar organization in the anterior third and posterior two thirds as presented in Figure 2-5 [22].

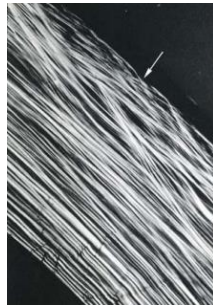


Figure 2-5: Optical polarization figure demonstrating the interweaving of the collagen lamellae in one third anterior stromal portion of the cornea, whereas the posterior two thirds demonstrate planar organization of the lamellae. The arrow in the figure signifies the anterior stromal surface [22]

The anterior stroma exhibits substantial weaving of continuous lamellae in the A-P direction while in the posterior stroma, the lamellae run nearly exclusively in the plane of the cornea. This variation in interweaving is expected to contribute towards variation in mechanical properties of corneal stroma [23].

Descemet's Membrane

Descemet's membrane (DM) is a thin, strong and structure less corneal layer [24]. DM is approximately 5 to 10 μm in thickness. The DM, like other basement membranes, consists of two distinct layers, a posterior layer adjacent to the endothelium and produced by the endothelial cells, and an anterior layer formed by collagen lamellae and proteoglycans. The thickness of the posterior non-banded layer of DM increases significantly with age, averaging approximately 2 μm at age 10 years and 10 μm at age

80 years [25]. The different organization of the DM in comparison to the collagen fibril organization in the stroma has been documented in literature [26]. DM plays a pivotal role in modulating corneal hydration levels and maintenance of the endothelial layer post-surgery. Considering the thickness of DM and its unique composition, its corneal function besides acting as a basement membrane, is that the DM plays acts as a mechanical support and as a liquid barrier [27].

The Endothelium

The endothelium is an extremely thin corneal layer about 4 to 6 μm thick consisting of a monolayer of hexagonal endothelial cells as shown in Figure 2-6 [28]. Endothelial cells are about 20 μm across and are conjoined at their borders with incomplete tight junctional complexes [10]. Endothelial cells (ECs) are essential in maintaining corneal clarity by acting as small pumps to pump excess fluid out of the stroma, as the stroma has the danger of swelling with water. The ECs are unique in reference to their regeneration ability; they do not regenerate at an adequate rate and this is the reason that EC loss leads to corneal transplantation [29], [30]. Generally, when an EC is lost, other ECs enlarge to fill up the gap. However, excessive damage to ECs can lead to corneal edema (swelling caused by excess fluid) and blindness, leaving corneal transplantation as the sole remedy.

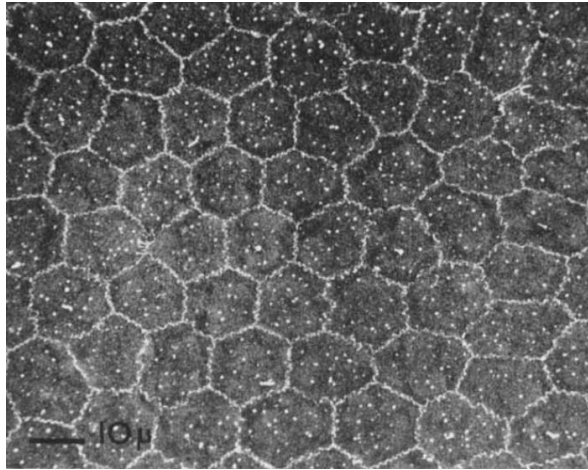


Figure 2-6: SEM of corneal endothelial layer [28]

Limbus

The limbus acts as the junction zone between the transparent cornea and the opaque sclera as shown in Figure 2-7 [31]. Besides, the limbus contains pathways for flow of aqueous humor. The limbus is not categorized as a separate tissue but, rather as the border zone separating cornea, conjunctiva, sclera, and uvea. Like geographic border zones around the earthly globe, there is no uniform agreement about the precise boundary lines of the sclera [31]. Limbus transitional zone is approximately 1.5 to 2.0 mm with the internal edge called as the corneal limbus whereas the external edge is called scleral limbus. Within the limbal zone, the orderly corneal collagen packing transitions to the coarse interweaving of scleral fibrils, and the fibril diameter increases significantly from the smaller fibril diameters in the cornea to the larger fibril diameters found in the sclera.

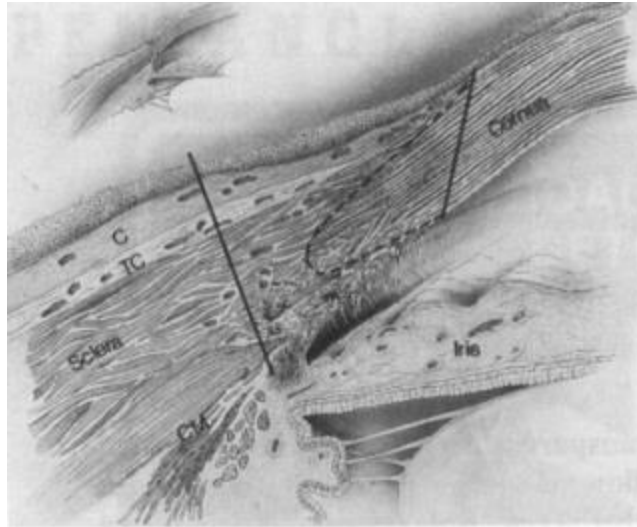


Figure 2-7: This figure shows the limbus where solid lines demarcate the pathologist's limbus whereas the dotted lines demarcate the histologist's limbus [31]

Sclera

The sclera constitutes the posterior five sixths of the corneal globe and gives the eye its white color. It is relatively avascular and consists almost entirely of collagen, containing a lesser amount of ground substance material than cornea [32]. The opaque nature of the sclera prevents light rays to scatter inside the eye globe. Sclera is mechanically stiffer than the cornea hence it has the ability to protect the intraocular contents from damage and mechanical detachment due to injury. The higher stiffness of the sclera allows the eye to maintain its shape, under the action of the intraocular pressure and contractions of extra-ocular muscles. The scleral thickness is non-uniform and it is a function of gender and age [33]. The bands of collagen bundles that form the sclera are predominantly oriented parallel to the scleral surface, however there is intersection among them as shown in Figure 2-8 [22]. Collagen fibrils that constitute the collagen bundles of the sclera are also predominantly parallel to each other and demonstrate extensive variation in diameter and spacing [34].

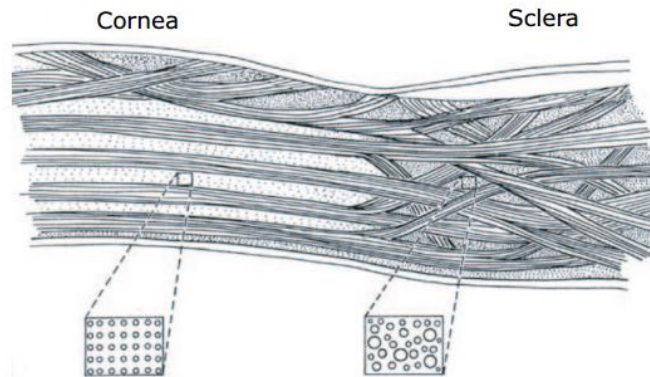


Figure 2-8: Figure representing the interlacing of collagen lamellae in the corneal stroma and sclera [22]

Methods Used for Material Characterization of the Cornea

The biological structure of the cornea demonstrates that material properties of the cornea should be nonlinear anisotropic viscoelastic in nature. But characterizing the material properties of the cornea in an adequate manner is a challenge that the scientific community has faced over the years. Various research groups have been working on obtaining the exact material properties of the cornea for decades and have employed different characterization methods such as uniaxial strip extensimetry, inflation techniques, and indentation tests [35], [36]. Uniaxial tensile testing, the oldest characterization method is usually performed on 3 to 4 mm long corneal strips with rectangular cross sections at predetermined anatomical directions. Some limitations of this technique are introduction of unwanted stresses in the strips due to the flattening of initially naturally curved strips, and its failure to characterize the material properties of the cornea in its natural state with intraocular pressure applied on the posterior side. In addition, designing tissue holders for tensile testing poses a challenge, since improperly designed holders can lead to tissue damage and/or tearing at the grasping location [27]. Inflation testing is considered more accurate since it captures the natural conditions of

the cornea with the equivalent of intraocular pressure applied to the cornea tissue at the posterior end while material characterization is taking place. Once the external liquid pressure is applied, imaging techniques are employed to accurately measure corneal deformation and then mathematical computations are performed to convert corneal deformation data to material properties of the cornea. Indentation testing is a material characterization method in which an indentation probe (e.g. atomic force microscopy probe) is utilized to measure localized material properties of the corneal tissue by pressing the tissue and analyzing its response. This method has proven to be extremely sensitive to indentation tip size, depth, and loading rates. This method provides a good means to measure localized in-situ material properties of the cornea in its natural state and theoretically it has the capability to measure material properties of individual layers of the cornea. However, the results achieved from this characterization method are not very precise and demonstrate a high range of values [37].

Chapter 3

An Overview On Performance Characteristics Of Laser In-Situ Keratomileusis (LASIK) And Identification Of Challenges

Introduction

Humans have always faced vision problems due to refractive errors, and in efforts to address them they developed various solutions that changed and evolved with time. The first notable remedy invented was that of spectacles, yet the person who could be credited with this invention is still unknown. Literature tells us that Marco Polo wrote a letter in 1270 about Chinese people using spectacles, however the Chinese claimed that spectacles originated in Arabia in the 11th century [38]. The Western world as we know it today became accustomed with optics in the thirteenth century with the Italians being the first to come up with spectacles in that era [39]. Monks and scholars in Europe were the first ones to start using spectacles for correction of myopia [38]. The evolution of spectacles started in the fifteenth century hereafter many designs were introduced until we finally settled onto the spectacles design being employed today.

In the late nineteenth century, eye care took a turn and scientists started investigating contact lenses. This change was propelled by F. E. Muller's invention of an eye covering that enhanced vision and could be worn with ease [40]. Though, it was not until mid-twentieth century that contact lenses were commercially introduced as small circular shaped lenses to rectify vision. Contact lenses alleviated a person from wearing spectacles which led to enhanced convenience, peripheral vision and aesthetics. The United States Food and Drug Administration (FDA) approved contact lenses in 1971.

The invention of contact lenses in early twentieth century prompted scientists to raise the question of eliminating lenses once and for all. Therefore, researchers directed

their attention towards refractive surgery and it was not long before experimental studies were being conducted. Barraquer was the first to introduce the concept of refractive surgeries to attain better visual acuity in 1960 [41], however the first LASIK surgery was performed by Pallikaris et al. in early 1990s [42].

Traditionally, mechanical microkeratomes (miniaturized mechanical blades) were utilized in refractive surgery procedures for making incisions. But due to advances in laser technology and the unique advantages it offers, lasers are gradually taking over the use of mechanical microkeratomes in refractive surgical procedures. Mechanical microkeratomes and femtosecond lasers have been employed for flap creation, excimer lasers are subsequently utilized for corneal remodeling. Srinivasan and Trokel were the first ones to use excimer lasers for refractive surgery procedures in 1983 [43]. Owing to the success of excimer lasers in LASIK procedures, the Kremer Excimer Laser was the first to be approved by FDA in 1998, followed by a host of other lasers to be employed in refractive surgeries [44]. Thus, technological advances in non-contact incision making have reduced the use of mechanical microkeratomes. LASIK surgeries today rely totally on lasers for incision making and corneal remodeling.

This chapter will present a brief review on the current challenges associated with LASIK surgery. In order to better understand these challenges, a brief explanation on the anatomy of the human eye and associated refractive errors or ailments is presented, followed by an explanation on LASIK. It continues by explaining laser-tissue interaction when a femtosecond laser is used to create the corneal flap or when an excimer laser is used to remodel the human cornea. It highlights the parameters that affect laser-tissue interaction and subsequently suggests approaches in which they can be optimized for enhanced incision quality. Aspects of the LASIK procedure which lead to post LASIK side effects are introduced and the role of lasers in alleviating them is discussed. Issues

presently encountered in LASIK, recent developments and open research questions yet to be answered are highlighted. For the purpose of discussion, this work refers to IntraLase 30-60kHz femtosecond laser (Abbott Medical Optics, Santa Ana, California, USA) [45] unless specified otherwise and the material related to mechanical microkeratomes will be mostly related to Bausch and Lomb Hansatome (Bausch & Lomb, Rochester, New York, USA) [46].

Refractive Errors

The adult cornea is about half millimeter thick and comprises of five layers: epithelium, Bowman's membrane, stroma, Descemet's membrane and the endothelium [47]. All these layers have a cumulative refractive effect that enables light to be refracted on the retina. In eyes with refractive errors such as near sightedness or myopia, light is focused in front of the retina (Figure 3-1) whereas in far sightedness or hyperopia light is focused behind the retina. Astigmatism however involves a phenomenon in which light rays entering from top and bottom are focused at one point and light entering from left and right side are focused at another point.

Clear vision demands perfect shape and alignment of the cornea and retina. However, refractive errors lead to an imperfect shape and alignment due to which lights rays do not focus onto the retina properly. These imperfections are known as refractive errors among ophthalmic circles [48]. All these refractive errors could be rectified by appropriately changing the shape of the cornea. Therefore a good understanding of the cornea is important for understanding LASIK.

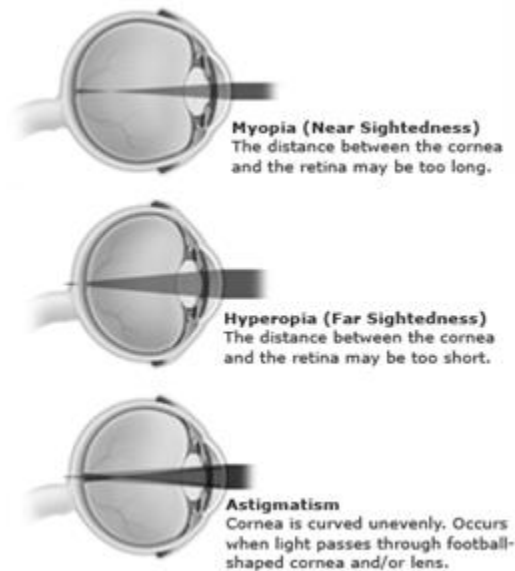


Figure 3-1: Refractive errors in a human eye [49]

Laser In-Situ Keratomileusis - LASIK

LASIK is an ophthalmic procedure used to rectify refractive errors, the steps followed in this procedure are shown in Figure 3-2 [50]. In the LASIK procedure, the patient's eye is affixed to a suction ring to prevent eye movements or loss of contact. Then a femtosecond laser or mechanical microkeratome is used to create an endothelium corneal flap. The flap is folded to reveal the underlying corneal tissue. An excimer laser is then used to change the shape of the revealed corneal tissue by controllably removing or ablating parts of the tissue. Thus, effectively changing the overall shape of the cornea and rectifying the preexisting refractive errors. After corneal remodeling, the flap is allowed to fall back in place where it reseats into the corneal groove without the need for stitches. LASIK is a preferred procedure because it avoids anterior stromal haze and pain that are frequently associated with other refractive surgeries such as photorefractive keratectomy (PRK), radial keratotomy (RK), automated lamellar keratoplasty (ALK) etc. These symptoms are not observed in LASIK because

LASIK avoids damaging the corneal epithelium. In the US, clinical trials for LASIK began in 1996 and FDA approval was granted in 1999 [51].

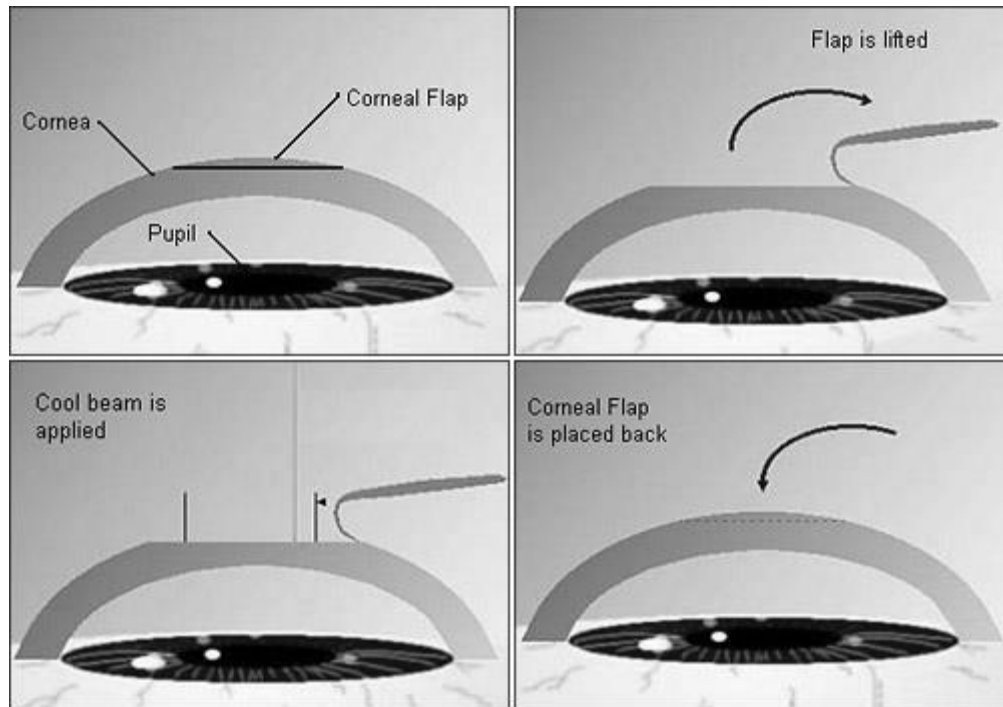


Figure 3-2: Steps for LASIK procedure [50]

Refractive errors such as near sightedness (myopia) can be corrected by making the cornea less round. Corneal flattening decreases the refractive power and increases the focal length, hence light is focused not in front of the retina but on the *fovea* (center of the macula region of retina). In hyperopia, the cornea is rounded in the center to increase the curve of the cornea and enable the eye to focus on the retina by employing the same tools and process outlined in the LASIK procedure [52]. Astigmatism can be corrected after measurement of the amount of abnormal eye curvature by an aberrometer. Subsequently, LASIK is performed and corneal tissue is remodeled so as to rectify the abnormality in the eye and perform correct focusing of light on the *fovea* [8]. Although

LASIK is a successful procedure, it cannot be employed yet to rectify eyes with refractive errors above +5.0 diopters of hyperopia and -12.0 diopters of myopia [53].

During all LASIK surgeries, immense care is taken to avoid generating abrupt steps on the corneal surface between treated and untreated corneal tissue. An abrupt change in corneal surface may lead to refractive regression [54] which introduces blurred vision, therefore it is highly desirable to establish a smooth transition between the treated and untreated corneal tissue. Studies have revealed that most of the excimer laser operation on the cornea should be limited to the center of the cornea known as the optical zone, which is determined by the size of the patient's *mesopic* pupil (size of pupil in normal daylight conditions). Intersection of treatment zone with the optical zone, is considered undesirable since it leads to disturbances in night vision [55].

Flap Creation In LASIK

The endothelium corneal flap creation is perhaps the most critical step that defines the success of the LASIK procedure. The corneal flap in traditional LASIK is usually a round shape with 9 mm diameter and depth of 140 to 180 μm . Owing to the fine nature of this incision, traditionally a healthy percentage of complications were observed due to misplaced or de-centralized corneal flaps. This was attributed to limitations of the traditional mechanical microkeratomes used in corneal flap creation. These shortcomings of mechanical microkeratomes paved the way for femtosecond lasers to be used for flap creation in LASIK. But recent developments in both laser and mechanical microkeratome technology have fairly enhanced the accuracy of corneal incisions [56]. A recent study conducted at Optical Express in UK revealed that flap displacement rate after LASIK was extremely low (0.012%) [57].

Comparison Of Femtosecond Lasers With Mechanical Microkeratomes

There is a wealth of literature available that discusses the capabilities of both femtosecond lasers and mechanical microkeratomes. Traditionally mechanical microkeratomes were used to create corneal flaps in LASIK procedures, but gradually femtosecond lasers are replacing them [58]. It is firmly established in the literature that femtosecond lasers have an advantage because they provide more options for the flap cutting profile. Femtosecond lasers reduce the time duration for flap creation and enable surgeons to create better quality corneal flaps that are thinner, more precise and accurate in dimensions [58], [59]. Flaps created by femtosecond lasers reduce the chance of infection as the laser light is the only element that comes in direct contact with the eye. The programmability afforded to motion systems guiding femtosecond lasers equips the surgeon with the ability to make customized cuts with respect to depth, profile and side-cut orientation [60]. Flaps created by femtosecond lasers have been observed to be of uniform thickness when going from the center of the cut to the periphery [61] and this enhanced accuracy has allowed surgeons to accept a wider range of candidates for LASIK surgery. Studies have also shown that femtosecond laser created flaps expedite recovery of the corneal sensation after LASIK surgery [62].

Mechanical microkeratomes are less expensive and easily available. Their accuracy and reproducibility has been significantly improved over the last few years. So much so that recently some research groups have not registered any significant differences in the performance of a mechanical microkeratome and a 15kHz femtosecond laser [56]. In LASIK, accuracy of corneal flaps created with mechanical microkeratomes depends largely on the ability of the surgeon and the quality of the blade being used [63], factors that lower the reproducibility of corneal flaps. This aspect was highlighted in a recent study where flaps created by mechanical microkeratomes had a standard

deviation of 18 to 24 μm for a flap thickness of 160 μm [64]–[66]. However, significantly improved results have been observed with a 60kHz femtosecond laser [58], [67], [68]. This was validated in a recent clinical study where a 60kHz femtosecond laser was shown to produce extremely reproducible results. Corneal flaps made by this laser system exhibited a mean deviation of 6.6 μm from the desired depth of 120 μm [69].

Modes Of Laser Tissue Interaction

The results of laser tissue interaction depend on the type of laser used and the health of the interacting tissue. In corneal flap incision, the tissue is transparent and as such all the modes of laser-tissue interaction such as absorption, transmission, reflection and scattering, as shown in Figure 3-3, must be considered and understood. In LASIK, we are interested in quantizing these aspects of laser tissue interaction because only after the effects of each of these phenomena are known, can we decide the appropriate laser type, laser power/energy and other process parameters to use. For example, if we are unaware of the amount of laser power that reflects or scatters once it strikes the cornea, we cannot decide the correct amount of laser power/energy to use. We might know the laser fluence level it requires to ablate a cornea, but since every eye is different it might react slightly differently with the interacting laser. Owing to these factors, further research into these areas is recommended, as this would provide the knowledge to define a procedure which will enable the surgeon to define exact laser parameters for each individual's eye at a personalized level. If excess energy is applied to the cornea this could lead to the generation of heat affected zones whereas, fluence levels below threshold fluence would not result in any ablation or cutting, thus leading to reduced quality of incisions while creating the corneal flap in LASIK.

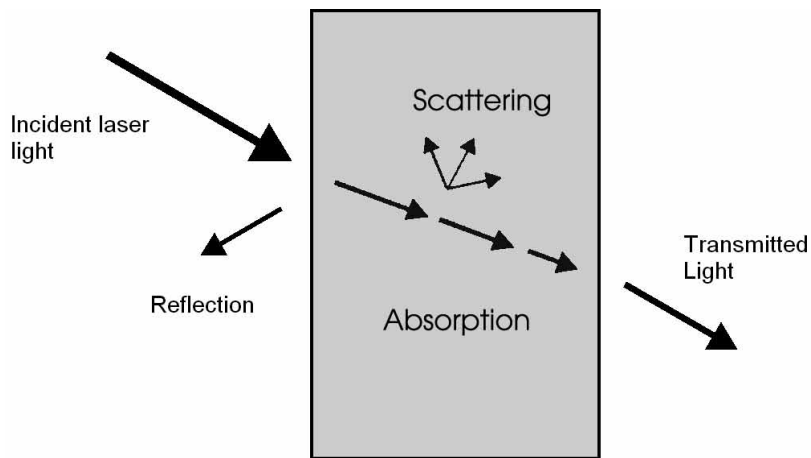


Figure 3-3: Laser tissue interaction [70]

The laser characteristics are not the only parameters that govern laser-tissue interaction but the type of tissue plays an important role in determination of the final outcome. When optical energy of the laser beam is imparted to a tissue it changes to other forms of energy according to the *first law of thermodynamics*. If the optical energy changes into thermal energy it is called *photo-thermal effect* and it causes an abrupt rise in the temperature of the tissue. This sudden influx of optical energy might initiate chemical reactions in molecular bonds of the tissue and this is known as *photo-chemical effect*. The laser energy sometimes creates a plasma effect in the tissue it interacts with; this plasma subsequently expands and generates a shockwave, this phenomenon is known as the *photo-acoustic effect*. Plasma usually travels in a radial direction towards the surface as it offers a radial path of least resistance. The generated plasma plume also provides hindrance to the subsequent laser pulses, which ultimately reduces the quality of incisions.

Lasers Used In LASIK

Femtosecond Laser

Femtosecond laser is named after its pulse width which is in the order of 10^{-15} second. These lasers operate in infrared or near infrared wavelengths (1053nm for LASIK [71]). Femtosecond lasers have been employed to ablate a variety of materials ranging from hard metals to soft corneal tissue [72], [73]. When using femtosecond lasers, every material possesses a deterministic ablation threshold which is defined as the minimum amount of fluence required to initiate ablation [72]–[75]. This ablation threshold fluence is a function of laser parameters; the laser pulse width, laser energy, laser pulse frequency (or pulse repetition rate) and focus spot diameter. The human cornea ablates at lower pulse energy if the laser beam is tightly focused, the frequency of pulses is high and the pulse duration is very small [76], [77]. *Beam waist* (radius of focused laser beam) can be decreased by expanding the laser pulse or by using a lens with a shorter focal length. However, both of these options are usually impractical due to limitations in the geometry of the optical system. Besides, the minimum beam waist is also dictated by diffraction if wave optics is to be considered [78]. Owing to these constraints, laser pulses with small duration and high frequency are used in LASIK. The IntraLase laser now marketed as iLASIK was the first femtosecond laser to be approved by the FDA in the United States in 2004. After the success of this laser, the FDA approved a host of other femtosecond lasers for LASIK procedures.

The success of femtosecond lasers can be largely attributed to the fact that they require small amount of laser energies for ablation which, leads to minimal heat affected zones [77], [79]. Ophthalmic applications of femtosecond lasers have various advantages because of the transparency of the eye. This enables incisions to be made at any depth and any angle [80]. However, the sequence of lasing in the cornea should start from the

depth of the corneal flap towards the surface. Since, refractive changes take place at the location where the focused laser light interacts with the tissue. Once the refractive index of a particular location changes, subsequent laser light pulses might be refracted to undesirable locations or blocked completely if the interaction location becomes opaque. Thus, when the laser light interacts with tissue, micro-cavitation bubbles are formed which induce a change in the refractive index of the cornea at that location. The cornea loses its transparency in that small region thus causing non-linear effects as described above due to refractive index changes.

Mechanism Of Tissue Ablation Under Effect Of A Femtosecond Laser

Ultrafast lasers induce photoablation in tissues. This process begins with the laser induced tissue optical breakdown, a process in which the laser pulse generates an electric field termed 'plasma formation' consisting of ions and electrons [81]. This plasma rapidly expands and in the process displaces surrounding tissue. This displacement of tissue is regarded as a shockwave [82]–[85]. Adiabatic expansion of the plasma is so fast that heat diffusion from the plasma does not get enough time to diffuse thermal energy to the surrounding tissue and as such the heat affected zones are almost nonexistent. The ions in the expanded plasma merge to form carbon dioxide gas, nitrogen gas and steam [86]. These gases combine to form a small bubble and this phenomenon is termed as 'micro-cavitation' [87]–[90]. This means that wherever laser light interacts with tissue it produces small gas bubbles and these bubbles further combine with each other to gently lift and separate the tissue resulting in a continuous incision. Tissue bridges have been observed when the laser feed rate is too high, however this can be avoided by selecting a suitable laser feed rate [87].

When compared with other lasers, femtosecond lasers have an added advantage since they operate at near infra-red wavelengths and as such are not absorbed by

optically clear tissues [75]. These ultrafast lasers have the capability to perform incisions with submicron depth of cut accuracy. Femtosecond laser systems are also outfitted with appropriate mechanical motion drive systems that could achieve great repeatability to generate a corneal flap cut profile [91], which makes them perfect candidates for ophthalmic surgery.

Why Femtosecond Lasers Are Suitable For Ophthalmic Applications

Femtosecond lasers can be employed to create incisions in the human eye due to their unique properties. These properties are ease of accessibility, lack of blood vessels in the corneal layer of the eye and transparent nature of the cornea. Femtosecond lasers are characterized by small beam waist and minimal heat affected zone. Hence, when a femtosecond laser pulse meets the cornea, the combination of their respective properties create a synergistic effect which results in extremely precise incisions with an accuracy of $118.9 \pm 6.6 \mu\text{m}$ depth of cut [69]. These reasons make femtosecond lasers the perfect tool for corneal flap cutting.

The human cornea comprises mainly of water and hemoglobin. Both of these compounds exhibit low affinity with electromagnetic waves in the near infra-red region. Femtosecond lasers operate in the near infra-red wavelength region therefore these laser pulses are not absorbed by the cornea. Hence, femtosecond laser pulses can travel through the cornea without interacting with the corneal tissue, but at the point of focus. The interaction of femtosecond laser pulses with the corneal tissue at the point of focus initiates *micro-cavitation* that causes ablation at this location. These factors enable femtosecond lasers to be utilized effectively for conducting LASIK surgery.

Excimer Laser

After a corneal flap creation by mechanical microkeratomes/femtosecond lasers, excimer lasers are subsequently employed for the corneal reshaping process in LASIK.

The excimer laser was invented by Nicolay G Basov in 1970 [92]. This laser has the capability to produce ultra violet (UV) waves of varying wavelengths that depend on the type of reactive gas element used in the laser such as chlorine and fluorine mixed with inert gases such as argon, krypton and xenon. Excimer laser and tissue interaction can be broadly divided into three categories; photochemical, thermal and ionization. We are interested in *photochemical* interaction since excimer laser and corneal tissue interaction is governed by this process [55]. In this type of interaction, the excimer laser pulses cause disintegration of molecules in the polymer chains of corneal collagens. This process of tissue ablation through photochemical interaction is termed as ablative photo decomposition [93]. The excimer lasers are called *cool lasers* because they do not cause a significant increase in the temperature of the corneal tissue. Hence, significantly reduced heat affected zones are observed in excimer laser corneal reshaping during LASIK [93].

Why Excimer Lasers Are Suitable For Ophthalmic Applications

The human eye corneal tissue absorbs wavelengths below 400nm whereas longer wavelengths are transmitted without affecting the tissue [94]. Studies conducted on corneal tissues show that 248nm wavelength of ultra violet (UV) light causes DNA mutation whereas 308nm introduces cataracts in the lens of the eye [93]. Therefore, 193nm is the suitable wavelength proposed for corneal refractive surgeries [93], [95].

The types of excimer laser procedures in LASIK include a broad beam excimer laser and scanning beam excimer laser. The broad beam excimer laser technique was initially used in LASIK with a laser beam diameter of about 6 to 8 mm and was found to have certain disadvantages [55]. In the scanning excimer laser beam technique, a beam of a smaller 2 mm diameter is applied to the cornea [96]. The small focus spot diameter of the scanning excimer laser technique in LASIK along with advances in high frequency

excimer lasers yield a smoother ablated corneal surface which enhances visual equity [97].

Impact Of Femtosecond Lasers On LASIK

Thin Flap Or Sub Bowman LASIK

The advancements in femtosecond laser technology with higher depth of cut accuracy pave the way for thin flap LASIK in an attempt to decrease the risk of ectasia. In thin flap LASIK, the flap thickness is of the order of 90 to 110 μ m. This provides the opportunity to treat higher refractive errors since a surgeon has the ability to preserve more of the stroma leading to reduced chance of corneal ectasia but it might increase the chances of interface haze [98] [60]. A recent study proved that thin flaps also have a low probability to develop ectasia because of their minimal biomechanical impact on the cornea [99]. Thinner flaps reduce the volume of corneal tissue affected by the laser. Hence, a reduced number of nerves require regeneration, which results in reduced healing time [100], [101].

Flap Cut Profile

The flap cut profile is an important parameter because it dictates some of the post LASIK complications. Automated, CAD programmed and machine manipulated femtosecond lasers enable a surgeon to define the flap cut profile in an effort to limit post LASIK complications (epithelial in-growth, dry eye etc.). Thus, the automation of the process using femtosecond lasers is an attractive option. Mechanical microkeratomes on the other hand, make incisions with similar side cut profiles which reduces the ability of a surgeon to control the LASIK procedure.

Stromal Bed Quality

The stromal bed quality depends on the frequency of femtosecond laser pulses. In a recent study, the stromal bed quality was monitored for a femtosecond laser with

frequencies of 15 and 30kHz. The 15kHz femtosecond laser produced good results similar to mechanical microkeratomes with a brand new blade. However, the 30kHz femtosecond laser produced significantly better results since higher frequencies enable a surgeon to use a smaller point of focus and lower energy per pulse. The lower energy per pulse reduced the heat affected zone, thus contributing to improved quality of incisions [102].

Flap Centration

The flap centration is important since an off centered flap conceals the vital middle portion of the cornea which requires remodeling. Smaller flaps are usually preferred since they decrease the probability of producing buttonholes [103]. However small flaps are difficult to make with mechanical microkeratomes. On the contrary, CAD driven femtosecond laser systems provide greater accuracy and repeatability thus enabling the surgeons to create exact sized flaps [83].

Post LASIK Complications

Epithelial In-Growth

LASIK requires an epithelium corneal flap be made. The epithelium is the outermost layer of the cornea and epithelium cells regenerate at a high pace. This high regeneration rate is precisely why this layer heals quickly and acts as a natural band aid to the LASIK surgery on the cornea.

Epithelial in-growth, a common post LASIK complication is the process of epithelium cell generation not just at the sides but also under the flap. This creates bumps in the flap, which in turn not only reduce the flap adherence to the cornea but also deteriorate visual equity. The number of patients who develop this condition varies between 1 to 20% [104]. This complication could be surgically addressed by re-lifting the

flap and manually *debriding* the LASIK flap. But even after this surgical procedure recurrence of epithelial in-growth has a probability of 40 to 50% [105].

The side cut profile of a corneal flap is quite important as it has a strong bearing on post LASIK performance of the eye, especially on issues related to epithelial in-growth. A major advantage of using femtosecond laser system for LASIK is the ability to manipulate and control the side cut angle. Studies have revealed that epithelial in-growth is dependent on the side cut profile and, this is precisely why femtosecond LASIK surgeries exhibit decreased occurrence of the epithelial in-growth problem [106]–[108]. Chances of epithelial in-growth are 20% higher for mechanical microkeratomomes as compared to femtosecond assisted LASIK procedures [109].

In a recent study, it was observed that patients undergoing LASIK to rectify hyperopic eyes had a greater chance of developing epithelial in-growth as compared to patients undergoing LASIK to rectify myopic eyes [110]. In this study, 1000 consecutive LASIK procedures were analyzed. Out of these, 3% of the myopic patients and, a staggering 23% of hyperopic patients developed epithelial in growth [110]. The vertical side cut incisions created by femtosecond lasers induce less mechanical trauma to the epithelium leading to decreased probability of epithelial cell migration, hence reduced chances of post LASIK epithelial in growth [111].

Early Flap Displacement After LASIK

Early corneal flap displacement after LASIK hinders both the vision and healing process of the eye. This post LASIK complication is quite rare yet highly undesirable because of its adverse effects on visual equity. In a recent study, 81238 eyes that underwent LASIK were monitored for twelve months after LASIK surgery for early flap displacement. In this period, 0.055% of hyperopic patients. Compared to 0.003% of myopic patients developed flap displacement [57].

Night Glare And Halos

This is a common post LASIK side effect which can be addressed by using wavefront guided excimer laser surgery. In this technique, an aberrometer is used to image the aberrations present in the patient's eye. This image is used to decide the laser application pattern. The excimer laser is then guided to deliver tightly focused laser energy in the predetermined pattern rather than a random pattern. The first wavefront surgery was performed in 1999 with FDA approval granted in 2002 [84].

The wavefront guided excimer laser treatment provides better visual equity as compared to traditional LASIK. In a study conducted at the Bascom Palmer Eye Institute at University of Miami, 98% of the patients received a 20/20 vision or better with wavefront guided excimer laser [112].

Epithelial Erosion

Epithelial erosion is a condition where the outer most layer of the cornea starts to deplete. The epithelium layer is a thin layer of cells which are highly regenerative and as such they are the first line of protection of the eye. From an engineering perspective, epithelial erosions are caused due to a tangential shearing friction force on the epithelium. Friction plays an important role in the manifestation of epithelial erosions. In a study conducted to analyze whether mechanical microkeratomome usage in flap creation always leads to epithelial erosions, it was found that friction between the edge of mechanical microkeratome and epithelium cells always exists which leads to enhanced chances of epithelial erosions. However, friction is not the only cause as only selective patients developed epithelium problems in this study [113]. Some studies indicate that epithelial erosion is dependent on patient's age, ethnicity and skin type, thus some people are more prone to this side effect than others [113].

Dry Eye

Dry eye is a major side effect noticed by patients as a post LASIK effect where 0.25% to 59.0% of LASIK patients complain of dryness issues [114]. Excess pressure applied by the suction ring on the eye is considered as one of the problems that might lead to the dry eye syndrome [115]. Besides, preoperative dryness can cause major complications after surgery. Therefore, it is highly recommended that proper actions be taken before surgery to enhance visual outcomes and patient satisfaction.

LASIK changes the corneal shape and has a neurotrophic effect on the cornea that affect the tear dynamics of the eye and pave the way for ocular surface dehydration [116]. LASIK conducted by femtosecond as compare to mechanical microkeratomes produce lesser effects of dry eye due to planar flap profile [117]. Also, decreased corneal sensation in post LASIK patients leads to dry eye syndrome [115]. Lack in corneal sensation can be attributed to the transection of corneal nerves due to corneal flap cutting. The anatomy of the human eye reveals that most of the corneal nerves enter through 3-o' clock and 9-o'clock positions (Figure 3-4). Therefore, flap hinge positions play a vital role in preserving corneal nerves. Nasal hinges preserve more corneal nerves than superior hinges (Figure 3-4), thus patients with nasal hinges have a higher probability to avoid dry eye syndrome as compared to patients with superior hinge [115], [117], [118]. Therefore, ideally LASIK corneal flaps with planar profile, constant depth of cut throughout the flap, predefined side cut angle and a broad nasal hinge, should result in better sealing of the corneal flap. Better sealing of the corneal flap leads to enhanced corneal sensation and ultimately reduced occurrence of dry eye syndrome.

A recent study though shows that LASIK surgeries conducted with femtosecond lasers or mechanical microkeratomes have the same probability to produce dry eye symptoms [119]. Another study claims that planar profiles do not play an important part in

quicker healing of eyes [120]. So in summary, researchers seem to have different views about LASIK conducted via femtosecond laser having a reduced tendency to generate dry eye symptom. But one thing is for sure, that dry eye remains the most important post LASIK complication and researchers are yet to find the answer to this problem.

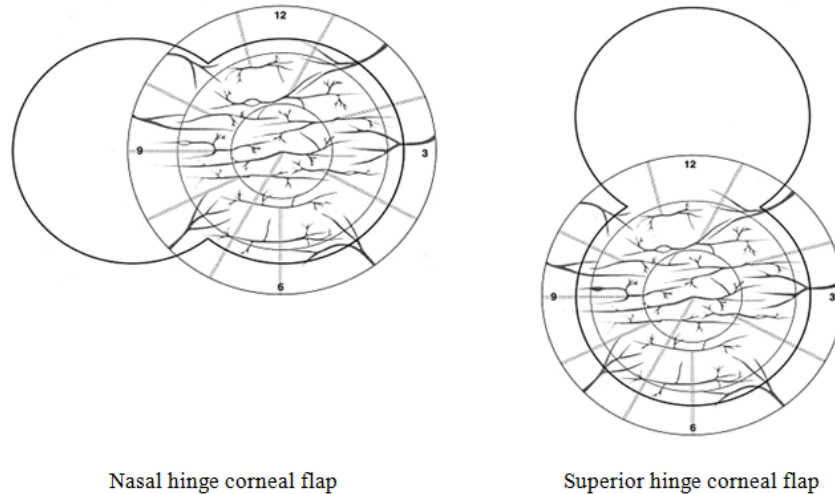


Figure 3-4: Flap configurations [115]

Conclusions

LASIK is an extremely widespread and effective refractive surgical procedure where 82 to 98% of the patients are satisfied with their corrected vision, visual recovery and quality of life after LASIK [74], [121]. This astoundingly high success rate associated with LASIK, which is higher than any other elective surgical procedures, has led to LASIK becoming one of the most popular medical elective surgeries.

LASIK is an elective procedure therefore patients harbor high expectations about post LASIK results. This creates an issue since a few minor post LASIK complications are quite common such as epithelial in-growth, dry eye, night glares and halos, etc. Hence, further research needs to be conducted in understanding the cause behind these complications in an effort to address and find solutions for them. Besides, some of the

tools used in LASIK such as femtosecond and excimer lasers demand further research, since accurate and reproducible incisions are of utmost importance in LASIK. Better understanding of the laser tissue interaction shall further improve the efficacy of LASIK and reduce post LASIK complications. Laser parameters such as; focused spot radius, spot separation and pulse energy in addition to optimized flap profiles require more research and better understanding. Whether the effect of these laser parameters is a function of age or race has yet to be evaluated.

Femtosecond assisted LASIK has proven to be an extremely reliable and effective process, yet a major barrier to the widespread adaptation of this procedure lies with the initial laser and auxiliary equipment purchase cost, besides their usage and maintenance costs. However, a recent market survey concluded that 68% of all LASIK flaps created in 2009 were created with a femtosecond laser [122], which is substantially higher than the 30% in 2006 [123].

Chapter 4

Application Of Finite Element Analysis To Study The Mechanical Behavior Of Cornea Due To Implantation Of An Intrastromal Corneal Ring

Introduction

Human eyes work when light rays enter through the cornea and get refracted due to shape and location of the cornea and natural lens. The cornea constitutes the transparent outer surface of the eye and is responsible for approximately 70 percent of the refraction that the incoming light rays undergo, thus making it the foremost place in order to restore visual acuity in eyes with refractive errors through shape modifications. Various eye diseases cause image formation away from the retina and many rectifications have been sought over the years in an effort to alleviate these defects. Intrastromal Corneal Ring (ICR) implantation is a relatively new surgical procedure which has enjoyed success in recent years [124]. The ICR implantation procedure requires the formation of a pocket in the stromal layer of the cornea with either a mechanical microkeratome or a femtosecond laser. Once the pocket is created, the ICR is inserted which causes the stromal tissue layers around the ICR to be pushed apart in order to make space for the ICR. The inserted ring plays an active role in modifying the shape of the cornea in order to improve visual acuity [3]. The amount of visual correction imparted to the cornea primarily depends on the geometry, diameter and cross section, of the ICR. Selecting the correct ICR geometry is therefore important to yield the desired cornea correction and as such structural analysis of the cornea with ICR implants can provide valuable insight into the biomechanics of the ICR implanted postoperative cornea.

Finite element (FE) analysis has been frequently utilized to analyze different organs, medical devices and implants [125]–[131]. FE modeling analysis has been

frequently used to model the cornea, and its usage has evolved over the years to encompass not just material properties but also the modeling technique. The eye models have evolved from 2D axisymmetric to 3D non-axisymmetric models of the cornea [10], [132]–[134]. Modeling approaches involved complete geometric eye models with cornea, limbus and sclera, and simplified models with just the cornea along with inclined roller supports [135]–[139]. Major evolution however, has been observed on the usage of material properties, with models starting with isotropic linear material properties to anisotropic nonlinear viscoelastic material properties for the cornea [10], [140]–[144]. Modeling approaches outlined by these research teams could potentially be followed as guides to model the biomechanics of the cornea with ICR implants. An exhaustive open literature survey was conducted to identify FE modeling techniques utilized to model and study the effect of ICR implantation on the corneal shape. Pinsky et al. (abstract only, 1995) [145] used a 2D model with isotropic linear material properties, and Kling and Marcos (2013) [146] employed a 2D corneal model with isotropic hyperelastic corneal material properties with hexagonal/triangular ICR implants.

The research presented in this chapter aims to develop a computationally efficient ICR implanted 3D axisymmetric FE model of a porcine cornea with isotropic hyperelastic material properties. A 3D axisymmetric model could be utilized to analyze segmented ICRs in future studies. The procedures followed and models developed in this chapter are based on the geometry of Myring ICR implant (Dioptex, Linz Austria), however they can be easily adopted and applied to study ICR implants of different characteristics. The presented FE model aims to provide more insight into the geometrical variations of the eye caused by the implanted ICR. FE modeling techniques have been utilized by others to analyze the cornea as mentioned earlier [132], [133], [135], [137], [139], [146]–[151], yet, to the best of our knowledge no papers available in

the open literature have utilized 3D axisymmetric numerical modeling of the cornea with 'Myoring' ICR implants and analyzed/discussed the effects of ICR parameters along with surgical conditions on the postoperative shape of the cornea.

This work develops and verifies a computationally efficient 3D FE model of the cornea by using ANSYS (Canonsburg, PA), a commercially available FE software tool. The hyperelastic material properties of the cornea and their application in the FE model are presented. A FE model of the full eye with cornea, limbus and sclera is developed and discussed. The full eye model is subsequently simplified by substituting limbus and sclera with angled roller support boundary conditions (BCs). The angle for roller BCs is determined by comparing FE model corneal apical displacement results with experimental results published in open literature. Moreover, to further gain confidence in the simplified FE modeling approach, the apical deformation results of the simplified FE model were compared with the apical deformation results of the complete eye FE model. The agreement between the FE modeling approaches and the limitations of the simplified FE model are discussed. Subsequently, the FE modeling procedure is extended to include ICR implants in the simplified cornea model. The changes in the corneal topography in response to the ICR implantation are evaluated and discussed. The discussion considers the effects on the corneal apical deformation due to variation in control parameters such as, diameter and thickness of the implanted ICR, ICR implantation depth, and diameter of corneal pocket. A sensitivity analysis was performed to evaluate the dominant control parameters affecting apical deformation through regression analysis.

Optics of the eye and refractive ailments

In the realm of biomechanics, the eye can be considered in simplistic terms as a pressurized spherical vessel. Light enters through one end (cornea) of the vessel (eye), it

is refracted due to the curvature of the entrance (cornea), and it focuses on the other side of the spherical vessel (retina). Due to optical diseases and irregularities sometimes the light focuses in front of the retina rather than on it and this condition is called myopia. There are three likely conditions which can lead to myopia (1) abnormally long eye ball, (2) an eye with an abnormally small radius of curvature which leads to abnormally high refraction of the incoming light rays, (3) abnormally high focusing power of the natural lens [152].

Over the years, various approaches have been sought to rectify myopia. The basic idea however behind all these procedures is to formulate a method whereby either refraction of the incoming light or length of the eyeball can be decreased as shown in Figure 4-1(a and b). The purpose of ICR implantation in the cornea is no different; it aims to alter the shape of the eye in an effort to ensure the focusing of light on the retina rather than in front of it. In simplistic terms, the ICR implants act as a structural reinforcement which if used properly can alter corneal biomechanics and achieve myopic rectification.



Figure 4-1: (a) Radius of corneal curvature increases which leads to a flatter cornea (b) Corneal curvature remains constant however the location of cornea is closer to retina (decrease in axial length of eyeball)

Materials and Methods

Structure of cornea

As discussed in chapter 2, the cornea primarily consists of three distinct layers, an outer epithelium layer, a middle stromal layer rich in collagen extracellular matrix

(ECM) and an inner endothelial layer [49], [153]. The epithelium and endothelium layers are essentially layers of cells that do not offer a significant amount of structural stiffness. On the other hand, the stroma acts as a structurally dominant layer since it is composed of interlaced collagen lamellae in an ECM interspersed with keratocytes [154]. These collagen lamellae when bonded together form collagenous layers that run parallel to the surface of the cornea, and combined these sheets constitute almost 90 percent of the cornea thickness [15]. Therefore, it can be safely stated that the stroma acts as the biomechanically dominant layer that undergoes stress stiffening behavior at high strains [154].

Material Properties Selection

It is widely accepted that corneal material properties are anisotropic and nonlinear viscoelastic in nature [155]. In this research, isotropic hyperelastic material properties similar to those used by Elsheikh et al. (2007) [156] as shown in Figure 4-2 were considered in an effort to improve computational efficiency as compared to employing nonlinear anisotropic properties. Moreover, isotropic hyperelastic material properties have been previously used to model the cornea by Kling and Marcos (2013) [146] and Elsheikh et al. (2010) [157]. Hence, using isotropic hyperelastic material properties can be considered as a valid assumption for a static structural corneal analysis.

The hyperelastic behavior of the corneal tissue is modeled for FE analysis using the Ogden 2nd order material model since it provided the best curve fit to the experimental data from Elsheikh et al. (2007) [156] as shown in Figure 4-2. Ogden material modeling was performed by utilizing the inbuilt modules of the FE modeling software, ANSYS Workbench 15, based on the Ogden strain energy function shown in Equation (4-1) [158].

$$U = \sum_{i=1}^N \frac{2u_i}{\alpha_i^2} (\lambda_1^{\alpha_i} + \lambda_2^{\alpha_i} + \lambda_3^{\alpha_i} - 3) + \sum_{i=1}^N \frac{1}{D_i} (J^{el} - 1)^{2i} \quad 4-1$$

Where λ_i are the principal stretches, N is a material parameter, J^{el} is the elastic volume ratio, u_i , α_i and D_i are temperature dependent material parameters. Material parameters calculated via ANSYS module were $u_1 = 727.74 \text{ Pa}$, $u_2 = 11.78 \text{ MPa}$, $\alpha_1 = 75.5$, $\alpha_2 = 0.0077$ and incompressibility parameters $D_1 = D_2 = 0$. The ICR implants are made of Polymethyl methacrylate (PMMA), a transparent thermoplastic polymer with linear isotropic properties; density of 1170 kg/mm^3 , Young's modulus of 1.8 GPa and Poisson's ratio of 0.48 [146].

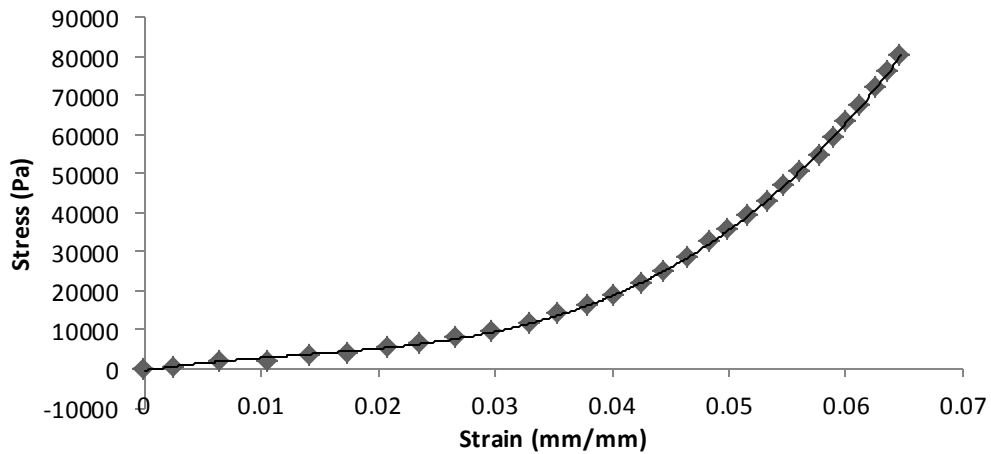


Figure 4-2: Stress strain material properties of the porcine cornea [156]

Finite Element Modeling

Modeling Methodology

Creating a complete 3D FE model of the eye presents a unique challenge because of the complexity of the physical system to be modeled. In a FE model that captures the exact physical condition, the modeling procedure would become quite complex. Some of the physical conditions that add to the complexity of the FE model are:

irregular size, shape and thickness of the cornea, intraocular pressure which varies from person to person, viscoelastic anisotropic material properties that depend on ethnicity, gender, age, health condition of the patient etc. Therefore, modeling the cornea with all its nonlinear complexity presents an enormous challenge and without the introduction of assumptions and simplifications, analysis would become computationally prohibitive. The model developed and presented in this work understandably considered some assumptions and simplifications which are discussed and explained.

FE Model Assumptions

The assumptions considered during the development of the FE model were, (1) the stress-strain functions in the model are assumed stable i.e. they do not change with repetitive loading, (2) the stress-strain function of the material during loading and unloading (hysteresis effect) are considered equal, (3) isotropic material properties were considered for the cornea, (4) viscoelasticity was not considered in the model, (5) prestresses on corneal layers due to curved natural state were ignored, (6) elastic material properties were considered for the limbus and sclera and (7) bonded contact was assumed between cornea, limbus and sclera.

FE Model Development and Simplifications

The first simplification focuses on reducing the size of the eye model by considering axisymmetry and reducing the model to a 2 degree sliver as shown in Figure 4-3. The eye model dimensions were taken as those presented by Woo et al. [159]. The material properties assigned to the different parts of the eye were, nonlinear isotropic hyperelastic material properties for the cornea as discussed earlier. Isotropic elastic material properties similar to the ones used by Kling and Marcos (2013) [146] were considered for the limbus and sclera with Young's moduli of 15 MPa and 33.6 MPa respectively and nearly incompressible Poisson's ratio of 0.49 was considered for both

the limbus and sclera. The loadings and BCs applied to the developed FE model are presented in Figure 4-4. Axisymmetry BCs B and C constrain the model from movement in the radial direction. BC C is fixed in all directions to suppress rigid body motion whereas BC D constrains the apical portion of the cornea for movement in the axial direction only. Loading A represents the intraocular pressure (IOP) of 3 kPa.

ANSYS solid tetrahedral elements (Solid 187) were used in this research since Solid 187 is a 10-node tetrahedral element with the ability to simulate hyperelastic material behavior. Appropriate mesh density for the FE model was evaluated by conducting a convergence study. The study was conducted by changing the number of elements when all other parameters such as model dimensions, BCs and loads were kept constant. While changing the number of elements care was taken to ensure that the quality of the elements in the mesh was not compromised and there was always more than one element in the thickness direction. The results of the convergence study were utilized to determine the minimum number of elements (9,310 elements) that yield a converged solution in an effort to decrease the computational cost of the subsequent set of analysis. The displacement results for the final full eye model are presented in Figure 4-5. The results show a maximum deformation of 0.37 mm at the apex of the cornea and this deformation is called apical deformation.

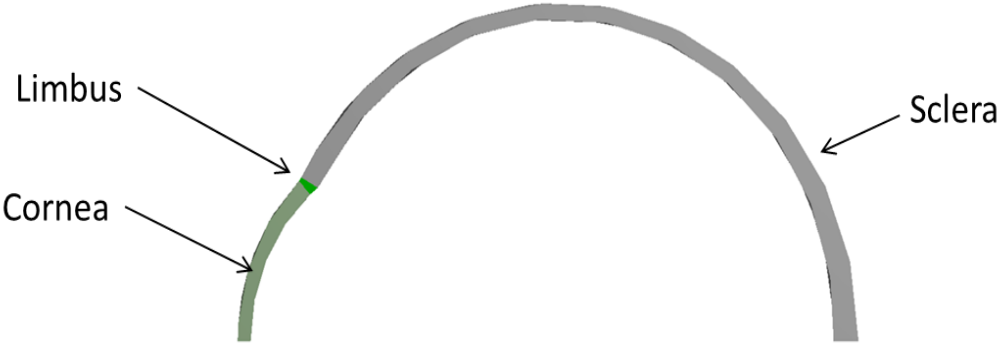


Figure 4-3: Full eye model with axisymmetric modeling assumption

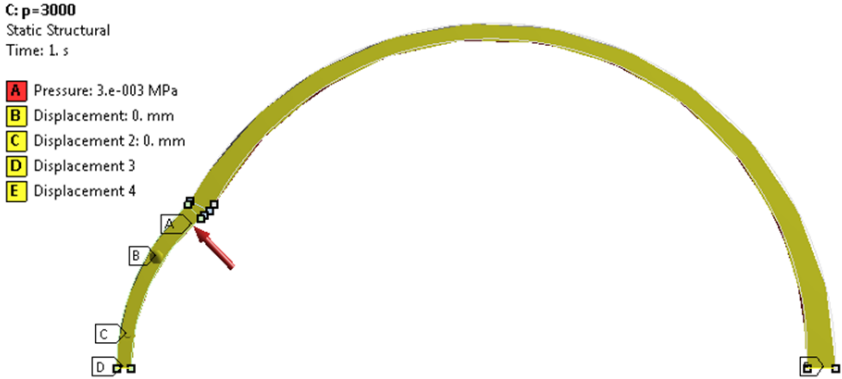


Figure 4-4: Applied loadings and BCs for the full eye axisymmetric model

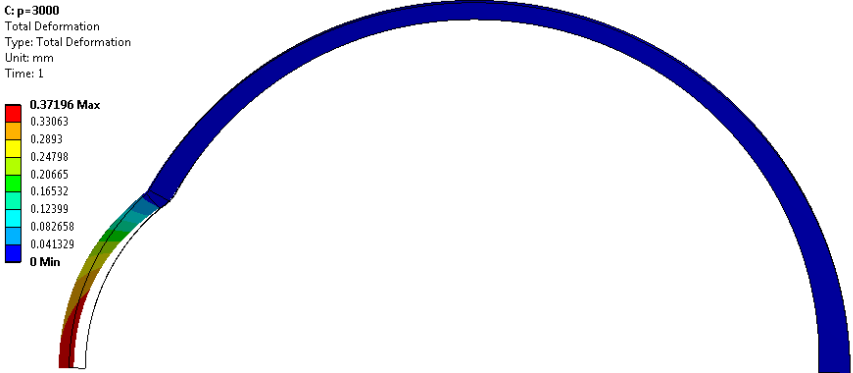


Figure 4-5: Full eye model displacement results

After developing the full eye FE model, the model was simplified to include only the cornea, the area of interest. This is a popular simplification procedure which has been previously employed by Orssengo et al. (1999) [138], Elsheikh et al. (2007) [156] and Han et al. (2013) [137] among others. It includes the introduction of angled roller supports at the corneal periphery as shown in Figure 4-6 in place of limbus and sclera. Similar to the cornea in the full eye model, the simplified cornea model was constructed with non-uniform corneal thickness of 0.52 mm at the center and 0.67 mm at the limbus [156], [159]. The remaining dimensions of the cornea model are shown in Figure 4-7. The correct angle for roller supports was evaluated by following an incremental methodology where the angle of roller supports were varied between 20 degrees and 50 degrees, and uniform intraocular pressure from 0 to 10 kPa was applied to the cornea model. The obtained displacement results were compared with inflation testing experimental results published by Elsheikh et al. (2007) [156]. The comparison of the FE model displacement results for varying roller support angles is presented in Figure 4-8. The results show that cornea model with 40 degree roller supports showed best agreement with the experimental results.

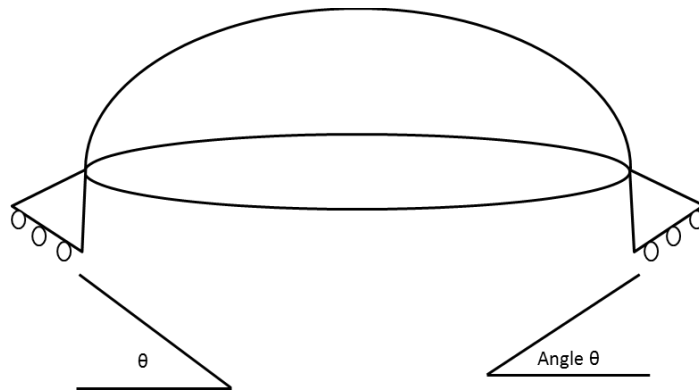


Figure 4-6: Simplified cornea model showing angle of inclined roller supports

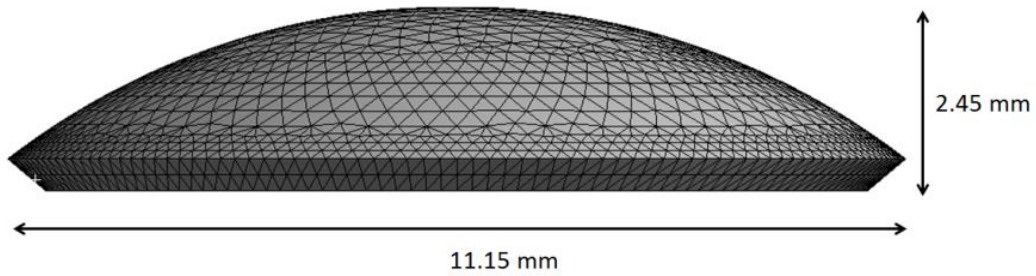


Figure 4-7: Dimensions of simplified FE cornea model

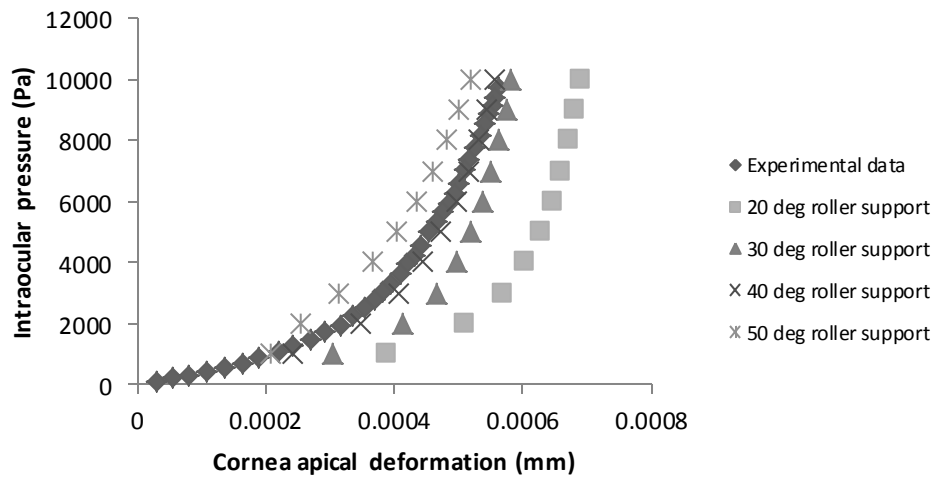


Figure 4-8: Corneal apical deformation and intraocular pressure for various angle supports and their comparison with experimental results

Advantages and Limitations of Simplified Eye Model

The displacement results of the full and simplified eye model (40 degree angular roller support BC) were compared with experimental results as shown in Figure 4-9. The results demonstrate that both full and simplified eye models show good agreement with the experimental data. Therefore, the simplified model was selected for further use since it improves computational efficiency while properly estimating the apical deformation.

Another parameter of significance in corneal studies is the radius of corneal curvature. An analysis was conducted to compare the radius of corneal curvature results obtained by the full and simplified eye models. The radius of curvature is evaluated according to Equation 4-2. The displacement equation describing the deformation of the cornea in Cartesian space is formulated using the FE displacement solution for a number of nodes on the deformed anterior corneal surface. A second order polynomial curve fit was used to represent the shape of the deformed cornea. This curve fitted equation is then employed in Equation 4-2 to evaluate the radius of curvature of the deformed cornea at the center of the cornea [160]. A representation of the process is provided in Figure 4-10, which shows the curve fit equations representing the shape of the deformed anterior corneal surface for simplified and full eye FE models.

$$R_{curvature} = \frac{[1 + (\frac{dy}{dx})^2]^{\frac{3}{2}}}{\frac{d^2y}{dx^2}} \quad 4-2$$

The application of the radius of curvature equation to the curve fitted equation representing the corneal topography without ICR implant as presented in Equation 4-3 is as follows:

$$R_{curvature} = \frac{(1 + (-51.234 * 2 * x + 0.5747)^2)^{\frac{3}{2}}}{-51.234 * 2} \Big|_{x=0.0055} \quad 4-3$$

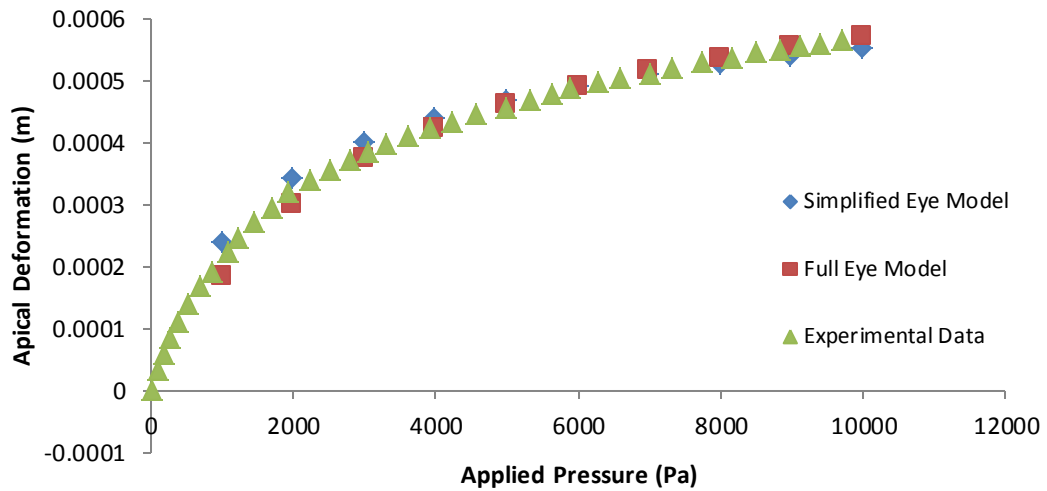


Figure 4-9: Corneal apical deformation vs intraocular pressure for full eye model, simplified cornea model and experimental results

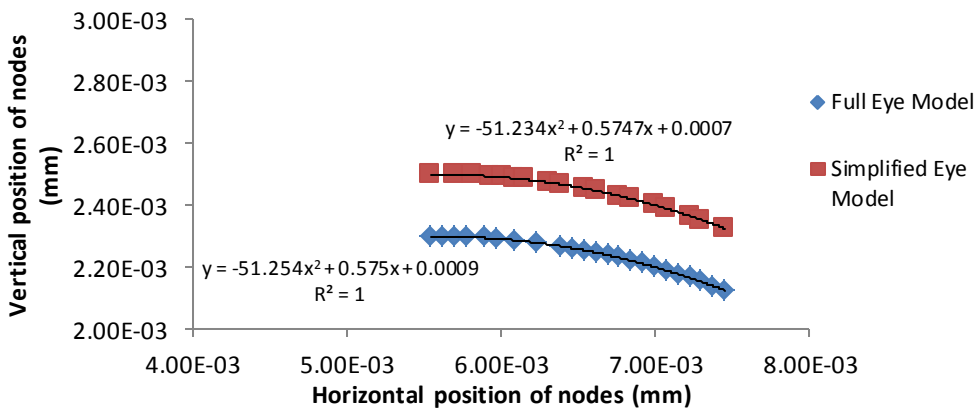


Figure 4-10: Nodal positions and displacement equations highlighting the topography of the cornea (Not to scale)

The radius of corneal curvature was evaluated at different intraocular pressure (IOP) levels while all other parameters were held constant, in order to evaluate the ability of the simplified FE model to properly estimate the radius of corneal curvature. The

comparative analysis results are presented in Figure 4-11 which demonstrate that as the IOP increases the radius of corneal curvature decreases in the full eye model whereas the radius of corneal curvature increases in simplified cornea model in addition to having different magnitudes. This comparison indicates that the simplified cornea model should not be employed to study the radius of corneal curvature since an increase in IOP should lead to a more curved cornea which entails a smaller radius of corneal curvature. This behavior was appropriately estimated by the full eye model. The reason for this lies in the manner in which the BCs have been defined for the simplified model. By employing, roller support BCs to replace limbus and sclera. At elevated pressures, the roller supports are constrained to move along their inclined plane which leads to an increase rather than a decrease in radius of curvature as shown in Figure 4-12. The deformed shape and the respective un-deformed wireframes highlight the difference in curvature for the two models that have the same corneal dimensions, material properties and loadings. Due to this limitation, the simplified cornea model was used to estimate only the effects of apical deformation on myopic rectification.

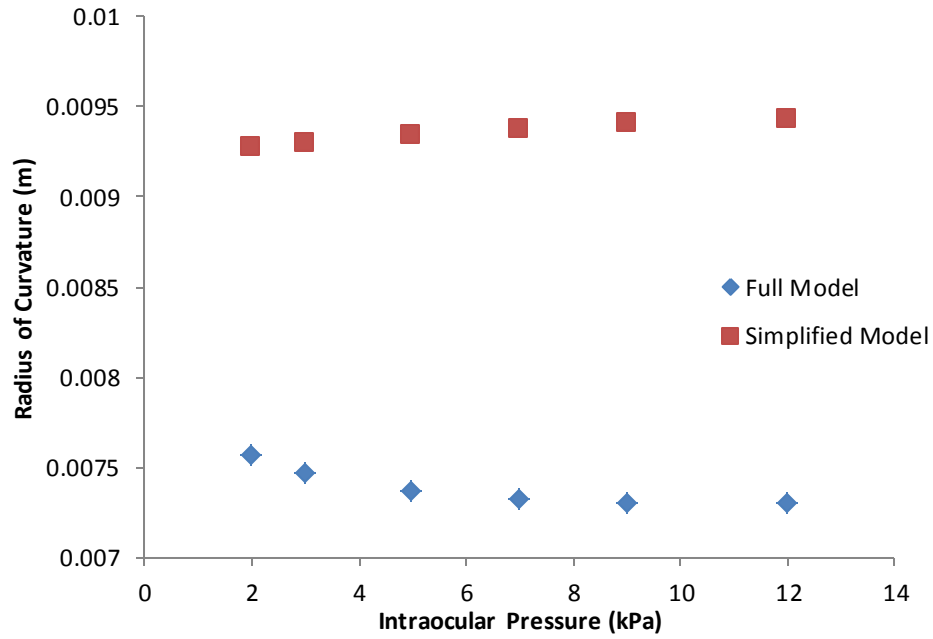


Figure 4-11: Radius of corneal curvature as a function of IOP

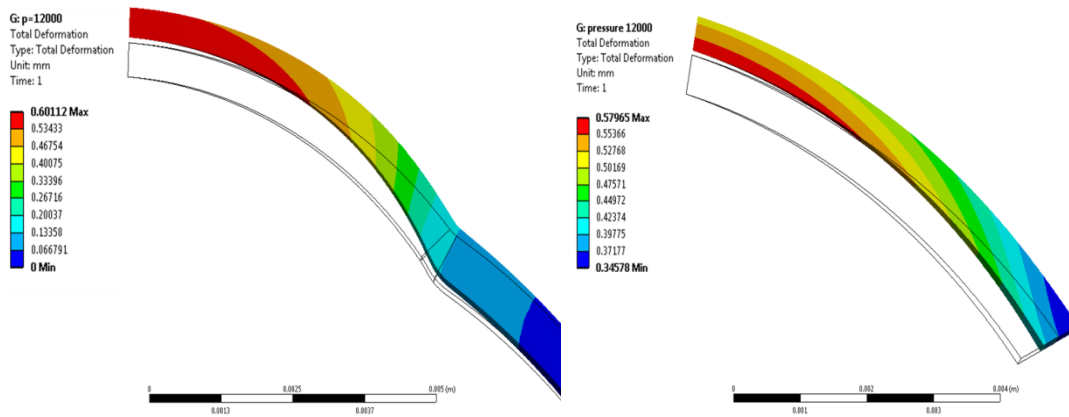


Figure 4-12: FE model displacement results for full eye and simplified cornea models with respective undeformed wireframes at an IOP of 12 kPa

Intrastromal Corneal Rings (ICRs)

The simplified cornea model was employed to study the effect of a 360 degree implanted ICR on the postoperative geometry of the cornea. In this study, the Myring implants by DiopTex, Linz Austria were used but any ICR could be easily modeled and studied. The Myring ICR is a circular shaped transparent PMMA implant with 5 to 8 mm diameter and a rectangular cross section with a constant width of 0.5 mm and incremental height from 0.15 to 0.30 mm in increments of 0.05 mm [161]. The rectangular cross section has a slight curvature of almost 8 mm at the top and bottom surfaces according to manufacturer specifications [162]. The selection of a specific ICR implant size for a patient depends on the topography of the patient's cornea and the extent of the preexisting optical ailment. Selecting the correct ICR is therefore challenging, and it is postulated that 3D FE modeling of the cornea with ICR implants can provide a valuable a priori insight into the effects of the ICR geometry and surgical conditions on the surgery outcomes.

The effect of ICR implants on the shape of the postoperative cornea is studied by utilizing the developed and validated simplified cornea model. The base model considered an ICR implant with 5 mm diameter and 0.3 mm thickness implanted in a pocket at 70% corneal depth with frictionless contact. While creating the ICR implanted cornea model, special attention was paid to accurately represent the displaced corneal tissue layers due to the insertion of the ICR implant in the cornea. The insertion of an ICR in the cornea causes the nearby stromal tissue layers to become slightly pre-stressed. However, in this static structural study, the overall effect of ICR as additional material (spacer element) was considered and the local effects of tissue pre-stressing were ignored. Due to the insertion of ICR in the cornea, the displaced corneal tissue layers leave space at the sides of the ICR implant and to model this aspect an approximate

semicircular pocket with diameter equal to the thickness of the ICR implant was created in the cornea model on the sides of the ICR as shown in Figure 4-14. Once the model was created, a mesh was generated as presented in Figure 4-14, zero normal displacement BCs were applied to the sides and bottom of the model (B, C, D loads) whereas an intraocular pressure (IOP) load of 3 kPa (load A) was applied to the model as shown in Figure 4-14. The generated mesh consisted of 6662 Solid 187 elements. Usage of hyperelastic corneal material properties rather than viscoelastic material properties entails that time dependent or step by step information is lost whereas, the FE model results would represent long term corneal deformation [144]. In an effort to promote computational convergence, a dense mesh and small sub-step size that captures the hyperelastic behavior were used.

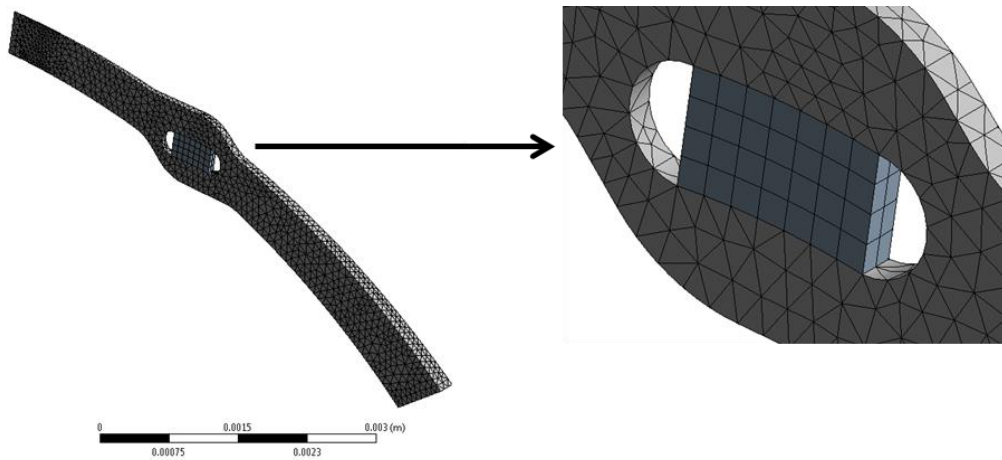


Figure 4-13: FEM model of cornea segment with pocket and ICR implant

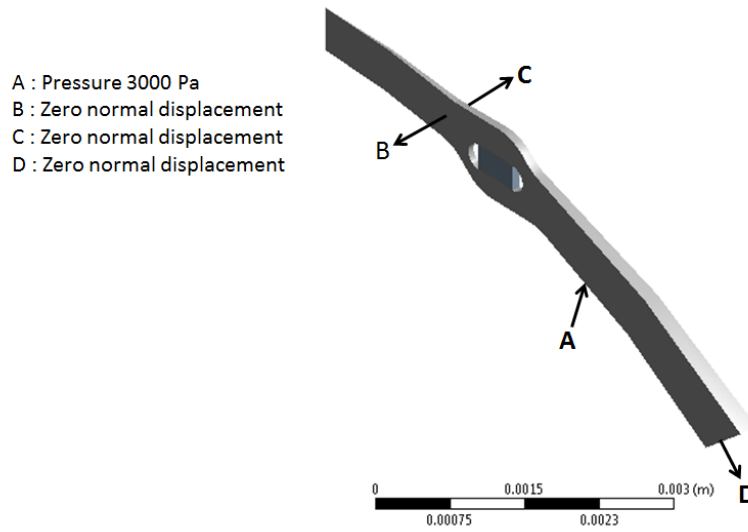


Figure 4-14: FEM model with loading and boundary conditions (BCs)

Results

The FE model results for a two degree axisymmetric cornea implanted with ICR demonstrate that the ICR implants provide structural support to the cornea and assist in rectifying myopia by reducing the apical position of the cornea from its initial location. Reduction in corneal apical deformation due to the implantation of an ICR entails that axial distance between the cornea and retina has decreased thus, the probability of light rays focusing on the retina increases leading to improvement in myopia. The biomechanical effect of ICR implantation on the corneal topography in the presented FE model can only be measured qualitatively by utilizing apical deformation of the cornea. A representative displacement result of the FE model highlighting the displacement regions is presented in Figure 4-15. The FE analysis results for an implanted ICR with 5 mm diameter and $(0.5 \times 0.3) \text{ mm}^2$ cross section produce a reduction in apical deformation of 0.0476 mm when compared with deformation results of a non ICR implanted cornea as shown in Table 4-1.



Figure 4-15: Representative FE model displacement results in meters of cornea segment with 5 mm diameter Myring with $(0.5 \times 0.3) \text{ mm}^2$ cross section

Table 4-1: Summary of FE model apical deformation displacement results

Without ICR (mm)	With ICR (mm)	Change in axial length (mm)
0. 438	0. 390	0. 048

Discussion

ICR implant thickness effects

The effect of variation in ICR implant thickness was studied with all other model parameters including material properties, implantation depth in the cornea (70%), diameter of corneal pocket (5 mm), ICR implant width (0.5 mm), and cornea dimensions kept constant. The thickness of the ICR implant was varied from 0.15 mm to 0.30 mm in increments of 0.05 mm. The results of variation in ICR thickness on the change in apical deformation of the cornea before and after implantation are shown in Figure 4-16. The results indicate that an increase in the thickness of the ICR implant is coupled with a marked decrease in axial length between the cornea and the retina. These results indicate that an increase in ICR thickness leads to commensurate improvement in myopia. An interesting phenomenon is observed at an ICR thickness of 0.2 mm where a

relative maximum is observed. The source of this relative maximum is unexplained and requires further investigation. Overall, the presented ICR thickness analysis is in qualitative agreement with clinical results published in open literature which highlight that an increase in ICR thickness leads to increased myopic rectification [3], [163]–[165].

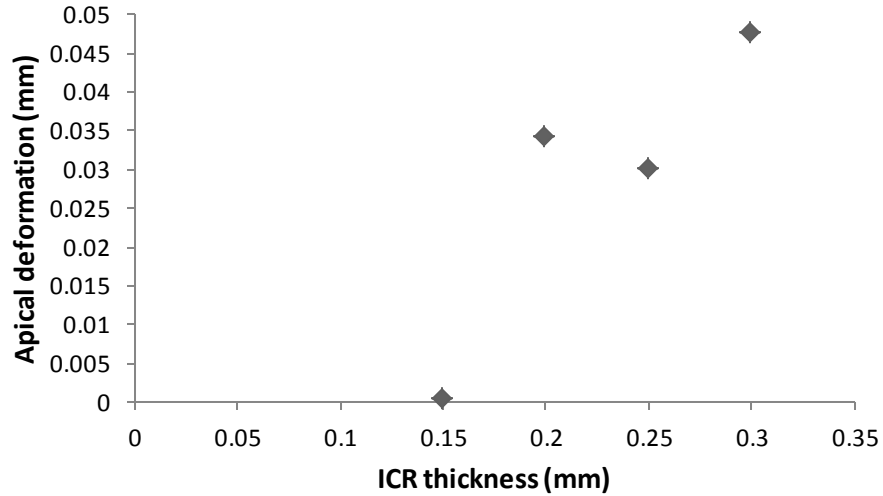


Figure 4-16: Change in corneal apical deformation (before and after ICR implantation) as function of ICR thickness

ICR implant diameter effect

The effect of variation in ICR implant diameter was studied with all other model parameters including material properties, implantation depth in the cornea (70%), ICR thickness (0.3 mm), ICR width (0.5 mm), and cornea dimensions kept constant. The diameter of the ICR implants was varied from 5 mm to 8 mm in increments of 0.5 mm. The results of variation in ICR diameter on the change in apical deformation of the cornea before and after implantation are presented in Figure 4-17.

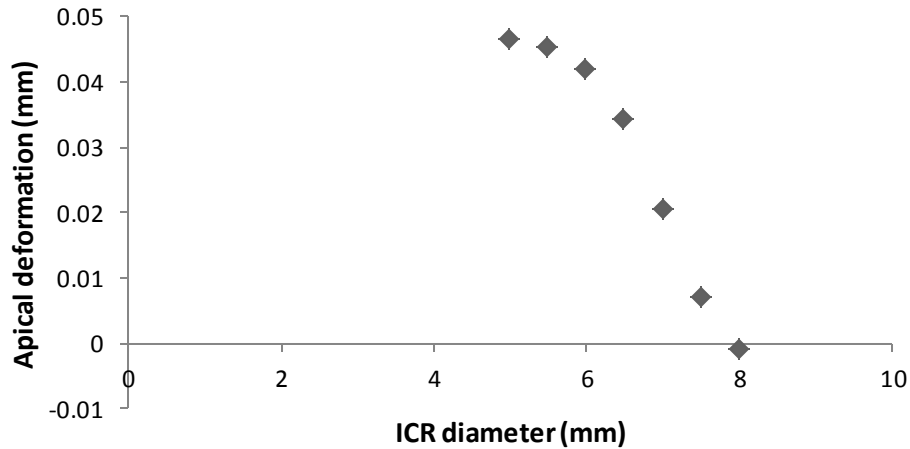


Figure 4-17: Change in corneal apical deformation (before and after ICR implantation) as function of ICR diameter

The results indicate that smaller diameter ICR implants result in a higher decrease in apical deformation (axial length) of the eye which results in increased rectification of myopia. An interesting observation is that, implantation of 8 mm diameter ICR results in an increase in axial length of the eye. This suggests that ICRs could also be utilized to rectify hyperopia (farsightedness). The presented FE model results suggest that a smaller ICR diameter leads to pronounced rectification of myopia which is in qualitative agreement with clinical results published in open literature which also highlight that smaller diameter ICRs yield higher myopic rectification [165]. Although, the FE model results and clinical studies promote the usage of a smaller diameter ICR for higher myopic correction, the optical zone and shape of the cornea of the patient eye must be considered because intersection of the ICR implant with the optical zone would lead to compromised visual results.

ICR implantation depth effect

The effect of variation in ICR implantation depth was studied with all other model parameters including material properties, ICR diameter (5 mm), corneal pocket diameter (5mm), ICR thickness (0.3 mm), ICR width (0.5 mm), and cornea dimensions kept constant. Implantation depth is defined as the corneal depth from the anterior end to the posterior end of the cornea. The ICR implantation depth was varied from 35% to 80% in increments of 5%. The results of variation in ICR implantation depth on the change in apical deformation of the cornea before and after implantation are shown in Figure 4-18.

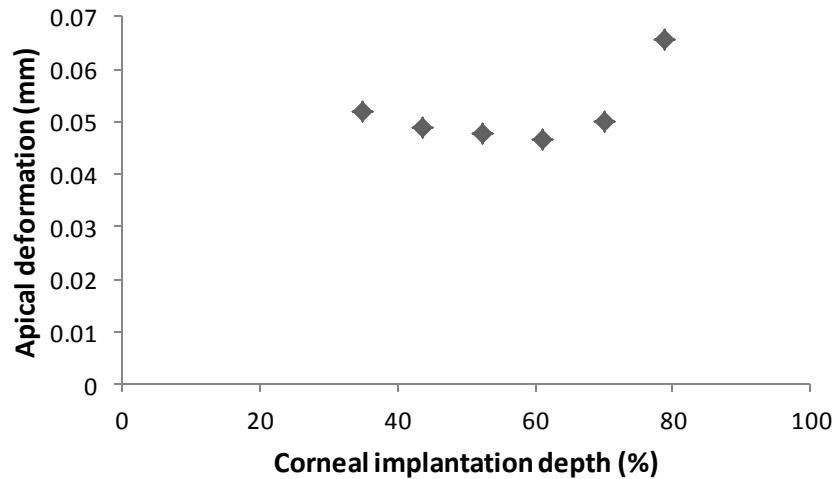


Figure 4-18: Change in corneal apical deformation (before and after ICR implantation) as function of ICR implantation depth

The results indicate that ICR implants have a similar effect on change in apical deformation for implantation depths between 40-75% of corneal thickness. Outside this region of corneal thickness, the change in apical deformation value increases. The predicted FE model results are in qualitative agreement with clinical experimental results available in open literature which suggest that ICR implantation in the corneal depth domain of 40-70% yield stable surgical outcomes [166]. An interesting observation in the

FE model results is that although a comparable/similar amount of corneal flattening is achieved even at a shallower corneal implantation depth e.g. 40%, yet higher ICR implantation depth is preferred since a deeper implanted ICR provides more biomechanical stability and longevity in postsurgical results. This is due to the fact that the cornea is always experiencing an intraocular pressure at the posterior end and an ICR implant near the anterior surface would be more susceptible to causing corneal tissue tearing.

Smaller diameter corneal pocket effect

The effect of variation in the diameter of corneal pocket was studied with all other model parameters including material properties, ICR diameter (5 mm), ICR thickness (0.3 mm), ICR width (0.5 mm), ICR implantation depth (70%), and cornea dimensions kept constant. The diameter of corneal pocket was decreased from 5.0 mm to 4.8 mm in steps of 0.05 mm. When a 5 mm diameter ICR was implanted, the results of variation in corneal pocket diameter on the change in apical deformation of the cornea before and after ICR implantation are shown in Figure 4-19. The FE model analysis results indicate a reduction in the apical deformation (axial length) of the cornea due to progressively smaller corneal pocket diameter for the ICR implant. The results of the presented FE model analysis demonstrate that reduction in corneal pocket diameter leads to myopic rectification. These results are in qualitative agreement with clinical study findings available in open literature that highlight the effectiveness of using smaller diameter corneal pockets for higher myopic rectification [3]. Albeit effective, smaller corneal pocket diameters for ICR implantation surgeries is usually not a preferred choice due to the application of excessive force by the ICR implant on the corneal tissue which can lead to undesirable effects such as waning of surgery effects over time. Since the pocket would enlarge and the ICR implant would lose a significant portion of its flattening force.

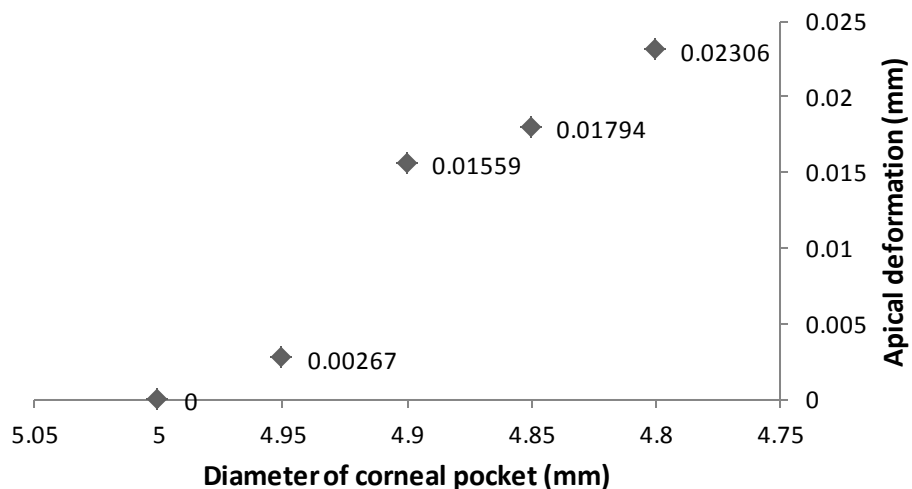


Figure 4-19: Change in corneal apical deformation (=5 mm value - smaller corneal pocket diameter value) as function of corneal pocket diameter

Sensitivity Analysis of the ICR implantation surgery control parameters

After analyzing the effect of different ICR implantation surgery control parameters on the apical deformation utilizing the developed FE models, a sensitivity analysis was performed to better understand the combined effects of the control parameters on the apical deformation. Design Expert (Minneapolis, MN) design of experiments (DOE) software package was utilized to perform the sensitivity analysis. The results of the sensitivity analysis are presented in Figure 4-20. The results highlight that apical deformation is more sensitive to ICR diameter as compared to ICR thickness, also apical deformation output is more sensitive to corneal pocket diameter as compared to ICR implantation depth. These results provide a qualitative mathematical relationship of the apical deformation as function of the control parameters, developed using simple linear regression model in the DOE software as presented in equation 4-4. Multiple linear regression model was considered but not pursued since the statistical significance level was below the considered significance level ($\alpha=0.05$).

$$D = 0.048 + 0.225It - 0.177Id - 0.00017IId + 0.165Cd \quad 4-4$$

Where D is the change in apical deformation, It is the ICR thickness, Id is the ICR diameter, IId is the ICR implantation depth, and Cd is the corneal pocket diameter. The presented equation provides a statistically significant relationship between apical deformation and the ICR implantation control parameters (in the ranges considered) because the presented equation has a P value of 0.0206 which is smaller than the considered significance level ($\alpha=0.05$).

The developed equation highlights that change in corneal apical deformation is strongly affected by change in ICR thickness, ICR diameter and diameter of corneal pocket. Out of these three parameters ICR thickness has the highest coefficient. But since the ICR diameter can be varied in a significantly larger range (3 mm) as compared to the ICR thickness and corneal pocket diameter. Both of which can only be varied in relatively smaller ranges (0.3 to 0.5 mm). Hence, ICR diameter is the control parameter that can have the highest impact on the apical deformation results and therefore myopic rectification.

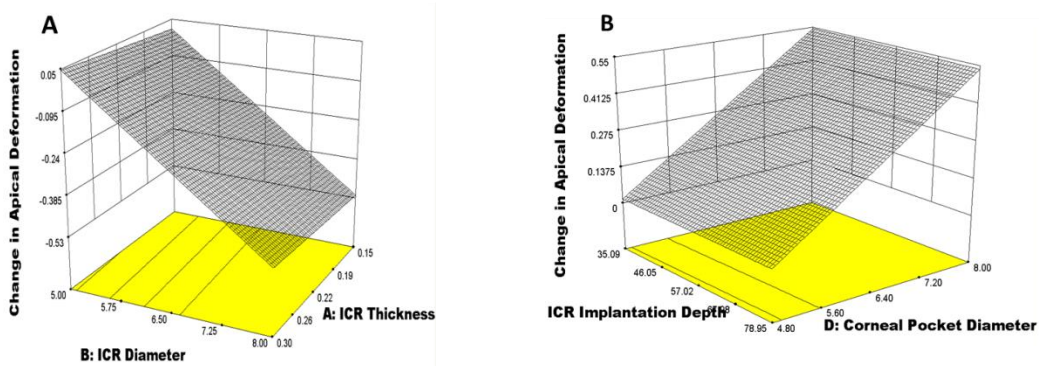


Figure 4-20: (A) Apical deformation as function of ICR diameter and ICR thickness (B) Apical deformation as function of ICR implantation depth and corneal pocket diameter

Conclusions

This chapter presented a 3D axisymmetric FE model of the cornea and its application to predict the postsurgical shape of the cornea after implantation of ICR for myopic rectification. It begins by explaining the importance of radius of corneal curvature and corneal apical deformation (axial length) of the eye in myopia. It presented the development of full eye and simplified cornea FE models the results of which are compared with published experimental apical deformation results to validate the models and procedures. The developed models are then compared with each other and published experimental results available in open literature to evaluate their relative merits. The comparison study revealed the limitation of the simplified eye model in evaluating radius of corneal curvature but not apical deformation.

Once the modeling procedures and output parameters had been determined, the computationally efficient and simplified cornea FE model was modified to accommodate an implanted ICR to study its effect on the corneal topography. Changes in corneal topography were evaluated by considering the change in apical deformation as a parameter due to the roller support BC utilized in the simplified cornea FE model. The developed FE modelling procedures were utilized to study the effect of changes in control parameters such as ICR thickness, ICR diameter, ICR implantation depth and diameter of corneal pocket on myopic rectification. The analysis results demonstrated dependency of myopic rectification on the control parameters. The analysis results suggest that smaller diameter ICR implants lead to pronounced flattening/rectification in a myopic eye. The ICR implant thickness analysis suggests that ICRs with thicker cross sections lead to pronounced rectification of myopia. The ICR implantation depth analysis results demonstrated that ICRs implanted at 40-75% corneal depth provide steady myopic rectification. In addition, a smaller corneal pocket for ICR implant analysis revealed that

smaller corneal pockets lead to a significant increase in rectification of myopic effects. Overall, the FE model based study of ICR implantation and control parameter analysis qualitatively agreed with published clinical studies. Lastly, a sensitivity analysis was conducted to evaluate the relative impact of the control parameters on the apical deformation utilizing simple linear regression. The developed equation highlighted that ICR thickness has the highest sensitivity but ICR diameter due to its higher range has the most pronounced effect on the change in apical deformation results. The presented modeling procedures can be further utilized to improve our understanding of the ICR implant surgery and the knowledge gained can be utilized to formulate the design for customized personalized implants that could improve ICR surgical outcomes.

Chapter 5

Descemet's Stripping Automated Endothelial Keratoplasty (DSAEK)

Allograft Insertion Devices: A Review

Introduction

After corneal refractive surgeries such as LASIK and ICR implantation, attention was directed towards partial thickness corneal transplant surgery called Descemet's stripping automated endothelial keratoplasty (DSAEK). The cornea is the outermost transparent part of the eye which covers the iris, pupil and anterior chamber (AC). The cornea comprises of five layers, namely: epithelium, Bowman's membrane, stroma, Descemet's membrane and endothelium [49], [167]. Each layer of the cornea has a designated function as already explained in chapter 2. This work will focus on the innermost layer i.e. the endothelium, an extremely thin layer responsible for keeping the cornea in its dehydrated state. Proper operation of the endothelial layer is vital for maintaining transparency of the cornea [168], [169]. The endothelial cells act as small pumps which suck fluid from the corneal stroma and pump it back to the AC hence maintaining corneal transparency. These cells regenerate at an extremely slow rate as compared to cell decay, since they are arrested in the G1 cell cycle [29], [30], therefore cell count decreases rapidly until the age of twenty five after which the rate of decay slows down [170], [171]. For clear vision, the endothelial cell count should stay above 500 cells/mm²; however diseases such as Fuchs' dystrophy, pseudophakic or aphakic bullous keratopathy, posterior polymorphous dystrophy, iridocorneal endothelial syndrome, endothelial decompensation and failed Penetrating Keratoplasty (PK) surgery, result in a decrease in endothelial cell count and eventually an endothelial layer transplant becomes necessary [172]. Numerous surgeries have been developed through

the years for endothelial layer transplant. These surgeries can be divided into two major sections, namely: full thickness keratoplasty and partial thickness keratoplasty/endothelial keratoplasty (EK) as shown in Figure 5-1 and Figure 5-2. Full thickness keratoplasty is widely used in the form of penetrating keratoplasty. Partial thickness keratoplasty is seen in the form of deep lamellar endothelial keratoplasty (DLEK), Descemet's stripping automated endothelial keratoplasty (DSAEK), and Descemet's membrane endothelial keratoplasty (DMEK). However, among all these procedures PK and DSAEK are the most popular choices among surgeons [173], [174].

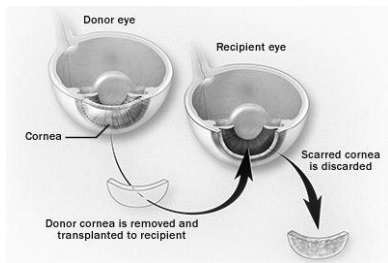


Figure 5-1: Full thickness penetrating keratoplasty (PK) [175]



Figure 5-2: Partial thickness endothelial keratoplasty (EK) [176]

In full thickness keratoplasty (penetrating keratoplasty), the complete donor cornea is removed and transplanted in the eye of the patient. In partial thickness keratoplasty, however, the objective is to replace only the diseased layer of the cornea. Which is usually just the endothelial layer, an extremely thin (10 μm) layer [177]. Therefore, cutting a corneal graft that comprises of just the endothelial layer is extremely challenging, hence corneal grafts of higher thickness have traditionally been used in partial thickness keratoplasty procedures. Due to advancements in cutting technology the thickness of the corneal graft has gradually decreased over the years, as highlighted in Figure 5-3.

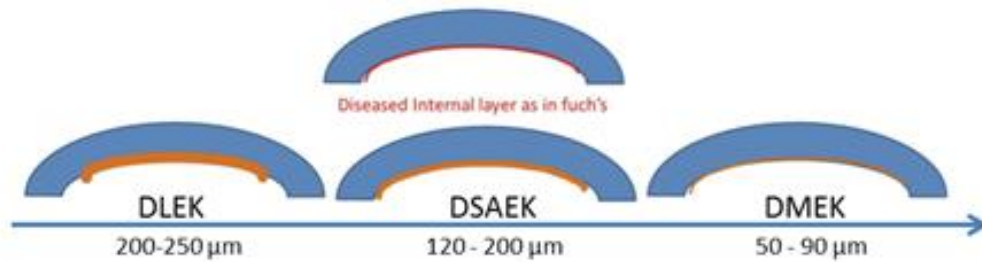


Figure 5-3: Types of partial thickness keratoplasty procedures [173]

In 2013, the number of corneal tissues used for transplant/keratoplasty in US alone was 72,736 [4]. This number was largely shared between penetrating keratoplasty (36,998) and endothelial keratoplasty (27,298) procedures. However, EK is catching up very quickly, showing approximately 12 percent increase from previous years and this number is expected to increase every year with improvements in health care and life expectancy [173], [178]. DSAEK is a type of keratoplasty that has become the gold standard in endothelial keratoplasty in recent years. Although this procedure is effective, fairly reliable and shows low rates of complications, it has continued to evolve in the last few years to achieve better results [179].

DSAEK is a type of selective corneal transplant procedure wherein the diseased endothelium and Descemet's membrane of a patient is replaced with a donor excised posterior allograft approximately 130 to 240 μm in thickness. This allograft comprises of the posterior stromal layer, healthy Descemet's membrane and the endothelium. This donor allograft once trephined, is inserted in the AC of the patient through a side incision created in the cornea, limbus or sclera. The advantages of EK are small incision size, structurally stronger cornea, requirement of few to no sutures, reduced operative time, lower risk of allograft rejection, economy, stability of refraction, and swift visual rehabilitation [180]–[190]. However, the disadvantages of DSAEK include significant initial loss in endothelial cells density (ECD), especially in the case of patients who have

shallow anterior chambers and high vitreous pressures. This intraoperative ECD loss occurs partially during microkeratome cutting of donor allografts, handling of corneal allograft and air bubble insertion in the AC [191], [192]. However, the major ECD loss occurs during allograft insertion and subsequent unfolding in the AC [172]. This loss in ECD is a major issue since it invariably leads to problems such as primary allograft failure and corneal opacity [187], [193], [194], hence it has a direct bearing on the success of the procedure [192], [194]. In addition to ECD loss, AC collapse is another frequent issue that depends on the incision size, allograft insertion mechanism and AC maintainer [195]. Since most of the issues affecting DSAEK outcomes stem from the allograft insertion technique, recently attention has been directed towards developing allograft insertion devices that aim to alleviate the trauma experienced by the allograft during the insertion and unfolding processes, in order to minimize endothelial cell loss and prevent AC collapse.

This chapter aims to compare the designs of various corneal inserters and discusses the performance of these insertion devices by reviewing and comparing their construction/design and the results of clinical studies conducted with them. Performance factors considered and analyzed are ECD loss percentage, AC collapse probability, ease of use, number of hands required by the surgeon for usage, required incision size, reusability and economy. Clinical studies conducted on the injectors were compared, although these studies were performed by different surgeons the comparison is still valid since ECD loss and success of the surgery are more dependent on the technique and devices used rather than the expertise of the surgeons performing them [196]. Another factor of variability was the difference in storage times of the donor allografts that were utilized in different clinical studies. However, a recent study has proven that allograft storage time is of little consequence when it comes to the ECD loss or the success of the

DSAEK surgery [197]. This literature review will provide helpful information about the current state of the art of the DSAEK inserters.

Endothelial allograft insertion devices

Traditionally forceps have been utilized for allograft insertion, however recently the need for corneal inserters was felt because corneal allograft inserted via forceps experiences more trauma resulting in more ECD loss. Thus, all the available inserters have been designed with the primary objective to protect the allograft from folding and reduce incision compression pressure (ICP). Therefore, almost all the inserters have shown better ECD results in clinical trials as compared with forceps [198]–[203]. Allografts inserted via forceps display a definite pattern of trauma such as parallel bands and orthogonal wrinkles due to the folding and compression of the tissue during insertion through the incision [187]. The initial trauma experienced by the allograft is even greater in patients with shallow anterior chambers, making allograft insertion and unfolding more challenging [204]. Reduction in initial endothelial allograft trauma was the main reason considered while developing a secure method in which the allograft is protected from incision compression pressure and folding effects. The insertion devices that have been developed can be broadly categorized into two groups based on their injection mechanism; namely pull through design (glides) and push in design (injector). Most of these devices require an incision size in the range of 3 to 5 mm to inject a lamellar allograft with a diameter greater than 8 mm and thickness of 130 to 240 μm [173]. Three glides and three injectors that are commercially available and extensively used will be introduced, discussed and compared (Table 5-1). The glides are the Endoglide, Macaluso inserter and Busin glide whereas, the injectors are the Endoserter, Endoshield/Endoinjector and Neusidl injector.

Endothelial glides

To operate endothelial glides, a corneal allograft is pulled inside the AC from the far side using forceps. This is a two hand technique with the inherent advantage that the allograft always unfolds in the correct orientation inside the AC. Besides, the allograft undergoes considerably less trauma during insertion as compared to insertion using forceps. Allograft displacement however, is possible due to AC maintainer interference, and high intra ocular pressure conditions can lead to AC collapse which becomes difficult to handle since glides require the use of both hands by the surgeon. Endothelial glides are available in different shapes and designs depending on the manufacturer, some of these glides have already received FDA clearance while others are still waiting.

Busin Glide

The Busin glide is a 126 mm long all metallic, FDA approved, reusable corneal allograft insertion device which was invented by Kobayashi and Busin. It consists of a handle with a pan at the end. The allograft is placed endothelial side up inside the marked space of the pan. This marked space is 8 mm in diameter and it aids in proper centering of the allograft. Once the allograft is in position, grasping forceps are used to bring the allograft towards the peripheral opening of the device. While proceeding towards the opening, the allograft rolls and takes the shape of the peripheral tip of the device. Having the allograft at the tip, aids in grasping it once the tip of the Busin glide is inside the AC. This non-tapered/elliptical peripheral opening of the Busin glide is inserted into the AC through a 5.0 mm incision in the eye (Figure 5-4) [205]. Note that at all times during this procedure the AC pressure is maintained via an AC maintainer. The opening of the Busin glide has a semicircular cutout which aids in grasping the allograft once inside the AC. The elliptical tip of the Busin glide protects the allograft from incision compression pressure and prevents folding of the allograft as well. The maximum

diameter of the allograft that the Busin glide can hold without overlap is 8 mm. Many surgeons place the Busin glide slightly outside the incision, to avoid AC collapse; however, this exposes the allograft to ICP and leads to endothelial trauma. Other surgeons insert the glide inside the incision to save the allograft from ICP; however, this increases the possibility of AC collapse, which in turn can lead to other complications [206]. The performance of this device is well documented with an ECD loss between 20 and 47.5% (6 months postoperative) [198], [199], [207], [208].



Figure 5-4: Busin Glide inserter [205]

Macaluso inserter

The Macaluso inserter as shown in Figure 5-5 is an all metallic reusable glide that takes its name from its inventor Claudio Macaluso [209]. This device is being used in Europe, however it has not yet been approved by the FDA for use in the USA. The Macaluso inserter employs a close chamber technique which aids in maintaining a well formed anterior chamber [210]. The allograft is placed endothelial side up on the concave winglet and some viscoelastic liquid is applied, the winglet has a circular region marked for aiding in centration of the allograft. The allograft is then grasped with forceps and pulled towards the opening of the insertion device. While proceeding towards the tip, the allograft rolls and conforms to the shape of the device tip. Once the allograft is in position at the tip, a plunger is used to seal the allograft inside the tip so that the allograft and cornea medium are confined in a closed space. The peripheral opening of the device has

a tapered elliptical shape with a 'V' shaped cutout to provide easier access for 23g coaxial grasping forceps. A 4.2 mm incision is usually recommended when using this device in DSAEK procedures. Also, at all times during the insertion, an anterior chamber maintainer is employed to maintain the shape of the AC. The maximum diameter of the donor allograft that can be held inside the Macaluso inserter is 8 to 8.5 mm, according to the manufacturer. However, what sets this inserter apart from other glides is the provision of a push plunger that seals the system from the environment. Hence, when the device is inserted inside the AC for allograft injection, AC and the inserter act as one sealed system, thus allowing the AC to remain stable. The metallic body of the Macaluso inserter makes it non transparent, however it can be sterilized and reused. There is not a lot of information available in the open published literature that discusses the clinical performance of this device. Therefore, more research needs to be conducted to assess the postoperative performance of this device.

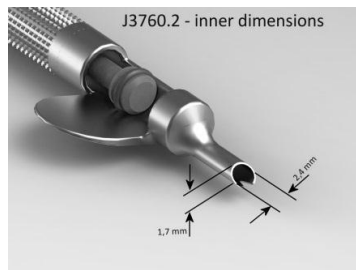


Figure 5-5: Macaluso endothelial inserter [211]

Tan Endoglide

The Tan Endoglide is an FDA approved, transparent, disposable endothelial allograft inserter invented by Donald Tan. It consists of a preparation base, glide cartridge and glide introducer (Figure 5-6). The allograft is placed endothelial side up on the Endoglide cartridge which is first slotted into the preparation base and some lubricating liquid is applied. Grasping forceps are introduced from the tip of the cartridge and the

endothelial allograft is pulled inside the cartridge. As the allograft is pulled towards the tip of the cartridge it takes the shape of the tip which induces a 'double coil' configuration shape to the endothelial allograft. Once the allograft is at the tip, the Endoglide introducer is connected to the back of the cartridge, sealing the back end in the process. The Endoglide is then flipped and inserted inside the AC through a 4.0 to 4.5 mm scleral or corneal incision [212], with the AC maintainer already inside the anterior chamber. Once the Endoglide is inside the AC, it seals it and creates a closed system. Since, it prevents fluid from flowing out through the incision or the glide itself, once the glide is in place the grasping forceps are introduced inside the AC from the opposite side and the allograft is gently pulled inside the AC. The tip of the Endoglide is oval in shape and can hold an allograft up to 250 µm in thickness. However, what sets the Endoglide apart is its 'double coil' tip shape which enables this device to use space more efficiently hence it enables the insertion of a larger diameter allograft through a relatively smaller incision. Various DSAEK clinical studies have been conducted using the Endoglide for allograft insertion and most of them show a decrease in ECD loss as compared to forceps insertion. The mean ECD loss is reported to be in the range of 13 to 26% (six months postoperative) [200], [202], [206].



Figure 5-6: Tan Endoglide [202]

Endothelial allograft injectors

To operate endothelial injectors, a corneal allograft is inserted in the AC using a pushing mechanism. These are usually single hand operated devices in which the allograft undergoes considerably less trauma during insertion as compared to using insertion forceps [199]. Some injectors have the added advantage of inbuilt capability to maintain the anterior chamber pressure hence an external AC maintainer is not required. The injector body is usually filled or coated with lubricating liquid before the allograft is inserted into the device. The inserted allograft takes the shape of the injector tip as it slides towards the opening. The lubricating liquid helps in reducing friction and protects the allograft from damage. Injectors are available in different shapes and designs depending on the manufacturer, some of these injectors have already received FDA clearance while others are still waiting.

Neusidl corneal inserter

This device is named after its inventor William B Neusidl. It is an irrigation incorporated, non-transparent, disposable corneal inserter that is FDA approved (Figure 5-7) [213].

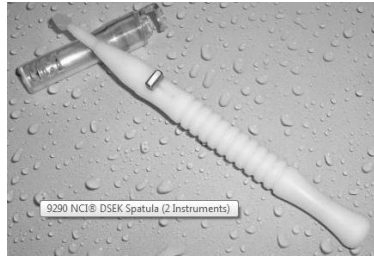


Figure 5-7: Neusidl Injector [214]

It consists of a body with a flexible platform upfront where the allograft is placed endothelial side up, once the surface has been lubricated [214]. The flexible platform can hold 8 to 8.5 mm allografts and ensures the delivery of the allograft is in the correct orientation, therefore eliminating the need for marking the stromal side of the allograft. A lever is used to extend the flexible surface, the allograft is placed on this surface and subsequently the lever is used to retract the flexible surface along with the allograft inside the injector. While moving inside the tapered elliptical opening of the device, the allograft conforms to the shape of the inner wall of the elliptical tip, while at all times avoiding touching or folding the endothelium. Once the allograft is securely retracted inside, the irrigation is attached and tested. The injector is then rotated such that it is oriented bevel down. In this orientation, the injector is inserted inside the AC through a 5.0 to 5.50 mm incision [201], the bevel down orientation aids in unfolding of the allograft inside the AC. A surgical stop is provided in the device which not only provides better sealing of the wound but also acts as an indicator for the surgeon that the recommended insertion has been achieved inside the AC. This however is a slight generalization since AC dimensions of patients vary slightly. During insertion of the allograft, the elliptical tip of the device protects the allograft from incision compression pressure and the irrigation pressure ensures a deep chamber. Having a deep chamber is essential since a deep chamber means more space for the allograft to unfold which in turn means that the

allograft will experience less trauma [215]. The irrigation provision in the Neusidl inserter is compatible with the standard cataract irrigation equipment hence an AC maintainer is not required. Various DSAEK clinical studies have been conducted using the Neusidl inserter for allograft insertion and most of them show a comparable or decrease in ECD loss as compared to insertion forceps. The mean ECD loss (six month postoperative) is in the range of 13 to 33% [216]. However, some surgeons have highlighted that the allograft sometimes sticks to the platform and requires shaking of the device to get it off the platform [201].

Endoinjector

Previously known as the Endoshield, the Endoinjector was invented by Yichieh Shiuey. It is a non-transparent, single use corneal allograft inserter which has the European CE mark approval and is awaiting FDA approval in the USA [217]. It consists of an injector body, injector cartridge and a foam tip plunger (Figure 5-8). The injector cartridge consists of a central ridge in the cartridge lumen which guides the allograft to form a double coil as the allograft is advanced, therefore preventing allograft rotation in the process (Figure 5-8). The balanced salt solution (BSS) soaked allograft is placed endothelial side up inside the loading area and fluid propulsion is used to guide the allograft forward to the beveled cartridge tip. The Endoinjector has been designed to atraumatically deliver 8 to 9 mm allografts inside the AC in the correct orientation [217]. Once the allograft is placed in the loading area and the wings of the cartridge are closed, the cartridge is loaded in the injector body and the wings are rotated clockwise for a right handed surgeon and vice versa. However, before the cartridge is loaded onto the injector body, Healon and BSS are used to plug and fill the cartridge in order to make the device act like a fluid chamber, thus making it a multi-step process. Once the cartridge is ready and loaded on the injector body, pressure is applied to the thumb rest to move the

allograft forward towards the end of the cartridge. Once the allograft is at the tip of the cartridge, an AC maintainer is inserted inside the AC. The Endoinjector is then rotated bevel down and inserted inside the AC through a 3.2 mm corneal incision, this bevel orientation aids in unfolding of the allograft inside the AC. During insertion of the allograft the Endoinjector protects the allograft from incision compression pressure and the AC maintainer ensures a deep chamber. There are few clinical studies reported in the open literature that utilize the Endoinjector for corneal allograft insertion in DSAEK. However, one study found the ECD loss to be 13% [217]. More results of clinical trials need to be published in open literature using this device so that the postoperative ECD performance of this device can be assessed and compared with other injectors.

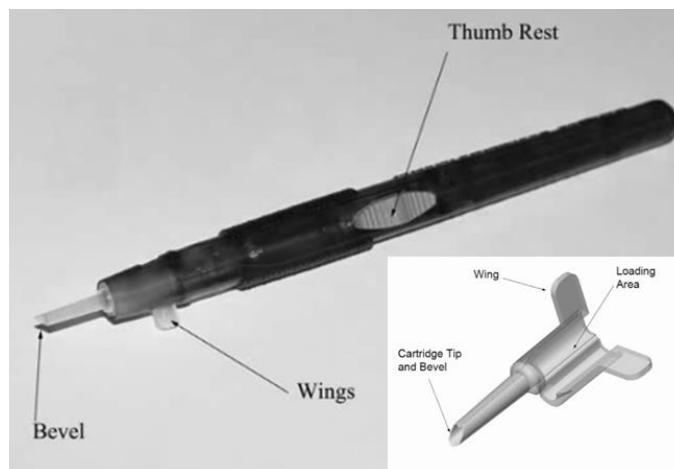


Figure 5-8: Endoinjector [217]

Endoserter

The Endoserter is an endothelial allograft insertion device invented by Keith Walter. It is an irrigation incorporated, non-transparent, disposable corneal inserter that is FDA approved (Figure 5-9) [218]. It consists of a flexible platform where the allograft is placed endothelial side up, once the device has been flushed with BSS by connecting the irrigation tubing to the lower end connector of the Endoserter [219]. This flexible platform

can accommodate allografts smaller than or equal to 8.5 mm in diameter and 175 μm in central thickness and ensures the delivery of the allograft is in the correct orientation. A rotating wheel is used to retract the allograft carrier inside the injector. While moving inside the tip of the injector the allograft conforms to the shape of the inner wall of the beveled tip, while at all times avoiding touching or folding the endothelium. The injector is then rotated bevel down and in this orientation the Endoserter is inserted inside the AC through a 4.0 mm incision. This bevel down orientation aids in unfolding of the allograft inside the AC. During insertion of the allograft the Endoserter protects the allograft from incision compression pressure and the irrigation pressure ensures a deep chamber. The irrigation provision in the Endoserter is compatible with standard cataract irrigation equipment. A recent DSAEK clinical study conducted using the Endoserter reported a mean ECD loss of 29% (six months postoperative) [201]. However, more results of clinical studies/trials need to be published in open literature using this device so that its postoperative ECD performance can be fully assessed.



Figure 5-9: Endoserter [219]

Discussion and Conclusions

Descemet's stripping automated endothelial keratoplasty (DSAEK) is an evolving procedure yet it has already demonstrated many advantages over traditional Penetrating Keratoplasty. Hence, it is gradually becoming the procedure of choice among surgeons.

Some challenges regarding its implementation still exist, which are being addressed to some extent with the use of endothelial inserters, since forceps have some inherent limitations. Using forceps is a simple technique, however forceps apply excessive pressure at the place of contact and they do not protect the allograft from incision compression pressure, which leads to higher postoperative ECD loss. In this chapter, six commercially available inserters were reviewed and their inherent advantages and limitations were discussed. Through this review, it can be safely concluded that each inserter has its own advantages and limitations regarding ECD loss percentage, AC collapse probability, ease of use, number of hands required by the surgeon for usage, required incision size, reusability and economy as presented in Table 5-1. However, the primary objective of every inserter is to reduce the amount of trauma experienced by the allograft in order to reduce the ECD loss sustained during the surgical procedure. All corneal inserters discussed in this work showed better postoperative ECD data as compared to traditional forceps insertion. However, among the six inserters discussed: Endoglide, Endoinjector and Neusidl corneal inserter seemed to show better ECD results according to published data.

Apart from ECD loss, another prominent issue faced by surgeons is flipping of the donor allograft inside the anterior chamber. Since visibility is low inside the AC, flipping of donor allograft poses a huge complication which can result in failure of the DSAEK procedure. All the six inserters discussed in the work do a very good job at this but since grasping forceps are used to insert donor allografts in glides, therefore glides have an almost perfect chance of donor allograft unfolding in the correct orientation.

The postoperative ECD comparison results presented in this review provide a valuable overview of the commercially available DSAEK inserters and present a much needed perspective regarding DSAEK allograft inserters. However, the ECD results

reviewed and compared in this work were acquired from clinical studies which involved patients from different demographics and utilized different mechanisms to measure postoperative ECD e.g. specular microscopy and vital dye staining with use of graphic software, therefore the comparisons made between the inserters lack a common denominator. To accurately compare the ECD loss efficiency of these inserters, all six of them should be used in a single study in the future. Such a study will be able to act as a bench mark regarding inserter comparison and will aid in identification of the inserter that imparts the least trauma to the allograft. Further, the trauma patterns can be studied and correlated with allograft insertion parameters such as orientation angle and insertion speed etc. so that technique of usage can be refined and standardized. As yet, most clinical studies have not involved more than two DSAEK allograft inserters.

Apart from ECD loss prevention and allograft unfolding orientation, other factors of note in DSAEK are AC maintainer requirement and incision size. Both of these factors are important and somewhat correlated, since a bigger incision size leads to hypotony in the AC which invariably leads to AC collapse and allograft failure. Whereas, a smaller incision entails reduced probability of AC collapse and requires less sutures thus reducing surgery time. Among the inserters reviewed, Endoinjector requires the smallest incision size of 3.2 mm. All of the inserters require an AC maintainer, except the Neusid inserter and Endoserter. An inserter that does not require an AC maintainer is a definite advantage, however having a smaller incision size can be a two edged sword since a smaller incision means less or no sutures and less chance of AC collapse, while at the same time a small incision correlates with more ECD loss [195], [208]. DSAEK is a relatively new and evolving surgical procedure with a good success rate. However, there is still room for improvement in this procedure to achieve better postoperative visual outcomes. The inserters reviewed in this work have their own advantages and limitations,

therefore further studies/research on the efficacy and these inserters should be performed. Using the results/feedback from these studies an effort can be made to improve the designs of the existing inserters and if possible new inserters can be developed that have the capability to address the identified issues.

Table 5-1: Characteristics of corneal inserters

Name	Company	Inventor	FDA Approved	Incision Size (mm)	Disposable /Reusable	Allograft Insertion technique	AC maintainer required	ECD loss (%) (6 months postoperative)
Kobayashi Busin Glide	Asico (Westmont, IL, USA)	Kobayashi & Busin	Yes	5.0	Reusable	pull in and pull out	Yes	20-47.5
Macaluso Inserter	E Janach (Como, Italy)	Claudio Macaluso	No	4.2	Reusable	pull in and pull out	Yes	Not reported
Endoglide	Angiotech (Vancouver, BC, Canada)	Donald Tan	Yes	4.0-4.5	Disposable	pull in and pull out	Yes	13-26
Neusidl corneal inserter	Fischer surgical (Arnold, MO, USA)	William B. Neusidl	Yes	5.0-5.5	Disposable	Pull in and push out (two way)	No	13-33
Endoinjector	Keramed (San Jose, CA, USA)	Yichieh Shiuey	No	3.2	Disposable	place in and push out (one way)	Yes	13
Endoserter	Ocular Systems (Winston-Salem, NC, USA)	Keith A. Walter	Yes	4.0	Disposable	Pull in and push out (two way)	No	26-31

Chapter 6

Finite Element Analysis of Descemet's Stripping Automated Endothelial Keratoplasty (DSAEK) Surgery Allograft to Predict Endothelial Cell Loss

Introduction

The literature review presented in chapter 5 on the existing commercially available DSAEK allograft inserters identified the advantages and limitations of the DSAEK surgical procedure. The review discussed the importance of allograft inserters in improving surgical outcomes as compared to forceps insertion and also how the inserters compare among themselves. Despite the success of the available DSAEK allograft inserters, some areas of improvement still exist and as such there is a definite need to better understand the surgery in an effort to design allograft inserters that will improve postsurgical outcomes.

DSAEK has made significant progress during the last few years, yet some areas of improvement are still present such as reducing postoperative endothelial cell (EC) loss, preventing anterior chamber (AC) collapse, simplifying the surgery to reduce the learning curve and reducing the surgery time [193]–[195]. These are major challenges being addressed to some extent with the use of surgical instruments such as endothelial inserters, since forceps, the traditionally used instruments have some inherent disadvantages [192].

Endothelial cell loss in DSAEK surgery takes place due to two major reasons, surgical trauma and mechanical trauma. Surgical trauma occurs when the endothelial cells on the allograft come in contact with another surface or surgical instrument [5]. Endothelial cells are very sensitive, and if proper care is not taken during the harvesting, folding, insertion and unfolding processes EC loss will take place. The other aspect that

leads to EC loss is mechanical trauma which exists due to bending stresses induced on the allograft at the folding crease possibly while in the folded state inside the injector/forceps tip before insertion in the AC [187], [220], [221]. Even though reducing the bending stresses is desirable, it can act as a two edged sword since extremely low bending stresses would make it difficult for the allograft to properly unfold inside the AC and this could inadvertently affect the DSAEK surgery outcomes.

The research presented in this chapter aims to correlate the post DSAEK surgery EC loss experienced by the allograft with mechanical stresses induced in the allograft during folding and insertion processes by employing finite element (FE) tools in a computationally efficient manner. It begins by introducing the allograft structure, composition, material properties and the role of material modeling in the usage of hyperelastic material properties in the presented FE model. It discusses the boundary conditions and loading procedure applied to the allograft in an effort to deform the allograft such that it replicates the shape it takes in commercially available injectors namely taco, forceps and double coil configurations [153]. Once the allograft assumes the proper deformed shape, the resulting stress distribution is evaluated and analyzed. The results of the FE model are compared and verified with clinical results published in the open literature to understand and develop the correlation between cell loss and stress distribution. The developed FE modeling procedures can be further utilized to predict EC loss in any given injector tip shape. In addition, the developed FE modeling procedures can be employed in the design of novel devices to control the location and magnitude of stress trauma on the donor allograft in an effort to decrease EC loss experienced by the allograft due to mechanical trauma and to facilitate natural allograft unfolding inside the AC. Thereby, improving the probability of success of the DSAEK surgical procedure.

Materials and Methods

As explained in chapter 3 the DSAEK allograft consists of the posterior stromal layer, Descemet's membrane (DM), and endothelium [222]. Among these three layers, the stromal layer is structurally dominant due to its higher stiffness and higher volumetric contribution in the DSAEK allograft [154]. The stromal layer possesses higher stiffness since it is composed of interlaced collagen lamellae in an extracellular matrix (ECM) interspersed with keratocytes [223]. Due to the collagenous nature of the stroma it demonstrates stress stiffening behavior as explained in chapter 4 which can be explained from the observation that at high strains, the corneal tissue activates its reinforcing constituents such as collagen fibrils to provide the necessary strength.

The mechanical properties of stromal layer of the cornea have been extensively studied over the years, and various research groups have been working on obtaining the exact material properties of the cornea by employing different characterization methods such as, uniaxial strip extensometry, inflation techniques, and indentation tests [35], [155], [224]–[226]. It is widely acknowledged today that the stroma behaves as an anisotropic nonlinear viscoelastic material [17], [141], [142], [227]. In this research, isotropic hyperelastic material properties were considered in the FE model for the stromal layer to improve computational efficiency. Moreover, isotropic hyperelastic material properties have been previously used to model the cornea by Kling and Marcos (2013) [146], Elsheikh et al. (2007) [156] and Elsheikh et al. (2010) [157]. In this work, the stromal material properties published by Elsheikh et al. (2007) [156] were utilized and are graphically presented in Figure 6-1. The presented material properties demonstrate stress stiffening behavior which is expected from collagenous tissue such as the corneal stroma. However, since the allograft used in the DSAEK surgery is composed of only the posterior part of the stroma, the stiffness of the stroma was reduced to 39.3% of its

original value according to the study by Dias et al. [228]. The method of volume fraction was utilized to modify the mechanical properties of the complete cornea to define mechanical properties of posterior stroma [229]. The method of volume fraction postulates that total stiffness of any composite material is the sum of the stiffness of the constituting materials multiplied by their fractional volumetric contribution.

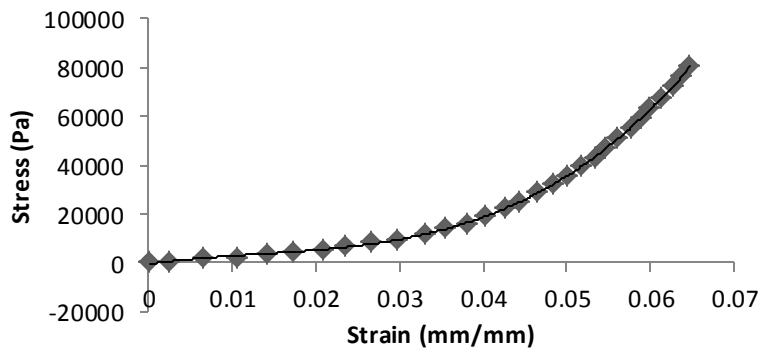


Figure 6-1: Stress strain material properties of the porcine cornea [156]

Hyperelastic materials follow a nonlinear yet elastic stress-strain relationship which is independent of strain rate. The behavior of a hyperelastic material is usually described by a polynomial whose coefficients are estimated based on experimental data. Among the various material models available, Mooney Rivlin and Ogden Material model have been frequently utilized by research teams to model the cornea with reasonable accuracy [139], [146], [230]. Likewise, in the presented research, the second order Ogden material model was selected since it provided the best curve fit for the material properties of posterior stroma/allograft.

Corneal Endothelium and its function

The endothelial layer is a monolayer of cells on the posterior corneal surface that forms a barrier between the cornea and the aqueous humor. The endothelial layer consists of polygonal cells, primarily hexagonal in shape with each having a dimension of

18 to 20 μm width by 5 μm (thickness). The channels between the endothelial cells transport fluid from the stroma into the anterior chamber. This movement of fluid counters a natural tendency for the stroma to swell and is necessary to maintain a transparent cornea. To properly understand the function of the endothelium, it is important to remember that unlike other tissues the cornea does not contain blood vessels. Therefore, oxygen and other important nutrients needed by the corneal cells cannot be delivered through conventional method. In the cornea, oxygen is provided by the surrounding air which passes into the tear film, and then into the cornea. Whereas, majority of the nutrients required by the cornea are present in the aqueous humor and under normal circumstances they are delivered to the cells due to the seepage of aqueous humor between the endothelial cells. These nutrients enter the cornea through seepage and deliver the nutrients to the corneal cells in the stroma. Once the aqueous humor enters the stroma and delivers the necessary nutrients the cornea starts to lose transparency which is why an exit mechanism is needed and it is provided by the endothelial cells which act as small pumps. Normally, the rate of fluid entering the cornea is equal to the rate of fluid “pumped” out of the cornea which is why the cornea remains transparent. But if, the number of endothelial cells decreases, there will not be enough cells to form a barrier to fluid flow or to “pump” out the fluid. This results in fluid build-up (edema) in the cornea, causing swelling, disruption of the complex corneal structure, and permanent corneal cloudiness. Thus, developing the need for a cornea transplant.

Causes of death of endothelial cells

In all biological systems, a balance between cell proliferation and decay is necessary for normal operation and corneal endothelium cells also adhere to this principle. Corneal endothelium layer is considered as a very delicate corneal tissue layer where cell numbers normally decrease with age till the age of twenty five, after which the

numbers largely remain steady. Yet, some diseases can cause the numbers to reduce even further. In general, all cells have a predefined finite lifespan, at the end of which the cells die/decay and other cells within the tissue divide and replace them. The fact that endothelial cell density decreases with age strongly indicates that endothelial cells do not divide at a high enough rate to replace the lost cells. To cope with the decrease in cell density, the remaining endothelial cells simply enlarge to fill the area where the dead cells were once located [231]. This method works well to a certain extent; however, if the cell density falls below a certain threshold, the remaining cells are no longer able to maintain the barrier between the cornea and aqueous humor and fluid freely enters the cornea, causing edema (swelling) and corneal blindness.

Endothelial cell death due to external stimuli

It has been recognized in literature that physical forces such as pressure, stretch and strain play a critical role in cell loss. Cells respond to external physical inputs through a process called mechanotransduction, and the process through which cells are lost due to external physical inputs is known as mechanical trauma [232]. Despite intensive investigation, the exact pathways by which mechanical signals are converted to biochemical responses are yet to be completely understood [232], [233]. It is suggested in literature that, physical forces act through receptor molecules such as integrins, focal adhesion proteins, and the cytoskeleton. These molecules in turn activate some protein kinase pathways (p38 MAPK and JNK/SAPK), which amplify the signal and activate enzymes (caspases) that promote apoptosis. These physical forces simultaneously activate other signaling pathways as well such as PIK3 and Erk 1/2 MAPK, which modulate the apoptotic response. The exact pathways to be activated are determined by the cell phenotype and the type of the physical stimuli [234].

Apoptosis is defined as the programmed cell death whereby, a strictly structured process maintains the number of cells of an organ. Cell numbers increase due to cell division and these cells replace apoptotic cell. Apoptosis occurs by several mechanisms e.g. caspase (a protein) dependent or independent pathway. One of the basic mechanisms of apoptosis is release of cytochrome-c (a protein) from inner membrane of mitochondria (known as cellular power house as ATP is generated here). This cytochrome-c is involved in ATP generation and hence its release from the inner membrane of mitochondria forces the cell to die.

Cell signaling is the most basic process of gene regulation e.g. when a person touches a hot/cold surface immediately the mind orders our body to retract the hand. This action is performed because the brain interprets the information sent by the hand via cell signaling and once the brain processes the signal it transmits a control action to the hand which in this case was the removal of the hand from the hot/cold surface. Cell signaling sequence involves diverse protein molecules that gets activated and deactivated in a chain to bring the response to perform certain cellular function by eventually impacting DNA in the nucleus of the cell. This signaling may be initiated by external stimulus or internal change in cellular environment [234].

Endothelial cells possess a set of signaling mechanisms. Therefore, when an external stimulus is provided to the endothelial layer signaling pathways are activated. The importance of this mechanism is greater in endothelial cells since corneal endothelium is non regenerative i.e. these cells do not divide once they are formed [231]. That is why apoptosis in corneal endothelium is harmful and cell scarcity leads to blindness thus paving way for a corneal transplant.

Allograft Folding Configurations

Reducing EC loss due to surgical and mechanical trauma is vital in improving the DSAEK surgery outcomes. To achieve this objective, inserters must impart relatively low bending stresses while at the same time facilitate proper unfolding of the allograft inside the AC such that further manipulation after AC insertion of the allograft is not required. Modeling the allograft behavior inside the injector and during insertion is therefore of utmost importance in order to understand the regions and magnitudes of bending stresses induced on the allograft since these stress levels correlate to EC loss.

A literature review on commercially available DSAEK injectors was conducted as presented previously, and it was concluded that although there are several commercially available DSAEK inserters, most of them employ three dominant configurations for allograft folding/unfolding [153]. Representative cross sectional views of the three dominant configurations are presented in Figure 6-2.

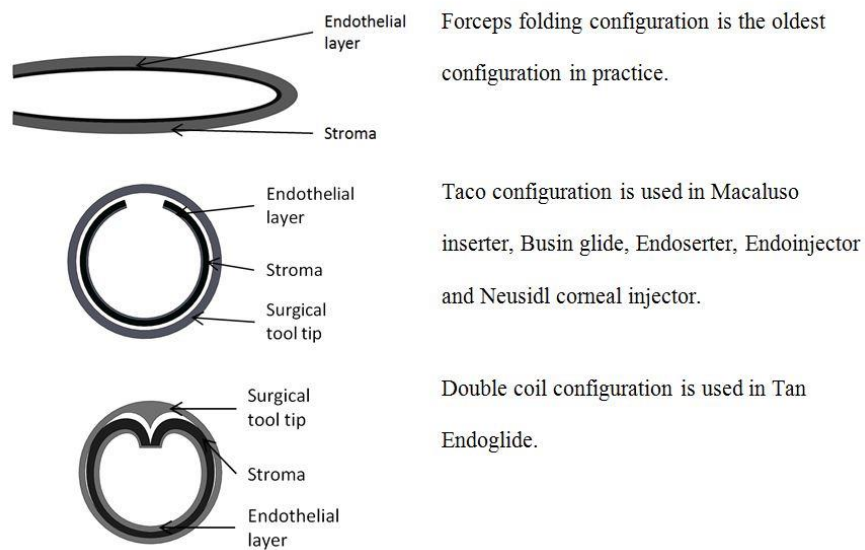


Figure 6-2: Cross sectional views of the three dominant folding configurations

All the inserters except forceps are designed such that the endothelial layer does not contact any other surface in order to reduce the probability of EC loss through surgical trauma and as such the endothelial layer is towards the inside of the fold.

Finite Element Modeling Methodology

The first step in developing a FE model involves geometry creation. The nominal round geometry of the excised allograft used in this research was 8 mm in diameter and consisted of non-uniform thickness of 0.20 mm at the center and 0.23 mm at the limbus. In an effort to improve the computational efficiency of the FE model, symmetry simplification condition along the folding axis was utilized. Once the part geometry was created, material properties and boundary conditions were assigned to the model.

FE Model Assumptions

The assumptions considered during the development of the FE model presented in this work were: (1) the stress-strain functions in the model are assumed stable i.e. they do not change with repetitive loading (2) the stress-strain function of the material during loading is considered equal to the stress-strain function of the material during unloading (3) isotropic material properties were considered for the cornea (4) viscoelasticity was not considered in the model (5) Pre-stresses on corneal layers due to curved natural state were ignored

FE Model Development

Ogden material models are frequently utilized for modeling the large strain nonlinear behavior of incompressible materials such as soft tissue. However, it is extremely important to mention that Ogden models do not provide any understanding into material behavior, but they are curve-fits of various polynomials to the experimental test data. The numerical values of polynomial coefficients resulting from the curve-fits are entered into FE analysis programs to estimate how the material behaves during

mechanical structural analyses. The hyperelastic behavior of the corneal tissue is modeled using the Ogden 2nd order material model since it provided the best curve fit to the posterior stromal material properties data [156]. Ogden material modeling was performed by utilizing the inbuilt modules of the FE modeling software, ANSYS Workbench 15, and is based on the Ogden strain energy function, U, as shown in Equation (6-1) [158].

$$U = \sum_{i=1}^N \frac{2u_i}{\alpha_i^2} (\lambda_1^{\alpha_i} + \lambda_2^{\alpha_i} + \lambda_3^{\alpha_i} - 3) + \sum_{i=1}^N \frac{1}{D_i} (J^{el} - 1)^{2i} \quad 6-1$$

Where λ_i are the principal stretches, N is a material parameter, J^{el} is the elastic volume ratio, u_i , α_i and D_i are material parameters dependent on temperature of the material.

ANSYS Solid tetrahedral elements (Solid 187) were used in this research since Solid 187 is a 10-node tetrahedral element with the ability to simulate hyperelastic material behavior. The density and quality of a mesh dictates the accuracy of the analysis. Therefore, attention was directed towards proper meshing in the model formulation as shown in Figure 6-3. The generated mesh consisted of 71,389 elements with eight elements in the thickness direction. The element aspect ratio is another important factor that governs mesh quality, and close attention was paid to ensure thin sleek elements were not present. The maximum aspect ratio was calculated as 13.8 whereas, average aspect ratio of all the elements in the mesh was estimated to be 1.95 using ANSYS statistics toolbox.

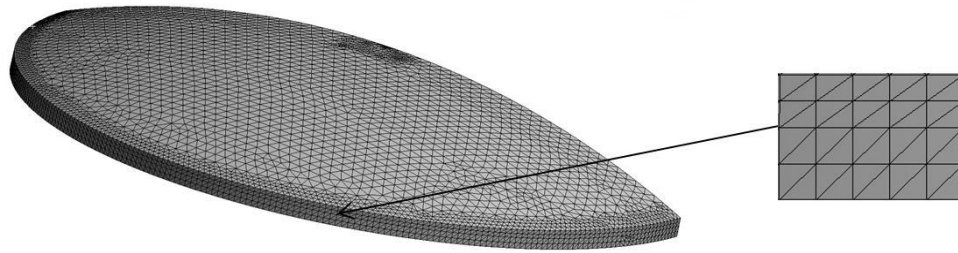


Figure 6-3: Meshing of the allograft in the FE model

In any FE structural simulation, the boundary conditions (BCs) and the loading magnitude and sequence must be properly defined. Since this research required the undeformed allograft to take the shape of the deformed allograft, a sequential loading procedure was devised to attain the correct deformed allograft shape in order to obtain the correct stress levels from the analysis. To ensure proper BCs and loading conditions were provided in a computationally efficient manner, symmetry condition of the allograft was utilized as shown in Figure 6-4 and Figure 6-5. Modeling the folding axis (on the plane of symmetry) of the allograft is challenging since the curved axis flattens gradually as load is applied to the allograft in an effort to deform it in the correct shape/configuration. To model this condition properly, the middle axis of the portion of allograft in contact with the base plate of the injector was fixed in all directions as shown in Figure 6-4, to ensure that the initial point of contact between the allograft and base plate is always maintained. Whereas, the portion of the allograft (folding plane) not in contact with the base plate was free to move in the vertical plane but fixed along the horizontal axis (motion constrained normal to the plane of paper) as shown in Figure 6-5, essentially accounting for and allowing the unconstrained physical movement of the allograft during bending.

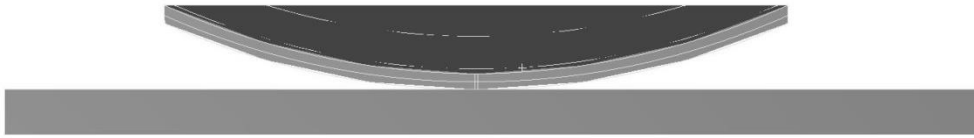


Figure 6-4: Modeling of the symmetrical plane boundary condition



Figure 6-5: Modeling of the symmetrical plane BC fixed in horizontal plane and free in vertical plane

BCs representing symmetry were kept consistent in all the allograft simulations performed to model all the folding configurations. In all the FE models, complex load sequence procedures were developed to force the allograft to take the desired deformed shape, in order to accurately model the stresses experienced by the allograft. The different loading procedures imposed on the allograft in the FE model simulations to achieve the correct deformed shapes are shown in Figure 6-6, Figure 6-7 and Figure 6-8.

The three allograft folding configurations analyzed were forceps, taco and double coil which were achieved using two loading approaches, namely, contact element displacement loading and pressure/displacement/force loading. Both loading approaches showed comparable results, however, a major hurdle in the implementation of contact element displacement loading approach was its computational inefficiency and expense, and the difficulty in accurately modeling complex configurations, therefore this technique was not pursued further and the pressure/displacement/force loading approach was

used. The next challenge was to identify the correct loading location, magnitude and sequence to ensure correct allograft folding. This process required several iterations involving loads of varying magnitude, direction and time sequence until the proper loading combinations yielded the desired allograft deformation configurations. During the various loading steps, the stresses generated in the allograft were observed and recorded to ensure that the maximum stresses experienced by the allograft occurred at the last loading step rather than in any of the intermediate loading steps.

Accurate modeling of the forceps configuration consisted of a two-step loading sequence where pressure load was applied to the allograft at two different locations as shown in Figure 6-6. The purpose of the first step was to bend the allograft with a pressure load (Load D) and the second was a pressure load (Load C) that performed the function of the pressure force applied by the forceps at the point of contact in the actual situation. Both loads were applied simultaneously to the allograft at their respective locations along the allograft width to ensure proper allograft folding as highlighted in Figure 6-6. The taco folding configuration presented in Figure 6-7, was achieved by applying a face pressure load (Load A) and an end pressure load (Load D). First, the face load was applied to deform the allograft in a curved shape, once the desired deformation was achieved, the end load D was applied in addition to the face load to pull the allograft and acquire the exact taco shape. Achieving the double coil configuration proved to be more challenging and as such, a four step loading sequence was utilized with three face pressure loads and one end pressure load to achieve the correct folding configuration as presented in Figure 6-8. First, load A was applied to deform the allograft and then end load D was applied to deform the allograft to a bent shape. Finally, load E and end load F were applied to force the allograft further towards achieving the correct folding shape that represented the double coil configuration.

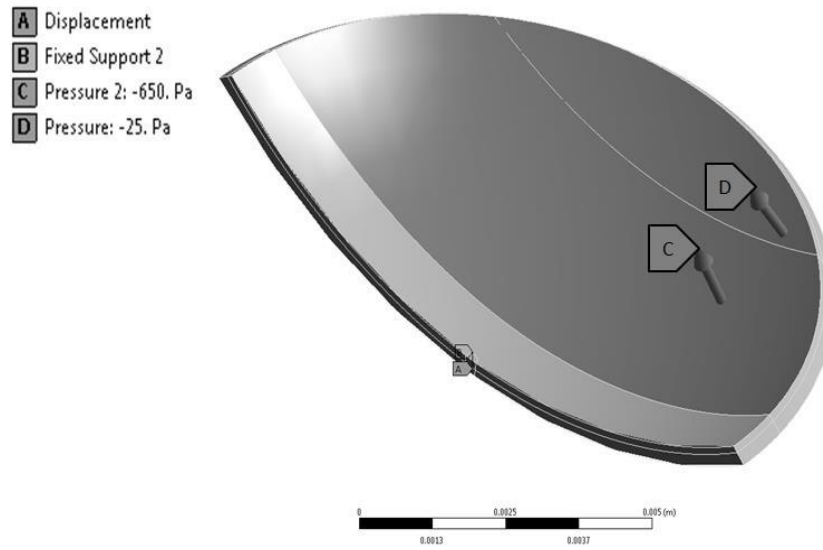


Figure 6-6: Loading sequence for 'Forceps' configuration

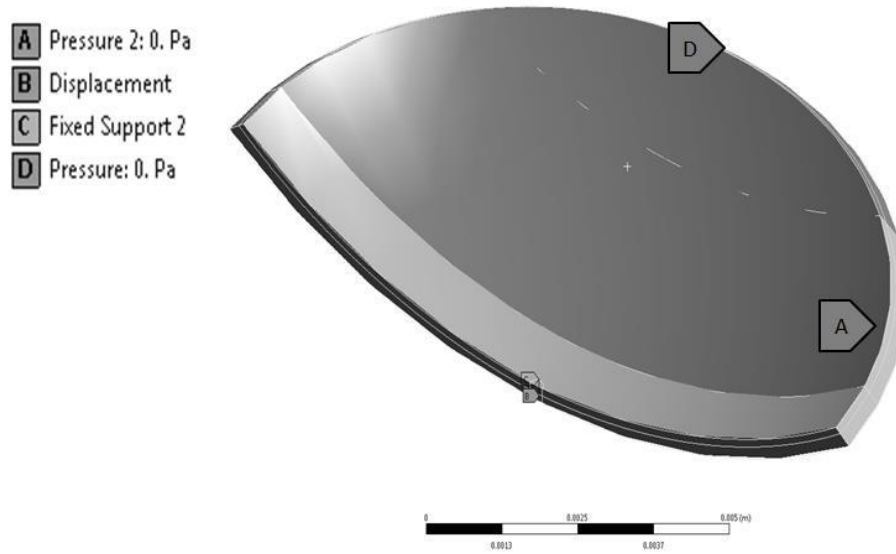


Figure 6-7: Loading sequence for 'Taco' configuration

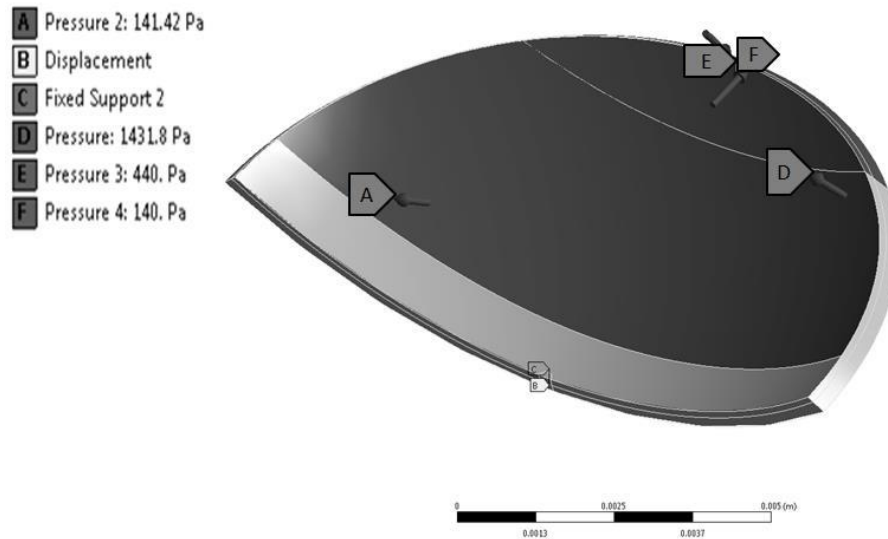


Figure 6-8: Loading sequence for 'Double Coil' configuration

Results and Discussion

A simplified model was developed to verify that the BCs and symmetry condition were properly implemented. The model and the corresponding results are shown in Figure 6-9 and Figure 6-10. Figure 6-9 shows the constrained end of the allograft, which models the symmetry condition whereas, Figure 6-10 shows the FE results of the model which highlight the shape acquired by the constrained end of the allograft under loading. These results were expected since bending will deform the shape of the constrained end by pushing it downwards at the periphery and this is what the FE results portray. The FE results shown in Figure 6-10 prove that the BCs and the symmetry condition were accurately defined in the model.

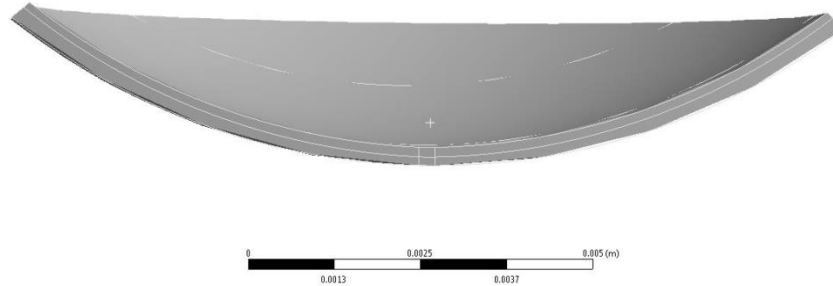


Figure 6-9: Undeformed allograft

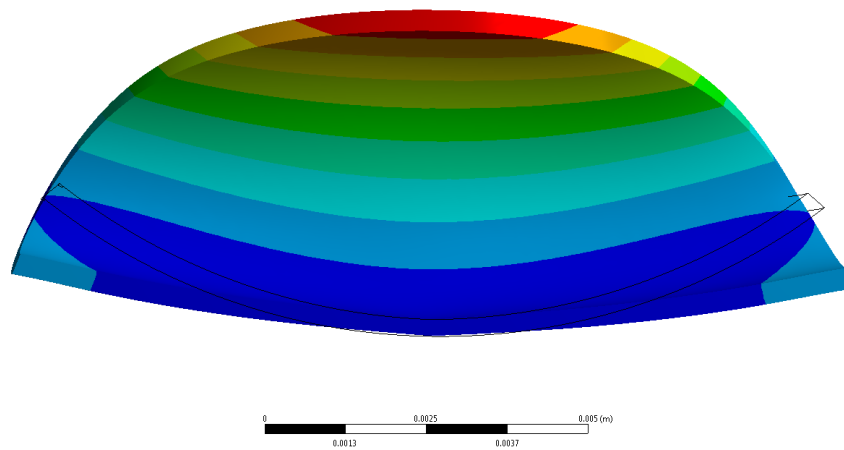


Figure 6-10: Deformed shape of the constrained symmetry plane that clearly experiences a downward pull

Once it was established that the symmetry condition has been accurately modelled, the loading conditions and sequences introduced earlier were imposed on the allograft to model the various folding states and analyze the stress distribution experienced by the allograft. The FE results of respective folding configurations are presented in Figure 6-11. The side view of the deformed state of the forceps folding configuration and the von Mises stresses on the allograft are presented in Figure 6-11(A)

and Figure 6-11(B) respectively. von Mises stresses represent an accurate stress state for ductile/hyperelastic materials. In the case of forceps configuration, after neglecting the stress singularity at the center, which is inevitable due to the unique nature of the BCs, as expected the high stress region is observed at the base where folding takes place. However, what is interesting is the fact that the stresses induced along the folding axis are on average 39 kPa which is relatively high. Therefore, a high amount of EC loss is expected in the forceps configuration. Moreover, the forceps configuration is unique since it employs a 'touching' technique wherein mechanical contact between the forceps and endothelial layer results in pronounced EC loss due to surgical trauma as shown in Figure 6-12(i) where EC loss due to surgical trauma is represented by the two circular grey regions. The presented FE model results for the forceps configuration only represent the EC loss due to mechanical trauma. The stress locations observed in the FE model results agree with the mechanical trauma EC loss pattern from experimental results published in open literature as shown in Figure 6-12(I and II) [5], [6], [208].

The side view of the taco configuration and the corresponding stresses generated on the allograft while in the deformed state are presented in Figure 6-11(C and D). After neglecting the stress singularity at the center, as expected the high stress region lies at the base along the folding axis. Moreover, it is observed that the magnitude of the stresses along the folding axis is on average 22.5 kPa which is considerably lower than the forceps configuration. This indicates that the mechanical trauma induced by the taco configuration is significantly lower than the forceps configuration. The taco configuration employs a 'no touch' technique hence EC loss is dominated by the mechanical trauma rather than surgical trauma as no physical contact with the endothelial cells is made. The observed FE model stress distribution results agree with the mechanical trauma EC loss

pattern from experimental results published in open literature as shown in Figure 6-12(III) [5], [208].

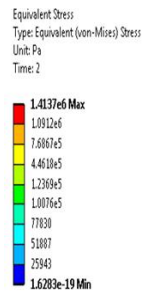
The side view of the double coil configuration and the corresponding stresses generated on the allograft while in the deformed state are presented in Figure 6-11(E and F). The presented results illustrate that high stresses induced in the double coil configuration are away from the folding axis unlike the taco and forceps configurations. Also, the magnitude of the averaged stresses in the double coil configuration is 51 kPa which is higher than the forceps configuration. Therefore, the presented stress magnitude results suggest that maximum EC loss due to mechanical trauma should occur in the double coil configuration. The double coil configuration like the taco configuration employs a 'no touch' technique hence EC loss is dominated by the mechanical trauma rather than surgical trauma. The EC loss pattern for allografts with double coil configuration is not available in the open literature, but since the presented FE modeling procedures correctly predicted the EC loss locations for both forceps and taco configurations, it can be concluded with sufficient confidence that allografts utilized in DSAEK surgery with double coil configuration will experience an EC loss pattern due to mechanical trauma as presented in Figure 6-11(F) (i.e. away from the folding axis). A summary of the maximum stress levels experienced by the allograft due to mechanical trauma for each folding configuration is presented in Table 6-1.

Table 6-1: Summary of maximum stress magnitude in allograft configurations

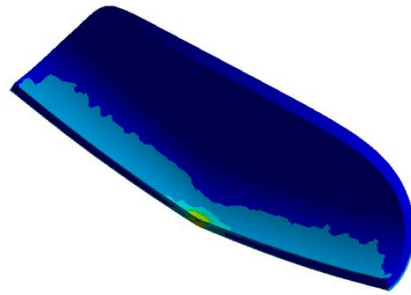
Forceps (kPa)	Taco (kPa)	Double Coil (kPa)
39	22.5	51



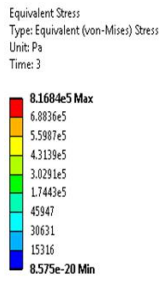
(a): Side View of allograft in 'Forceps' configuration



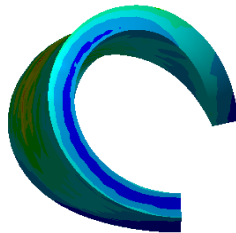
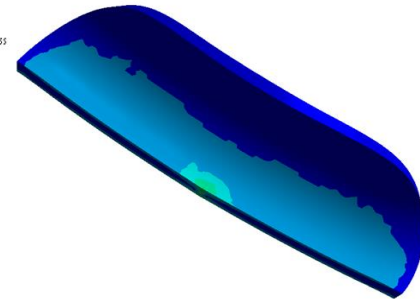
(b): 'Forceps' configuration von Mises stress level



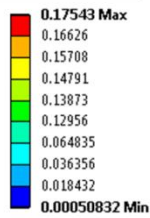
(c): Side View of allograft in 'Taco' configuration



(d): 'Taco' configuration von Mises stress level



(e): Side View of allograft in 'Double Coil' configuration



(f): 'Double Coil' configuration von Mises stress level

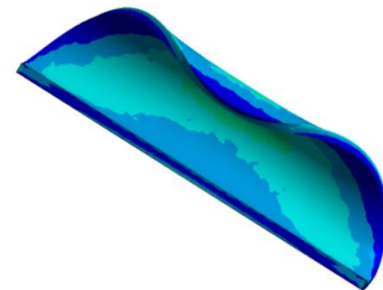
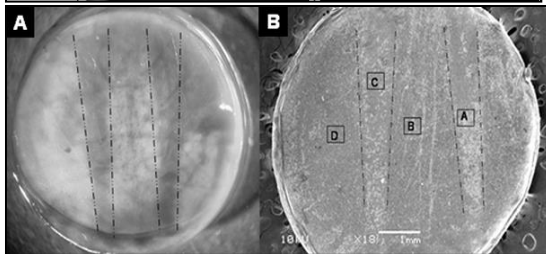


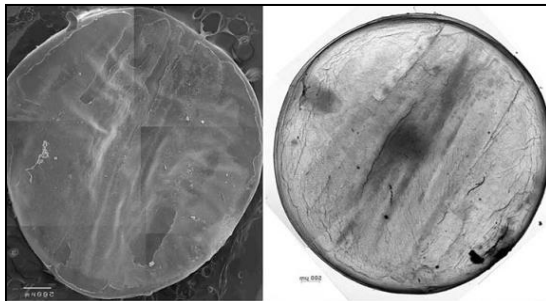
Figure 6-11: FE model results

Group (mean % damage)	Vital Dye Stain	Processed Image
1 Control group with trephina tion only (8.64%)		
2 5mm non- coapting Forceps Insertion (18.39%)		

(I) This figure published by Terry et al. shows the EC loss after forceps were used for the DSAEK surgery. The black spaces on the allograft shown in the processed images in the right column represent healthy cells whereas the grey region represents damaged cells. The cell damage pattern clearly indicates cell death due to surgical trauma where forceps were used to grasp the allograft (two circles) and the lines along the folding axis represent cell damage due to bending stresses/mechanical trauma [208]



(II) This figure published by Mehta et al. shows the EC loss after forceps insertion in DSAEK. The dark grey color represents damaged cells. The same cell damage pattern has been divided into different regions in figure B. Region A and C represent cell damage due to direct contact. Region B represents cell loss due to folding (bending stresses) and region D represents random cells that were damaged [5]



(III) This figure published by Hwang et al. shows the EC loss after taco insertion configuration was employed in DSAEK. The figure on the left represents allograft condition before the surgery and the figure on the right presents the postsurgical allograft with dark grey region representing damaged cells whereas the light grey region represents healthy cells. The cell damage pattern clearly indicates cell death in the folding axis region (maximum bending stress region) [6]

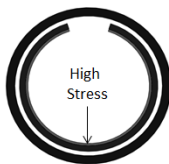


Figure 6-12: EC loss clinical experimental results

Conclusions

The work presented in this chapter highlights existing limitations of the DSAEK surgical procedure, the role of allograft inserters in alleviation of those limitations, and the expected mechanical trauma experienced by the allografts due to the utilization of commercially available and commonly utilized allograft inserters. The importance of EC loss and the correlation between the EC loss and mechanical stresses developed in the allograft was discussed. The procedure for developing a FE model was introduced. The model development procedure including loading sequences and boundary conditions, were explained and the challenges faced in model development were discussed. The FE structural analysis of the allograft as a method to predict the location and magnitude of EC loss was introduced and discussed. The FE model was utilized to capture the stress distribution generated in the allograft while undergoing forceps, taco and double coil configurations. The results of the analyses revealed both the location and magnitude of high stress regions which for forceps and taco configurations were qualitatively in agreement with clinical EC loss data available in the open literature. The FE model results provide insight into the regions of EC loss expected in the double coil configuration for which clinical data was not available in open literature. Confidence can be placed in the FE model results for the double coil configuration since the presented FE modeling procedures correctly predicted the qualitative EC loss magnitude and location for forceps and taco configurations. The FE model procedures developed and presented in this study can be further utilized to study and improve existing insertion configurations and develop improved allograft insertion devices to distribute stresses on the donor allograft such as to reduce EC loss and facilitate allograft unfolding especially in constrained ACs. Success in decreasing EC loss and facilitating allograft unfolding will lead to improvement in the probability of success of the DSAEK surgical procedure.

Chapter 7

Design of a Novel Allograft Insertion Device for Descemet's Stripping Automated Endothelial Keratoplasty (DSAEK) Surgery

Introduction

Finite element structural analysis results of the DSAEK allograft presented in chapter 6 provided the necessary information and background for the design and development of a novel DSAEK allograft inserter that should improve postsurgical outcomes. DSAEK has made significant progress during the last few years yet, there is still room for improvement, especially when the patient has a shallow/constrained AC, since, extra allograft manipulation is required for proper allograft unfolding inside a constrained AC. This extra manipulation leads to higher EC loss, increase in surgery time and complicates the surgical procedure which leads to an increase in the learning curve. Shallow ACs are commonplace, granted that a vast majority of Asian patients have shallow ACs but apart from demographics, AC dimensions also depend on patient age, ocular health and gender [204], [235]. Therefore, patients from all demographics could have shallow ACs [235], [236]. Hence, depending on the size of a patient's AC, a surgeon might have to modify his/her DSAEK surgical technique and this creates the need for a specialized DSAEK inserter for patients with shallow ACs.

This research presents a conceptual design and preliminary analysis of a novel DSAEK allograft inserter that could improve DSAEK surgical outcomes for constrained ACs by reducing the postsurgical EC loss due to mechanical and surgical trauma, facilitating allograft unfolding inside the constrained AC, reducing probability of AC collapse, protecting the allograft from incision compression pressure (ICP) and utilizing the inserter tip space more efficiently to carry a larger diameter allograft. The design and construction of the novel DSAEK allograft inserter that we like to call the 'binocular

inserter' are presented and explained to demonstrate its features. The binocular inserter design includes a provision for AC maintainer which can be utilized to pump AC maintenance fluid inside the AC during the surgery to avoid an AC collapse. The injector body and tip are fabricated of a suitable material with high stiffness to ensure that ICP is not transmitted to the allograft. When the allograft is inserted inside the inserter tip, it deforms into a configuration which reduces EC loss due to surgical trauma. The binocular inserter tip space utilization is evaluated through a mathematical study that compares the binocular inserter with commercially available DSAEK allograft inserters. Finally, a FE study is performed to evaluate the allograft unfolding capability of the binocular inserter. The stress distribution on the allograft while in the deformed state was also utilized to evaluate the EC loss due to mechanical trauma. The FE model for the binocular inserter is developed by utilizing the procedures presented in chapter 6.

This chapter begins by revisiting the allograft structure, composition and material properties. Before introducing the binocular inserter it briefly reviews the allograft folding configurations being utilized in the existing and commercially available DSAEK inserters as presented in chapter 6. The desirable attributes for a DSAEK allograft inserter for delivering allografts in constrained ACs are highlighted and the design of the binocular inserter is evaluated based on those desirable attributes. The construction material and design of the binocular inserter were discussed to demonstrate how the binocular inserter design fulfils the DSAEK allograft inserter desirable attributes.

Materials and Methods

As discussed in chapter 6, a DSAEK allograft consists of the posterior stromal layer, Descemet's membrane (DM), and the Endothelium [49], [153]. Although this information was provided in chapter 6 however, it is revisited again for the purpose of completeness.

The stromal layer possesses the highest stiffness since it is composed of interlaced collagen lamellae in an extracellular matrix (ECM) interspersed with keratocytes [154], [237]. This stress stiffening behavior of the corneal stroma can be explained with the help of the results of earlier studies conducted by Woo et al.(1972) [159] and Hjortdal (1993, 1998) [21], [238]. These studies on corneal microstructure revealed that the stress-strain relationship of the corneal stroma is divided into two distinctive phases: a low stiffness matrix regulated phase at lower strains, followed by a high stiffness phase at high strains where the corneal tissue activates its reinforcing constituents such as collagen fibrils to provide the necessary strength.

As discussed previously, mechanical properties of the stromal layer of the cornea have been extensively studied over the years, and various research groups have attempted to obtain the exact material properties of the cornea by employing different characterization methods [35], [36], [239]–[241]. It is widely acknowledged today that the stroma behaves as an anisotropic nonlinear viscoelastic material [140]–[144], [149], [227]. In this research, isotropic hyperelastic material properties were considered for the stromal layer to reduce the complexity of the model and improve computational efficiency. Moreover, hyperelastic material properties have been used previously to model the cornea by Kling and Marcos (2013) [146], Elsheikh et al. (2007) [156] and Elsheikh et al. (2010) [157]. The material properties utilized in this study are graphically presented in Figure 7-1 [242].

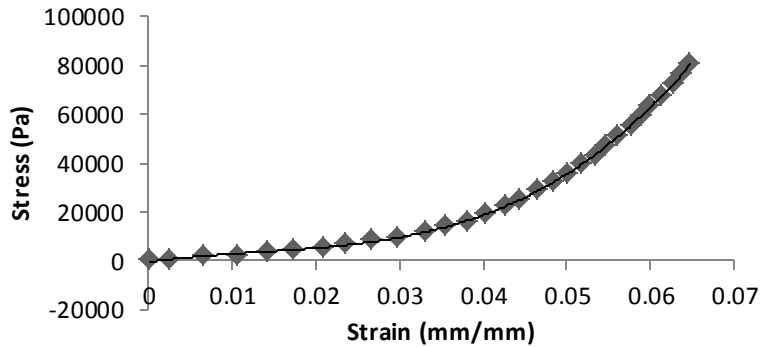


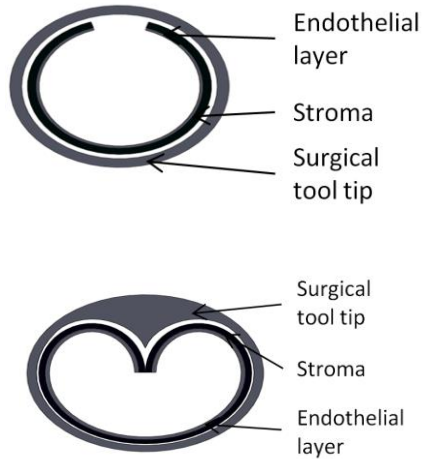
Figure 7-1: Stress strain material properties of the porcine cornea [156]

The allograft material properties appear to be highly nonlinear and undergo stress stiffening. The dominant posterior stromal layer exhibits elasticity with minimal hysteresis [27]. Therefore, the allograft material can be categorized as hyperelastic, and to utilize it in the FE model, material modelling needs to be performed. Hyperelastic materials follow a nonlinear yet elastic stress-strain relationship which is independent of strain rate. Therefore, polynomial equations can be used to describe the behavior of a hyperelastic material. The coefficients of these polynomial equations are estimated based on experimental data. Two models that have predominantly been utilized by researchers to model soft tissue are Mooney Rivlin and Ogden material models [146], [156]. In this work the second order Ogden material model was selected since it provided a better curve fit to the experimental data.

Allograft Folding Configurations

The two most common folding configurations being utilized in commercially available DSAEK allograft inserters are presented in Figure 7-2 [153]. Both of these folding configurations aim to improve DAEK surgery outcomes. The folding configurations presented in Figure 7-2 are effective in their own respective manner. However, there is room for improvement especially in the case of allograft unfolding inside shallow ACs.

The inserter design proposed in this work aims to address the limitations associated with the current designs by introducing a new folding configuration on the allograft that produces a stress distribution which will reduce EC loss and facilitate allograft unfolding especially inside a constrained AC.



Taco configuration is used in Macaluso inserter, Busin glide, Endoserter, Endoinserter and Neusidl corneal inserter.

Double coil configuration is used in Tan Endoglide.

Figure 7-2: Cross sectional view of prevalent DSAEK allograft folding configurations

Proposed Allograft Inserter Design

The proposed allograft inserter as shown in Figure 7-3(a and b) aims to (1) facilitate the allograft unfolding process inside the AC by providing a lateral push to the allograft due to the hump, (2) utilize inserter tip space in a more efficient manner to accommodate a larger diameter graft or reduce the incision length, (3) modulate the EC loss due to mechanical trauma by reducing the magnitude of stresses by moving from one high stress region allograft configuration design to two moderately high stress regions, (4) reduce EC loss due to surgical trauma with the 'no endothelial' touch feature of the inserter, (5) protect the allograft against incision compression pressure (ICP) and (6) minimize the probability of an AC collapse by employing an AC maintainer. The binocular inserter design and construction will be discussed and explained to

demonstrate its capability in reducing EC loss due to surgical trauma, protecting the allograft against ICP and minimizing the probability of AC collapse. A FE model for the allograft in the binocular configuration was developed to evaluate the stress distribution on the allograft, identify EC loss regions, and predict natural allograft unfolding inside the AC. A geometric analysis was performed to evaluate and compare the maximum size allograft holding capacity of the binocular injector with existing inserters.

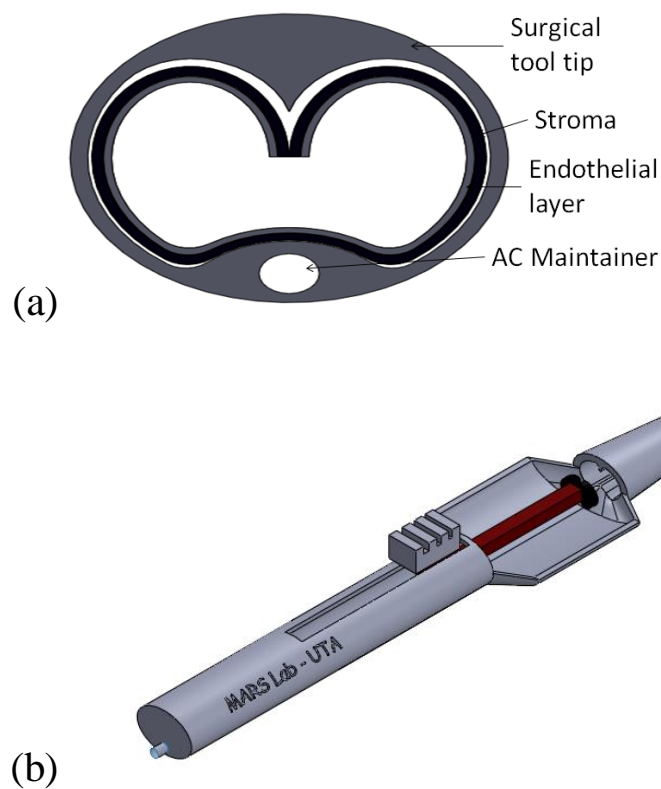


Figure 7-3: (a) Cross sectional view of the Binocular Inserter tip with the allograft folding configuration (b) Preliminary CAD rendering of Binocular tip inserter

Operation of the Proposed Binocular Inserter Design

The presented preliminary design of the binocular inserter will follow the glide mechanism to deliver the allograft inside the patient's eye, as explained in chapter 6.

Allograft delivery through the binocular inserter is expected to be performed by following these steps; (1) the plunger will be pulled back with the help of the thumb rest, (2) the prepared allograft will be placed on the tray, (3) grasping forceps will be used to pull the allograft inside the inserter tip up to the opening of the tip, (4) once the allograft is inside the tip, the plunger will be moved forward to make the tip airtight, (5) the binocular inserter tip will be inserted inside the AC via a corneal incision, (6) holding forceps will be inserted inside the eye from the other end of the AC and the allograft will be pulled inside the AC, and (7) once the allograft is inside and has unfolded air bubble will be added inside the AC and the binocular inserter will be pulled out of the incision.

Binocular Inserter Construction

The body of the binocular injector will be fabricated of a suitable and approved biocompatible material. The material should possess suitable properties of mechanical strength, melting point, glass transition temperature, transparency and low surface friction. The device material needs to be structurally stiff specially at the tip, to prevent tip geometry changes. The material should be sterilizable to allow reuse of the device. Transparency of the material used to fabricate the inserter would allow the surgeon to observe the orientation of the graft inside the device and during insertion. A low friction inserter material is desirable since friction opposes the motion of the graft and could lead to more ECD loss especially during the process of pulling the graft inside the AC. This ECD loss occurs due to the tension induced in the graft at the place where graft and pulling forceps interact. A preliminary conceptual inserter was manufactured via 3D printing technology as presented in Figure 7-4.

The binocular inserter is equipped with an AC pressure maintainer connection. The tip of the injector has a small hole that delivers the fluid inside the AC for maintaining the pressure inside the AC in order to avoid an AC collapse as shown in Figure 7-3(a).

Maintaining AC pressure during the surgery is important since an AC collapse not only increases EC loss but makes it almost impossible for the allograft to unfold inside the AC hence leading to failure of the DSAEK surgery. The design of the binocular inserter tip ensures that the tip structure bears the complete pressure of the wound when the inserter tip enters the AC, therefore protecting the allograft from ICP. Moreover, the binocular inserter tip design ensures that the endothelial layer on the allograft does not come into contact with any external surface as shown in Figure 7-3(a) hence protecting the allograft from surgical trauma, as endothelial cells are very sensitive and contact with any external surface can lead to their death.

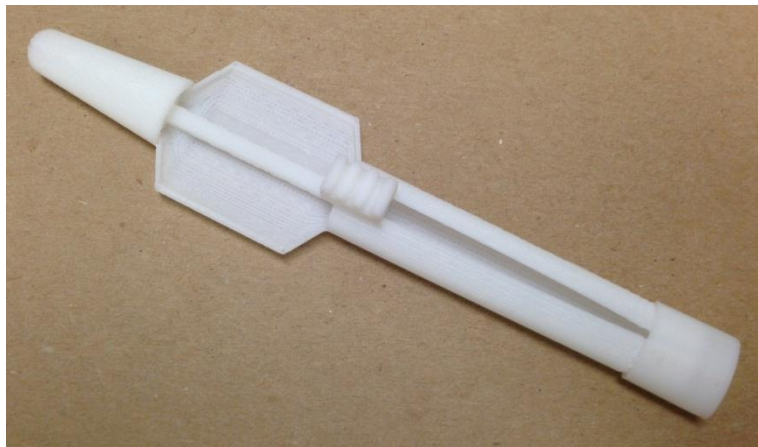


Figure 7-4: Preliminary inserter design manufactured using ABS via 3D printing technology

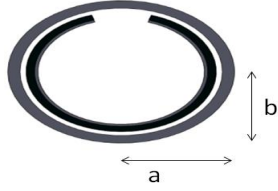
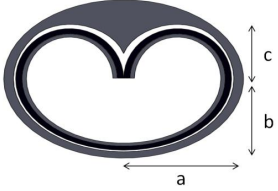
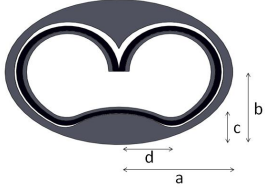
Allograft Tip Shape Analysis

The incision size in a DSAEK surgery is an important parameter since small incision sizes have the advantage of faster healing time. An incision size of 3.2 to 5.5 mm with an average of 4.5 mm is usually required for DSAEK. However, with an incision of 4.5 mm different inserters have varying capability for maximum size allograft holding, which is an important parameter for any inserter design. This difference in allograft

holding capability for inserters with the same outer shape and dimensions arises from the internal shape of the inserter tip. This aspect of the DSAEK allograft inserter design is studied to evaluate the internal perimeter of all available inserter tips and their results are compared with the binocular inserter.

While conducting the analysis, the outer tip shape, perimeter and material thickness were kept constant for all inserters, in an effort to understand the impact of internal tip design on the maximum size allograft holding capability. For an incision size of 4.5 mm the outer perimeter of the inserter tip cannot exceed 9 mm for proper fitting, considering 0.1 mm tip material thickness. In all the calculations, ellipsoid shape perimeter was calculated to 0.04% accuracy using the Ramanujan II method [243]. The length of curved corners was evaluated using the mathematical function that represents that shape and then calculating its length with the given dimensions. In all calculations, the internal major axis length '2a' was considered to be 2.8 mm and the internal minor axis length '2b' was considered to be 2 mm.

Table 7-1: Summary of nomenclature for the inserter tip geometry analysis

		
Ellipsoid (Taco)	Double Coil	Binocular

The inserter tip geometry for the various allograft folding configurations and the nomenclature used for the analysis are shown in Table 7-1. The allograft size holding capability of an ellipsoid tip was calculated using the Ramanujan II method [243]. The allograft size holding capability of a double coil inserter tip was calculated by dividing the

tip shape into two parts, a big ellipse that represents the bottom portion of the allograft and two smaller ellipsoids that represent the upper portion of the allograft. The allograft size holding capability of the binocular inserter tip was evaluated by following three steps. In the first step, the process outlined for double coil is followed. Then, arc length covered by the bump is subtracted from the previously calculated sum and then finally, the circumference of the bump is added to the total. The formulae and details of the evaluation of the allograft length/size or diameter holding capability for the various configurations are presented in Appendix A.

Table 7-2: Summary of maximum diameter allograft carrying capability for the folding configurations

Inserter Configuration	Taco	Double Coil	Binocular
Maximum Allograft Diameter (mm)	7.6	8.1	8.54

The results of the allograft size analysis show that binocular inserter with the same tip geometry and exterior dimensions is the most effective at utilizing inserter tip space allowing the inserter to accommodate a larger diameter allograft as compared to other tip geometries as shown in Table 7-2.

Finite Element Modeling

Endothelial cells are lost due to mechanical trauma when high bending stresses are induced on the allograft while it is in the folded state inside the inserter tip. Reducing the bending stresses is desirable however, it can act as a two edged sword since low bending stresses would make it difficult for the allograft to unfold properly inside a constrained AC. The binocular inserter aims to unfold the allograft especially inside a

shallow AC while at the same time reduce EC loss due to mechanical trauma. The stress distribution generated on the allograft in the binocular configuration is evaluated using a FE analysis. A FE model was developed in an effort to understand the stress magnitude and distribution in the deformed state (shape of binocular inserter) to predict the natural allograft unfolding capability inside the AC and the postsurgical EC loss.

Allograft unfolding inside the AC depends on the location and amount of bending stresses induced on the allograft inside the inserter tip. Once inside the AC, the allograft naturally wants to relieve itself of those stresses through unfolding. Allograft unfolding inside the AC receives resistance from its environment through contact with the walls of the AC and if the magnitude of the bending stresses is not high enough the allograft will fail to unfold. The methods and procedures developed in chapter 6 are employed to evaluate the stress distribution generated in the allograft for the binocular configuration.

During FE model development, a complex load sequence procedure was developed and followed to force the allograft to take the desired binocular deformed shape, in order to accurately evaluate the stresses experienced by the allograft. The loading procedure followed for allograft to achieve the correct binocular deformed shape is shown in Figure 7-5. BCs A and B represent symmetry conditions and loadings C to F are sequentially applied to deform the allograft in the correct shape.

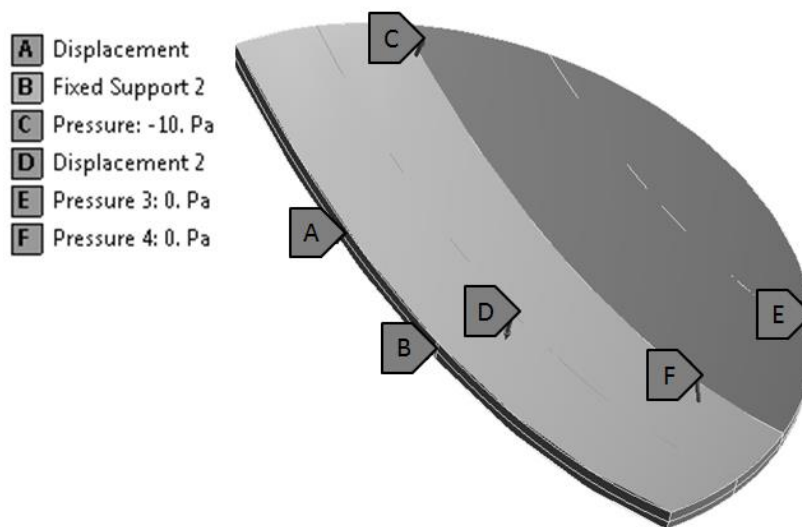


Figure 7-5: BCs and loading sequence for binocular configuration

Results and Discussion

DSAEK surgery was explained and its limitations especially for patients with shallow anterior chambers were highlighted. To improve the outcomes of the DSAEK surgery in patients with shallow ACs a new allograft inserter called binocular inserter was proposed in this research study. The performance of the binocular inserter was evaluated for efficient allograft space utilizing, EC loss handling due to surgical and mechanical trauma, ICP transmission, allograft unfolding inside a constrained AC and maintenance of AC during DSAEK.

The results of the allograft size analysis show that binocular inserter configuration is most effective at utilizing inserter tip space. Since, binocular configuration with the same outer dimensions allows the inserter to accommodate a larger diameter allograft as compared to other tip geometries as shown in Table 7-2. This analysis demonstrates the ability of the binocular configuration to accommodate a large diameter allograft through a relatively smaller incision size. This is an important feature since

smaller incisions reduce wound healing time and reduce the possibility of an AC collapse during surgery.

The results of the FE model analysis are presented in Figure 7-6, where Figure 7-6(a) presents the side view of the deformed allograft and Figure 7-6(b) presents the von Mises stress distribution generated on the allograft in its deformed state. The von Mises stress results reveal the expected locations for postsurgical EC loss due to mechanical trauma as the high stress regions. In contrast to other inserter tip designs [242], the binocular configuration distributes the localized stresses, therefore effectively reducing the total stress levels encountered by the graft. The maximum stress developed in the binocular configuration is 47 kPa which is higher than taco and forceps but lower than double coil. Also, the distributed stresses in the binocular configuration are expected to aid in a two-step unfolding sequence that will facilitate natural unfolding of the allograft even in constrained ACs thus reducing additional trauma experienced by the allograft. The two moderately high stress regions indicated in the stress results presented in Figure 7-6 (b) induce bending moments to that allograft at strategic locations which will assist the allograft to unfold inside a constrained AC. The high stress region located near the plane of symmetry provides the lateral push to the allograft inside the AC whereas, the high stress region away from the plane of symmetry provides the force for allograft unfolding inside the AC. The combination of both these actions will facilitate natural allograft unfolding. It is important to mention that none of the existing designs of allograft inserters include a lateral push feature which is why natural allograft unfolding inside the constrained AC proves to be more challenging.

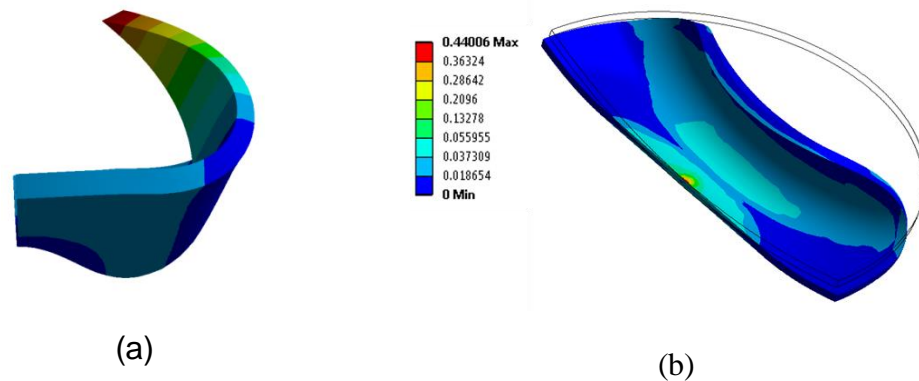


Figure 7-6: (a) Side View of the allograft for the binocular configuration (b) von Mises stress level of allograft for the binocular configuration

Conclusions

The limitations of the DSAEK surgical procedure with the current state of the art allograft insertion instruments were introduced and a novel DSAEK allograft inserter concept, binocular inserter was presented. The design of the novel binocular inserter was analyzed for its ability to improve DSAEK surgical outcomes especially in constrained ACs. The design of the binocular inserter was evaluated for its capability to reduce EC loss due to surgical and mechanical trauma, unfold in a constrained AC, reduce the probability of AC collapse, efficiently utilize inserter tip space to carry a larger diameter allograft and protect the allograft against ICP. The binocular inserter design has the provision for an AC maintainer to provide pressure inside the AC and prevent AC collapse. The inserter design ensures that the endothelial cells on the allograft do not come into contact with any external surface therefore protecting the allograft from surgical trauma. A FE model was developed to predict EC loss due to mechanical trauma and the natural allograft unfolding. The results show that the binocular configuration distributes the stress concentration area into two areas, therefore reducing the stress levels while also inducing a two-step allograft unfolding process that should assist

allograft unfolding in constrained ACs due to the lateral push experienced by the allograft. A geometric analysis was also performed to evaluate the tip space utilization in the binocular configuration and the results suggest that the binocular configuration utilizes inserter tip space better than the available inserters. Hence, it has the capability to carry a larger diameter allograft for the same incision size. Overall, the binocular inserter design is expected to improve DSAEK surgical outcomes especially for patients with shallow anterior chambers.

Chapter 8

Summary, Conclusions and Recommendations for Future Research

The work presented in this dissertation highlights the importance of biomechanics in corneal analysis by studying a number of surgical procedures used to alleviate ocular conditions such as myopia and partial thickness corneal transplant. It begins with a comprehensive literature survey of the LASIK surgery. Discussing the role of lasers and highlighting the challenges faced in the surgical procedure. Another refractive surgical procedure called intrastromal corneal ring (ICR) implant surgery was studied by developing a computationally efficient finite element (FE) model of the cornea. The developed FE model was utilized to study the effect of varying ICR thickness and radius, ICR implantation depth and radius of corneal pocket on the postsurgical outcomes. The FE analysis results demonstrated the ability of ICR implants to rectify myopia and underlined the dependency of the myopic rectification on the analyzed control parameters. These outcomes provided insight into the surgery that can be utilized to improve the surgical procedure and develop novel/improved ICR implant designs.

After analyzing the ICR implant surgery, attention was directed towards a partial thickness corneal transplant surgery called Descemet's Stripping Automated Endothelial Keratoplasty (DSAEK) surgery. A rigorous literature survey was conducted to document and understand the prevalent techniques and instruments being utilized to perform the surgical procedure. The shortcomings of the DSAEK surgical procedure were introduced and the techniques/devices being utilized to overcome them were discussed. To develop a better understanding of the surgery, a computationally efficient finite element (FE) model of the DSAEK allograft was developed. The FE model was used to evaluate the stresses generated on the allograft while in the popular folded states such as forceps, taco and double coil. The FE model stress distribution results were correlated with

endothelial cell (EC) health data available in open literature. The results demonstrated that a correlation exists between postsurgical EC loss due to mechanical trauma and the stress distribution developed on the allograft while in the folded state. The FE model results also suggest that highest EC loss due to mechanical trauma is experienced by the double coil configuration followed by forceps and taco configuration. The results of the FE model provide an insight into the cause of EC loss and importance of high stress locations on allograft in reference to allograft natural unfolding inside the AC.

The knowledge gained from the development of the DSAEK allograft FE model and the requirement for natural allograft unfolding inside the AC were used towards the design and development of a novel DSAEK allograft inserter we call the binocular inserter. The design of the binocular DSAEK inserter was analyzed and evaluated for its capability to improve DSAEK surgical outcomes especially in constrained ACs by evaluating its capability to reduce EC loss due to surgical and mechanical trauma, naturally unfold the allograft in a constrained AC, reduce the probability of AC collapse, efficiently utilize inserter tip space to carry a larger diameter allograft to reduce the incision size and protect the allograft against ICP. The prototype conceptual design of the binocular inserter showed that it should be capable to meet the desired performance objectives. The performance of the binocular inserter for natural allograft unfolding and EC loss due to mechanical trauma was evaluated by developing a FE model. The FE results demonstrated that the binocular configuration distributes the stress concentration into two regions, thereby reducing the stress levels while facilitating a two-step allograft unfolding process that should assist in natural allograft unfolding especially inside constrained ACs. Moreover, a mathematical analysis was performed to evaluate the tip space utilization in the binocular configuration and the results of the analysis suggest that the binocular configuration utilizes inserter tip space better than the existing inserters.

The proposed inserter can accommodate a larger diameter allograft for the same incision size or reduce the incision size requirement for delivering the same size allograft. Overall, the unique characteristics of the proposed binocular inserter design fulfil the desired criteria and has the potential to improve DSAEK surgical outcomes especially for patients with shallow ACs.

Recommendations for Future Research

The work presented in this dissertation document utilizes biomechanical concepts to analyze the cornea post ocular surgeries such as DSAEK, ICR implantation and proposes a novel allograft inserter, the Binocular Inserter. A number of future research directions could be pursued based on work presented in this dissertation as listed below:

- Conduct a study to compare the effects of employing anisotropic/orthotropic corneal material properties with nonlinear hyperelastic properties used in this work by using the developed FE models and procedures.
- Investigate the source of the relative maximum in ICR thickness analysis for ICR implantation surgery FE analysis.
- Study DSAEK allograft natural unfolding inside different sized ACs for the existing and proposed binocular inserter.
- Utilize the full eye FE model for ICR studies in the future because of its ability to evaluate both the corneal curvature and apical deformation.
- Study the effects of segmented ICR implants on the corneal topography using the full eye FE model.
- Optimize the binocular inserter tip geometry to reduce EC loss and improve natural allograft unfolding by evaluating the sensitivity of hump height and location on allograft utilization through FE analysis.

- Fabricate the binocular inserter and perform initial clinical trials using eye bank or animal corneas to assess its performance.
- Perform a controlled clinical study utilizing all six commercially available DSAEK allograft inserters and evaluate their postsurgical EC loss as compared to the binocular inserter.
- Research different geometry mapping techniques that could be utilized to deform a model geometry in the desired shapes without the use of complex loading sequences for FE analysis.
- Research the application of presented FE modeling techniques to analyze other corneal surgeries such as DMEK, Corneal Inlays etc.

Appendix A

Allograft Tip Space Utilization Analysis

Allograft length calculation for an ellipsoid inserter tip

Allograft size holding capability of an ellipsoid tip was calculated as shown below.

$$P = \pi(a + b) \left[1 + \frac{3h}{10 + \sqrt{4 - 3h}} \right]$$

$$\text{Where, } a = 1.4 \text{ mm}, b = 1.0 \text{ mm}, h = \frac{(a-b)^2}{(a+b)^2} = 0.0278 \text{ mm}$$

$$P = 7.6 \text{ mm}$$

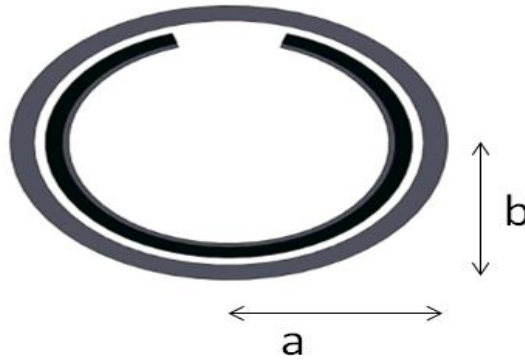


Figure A-1: Nomenclature of an ellipsoid inserter tip

Allograft length calculation for a double coil inserter tip shape

Allograft size holding capability of a double coil inserter tip was calculated by dividing the tip shape into two parts, a big ellipse that represents the bottom portion of the allograft and two smaller ellipsoids that represent the upper portion of the allograft.

$$D = (\text{lower half ellipsoid} + 2 \text{ upper half ellipsoids})$$

$$D = \frac{1}{2} \left\{ \pi(a + b) \left[1 + \frac{3h}{10 + \sqrt{4 - 3h}} \right] \right\} + 2 \frac{1}{2} \left\{ \pi(a_1 + b_1) \left[1 + \frac{3h_1}{10 + \sqrt{4 - 3h_1}} \right] \right\}$$

$$\text{Where, } a = 1.4 \text{ mm}, b = 1.0 \text{ mm}, h = \frac{(a-b)^2}{(a+b)^2} = 0.0278 \text{ mm}, h_1 = \frac{(a_1-b_1)^2}{(a_1+b_1)^2} = 5.95 \times$$

$$10^{-4}, a_1 = \frac{1}{2}a = 0.7 \text{ mm}, b_1 = c = \frac{2}{3}b = 0.6667 \text{ mm}$$

$$D = 8.1 \text{ mm}$$

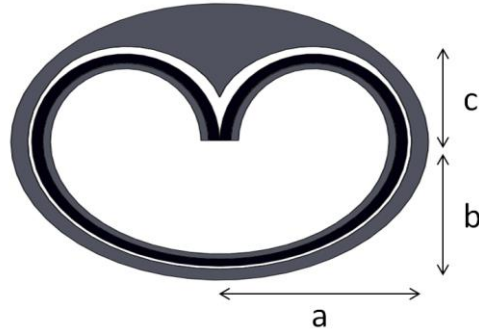


Figure A-2: Nomenclature of a double coil inserter tip

Allograft length calculation for a binocular inserter tip shape

Allograft size holding capability of the binocular inserter tip was evaluated by following three steps. In the first step, the process outlined for double coil is followed. Then, arc length covered by the bump is subtracted from the previously calculated sum and then finally, the circumference of the bump is added to the total.

$B = (2 \text{ half ellipsoids (H)} + \text{half ellipse (E)} - \text{arc length covered by bump (A}_b) + \text{circumference of bump (C}_b))$

When $a = 1.4\text{mm}$, $b = 1.0\text{mm}$, $h = 0.0278\text{mm}$, $d = 0.4\text{mm}$, $h_1 = 5.95 * 10^{-4}$, $a_1 = 0.7\text{mm}$, $b_1 = c = 0.6667\text{mm}$, $w = \frac{x}{a} = \frac{d}{a} = 0.2857\text{mm}$, $e = \frac{\sqrt{a^2 - b^2}}{a} = 0.69985$, $c = 0.4\text{mm}$ and $r = \frac{(2d)^2 + 4c^2}{8c} = 0.4\text{mm}$

$$2H = 2 \frac{1}{2} \left\{ \pi(a_1 + b_1) \left[1 + \frac{3h_1}{10 + \sqrt{4 - 3h_1}} \right] \right\} = 4.2941 \text{ mm}$$

$$E = \frac{1}{2} \left\{ \pi(a + b) \left[1 + \frac{3h}{10 + \sqrt{4 - 3h}} \right] \right\} = 3.7961 \text{ mm}$$

$$A_b = 2(a) \int_0^w \left[\frac{\sqrt{1 - e^2 w^2}}{\sqrt{1 - w^2}} \right] dw = 2(1.4) \int_0^{0.2857} \left[\frac{\sqrt{1 - (0.69985)^2 w^2}}{\sqrt{1 - w^2}} \right] dw = 0.806 \text{ mm}$$

$$C_b = 2r \left[\sin^{-1} \left(\frac{2d}{2r} \right) \right] = 1.2566 \text{ mm}$$

$$B = 2H + E - A_b + C_b = 4.2941 + 3.7961 - 0.806 + 1.2566$$

$$\mathbf{B = 8.5408 \text{ mm}}$$

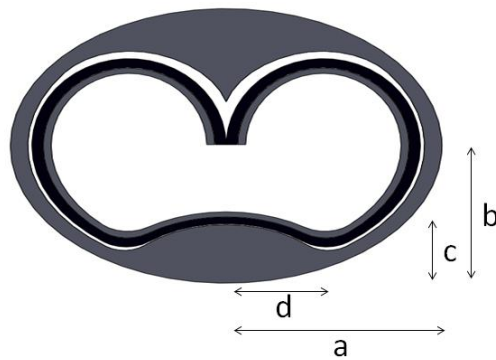


Figure A-3: Nomenclature of binocular inserter tip

References

- [1] D. A. Quillen, "Common causes of vision loss in elderly patients.," *Am. Fam. Physician*, vol. 60, no. 1, pp. 99–108, 1999.
- [2] American academy of Ophthalmology, "Eye health statistics at a glance," 2011.
- [3] D. J. Schanzlin, "Studies of intrastromal corneal ring segments for the correction of low to moderate myopic refractive errors.," *Trans. Am. Ophthalmol. Soc.*, vol. 97, p. 815, 1999.
- [4] Eye bank Association of America, "2013 Eye Banking Statistical Report," Washington DC USA, 2013.
- [5] J. S. Mehta, Y.-M. Por, R. W. Beuerman, and D. T. Tan, "Glide insertion technique for donor cornea lenticule during Descemet's stripping automated endothelial keratoplasty," *J. Cataract Refract. Surg.*, vol. 33, no. 11, pp. 1846–1850, 2007.
- [6] H. Hwang and M. Kim, "Endothelial damage of a donor cornea depending on the donor insertion method during Descemet-stripping automated endothelial keratoplasty in porcine eyes," *Jpn. J. Ophthalmol.*, vol. 53, no. 5, pp. 523–530, 2009.
- [7] M. E. Associates, "Anatomy of human eye," 2012. [Online]. Available: <http://www.mastereyeassociates.com/eye-anatomy-eye-problems/>.
- [8] L. J. Kugler and M. X. Wang, "Lasers in refractive surgery: history, present, and future," *Appl. Opt.*, vol. 49, no. 25, pp. F1–F9, 2010.
- [9] E. E. Center, "Introduction to LASIK," 2011. [Online]. Available: <http://www.eagleeyecentre.com.sg/lasik.html>.
- [10] J. W. Ruberti, A. S. Roy, and C. J. Roberts, "Corneal biomechanics and biomaterials.," *Annu. Rev. Biomed. Eng.*, vol. 13, pp. 269–95, Aug. 2011.

- [11] D. Ljubimova, *Biomechanics of the human eye and intraocular pressure measurements*. Department of Mechanics, Royal Institute of Technology, 2009.
- [12] C. Hanna and J. E. O'BRIEN, "Cell production and migration in the epithelial layer of the cornea," *Arch. Ophthalmol.*, vol. 64, no. 4, pp. 536–539, 1960.
- [13] M. J. Hogan and J. E. JA Weddell, "Histology of the human eye: an atlas and textbook," 1971.
- [14] N. Lagali, J. Germundsson, and P. Fagerholm, "The role of Bowman's layer in corneal regeneration after phototherapeutic keratectomy: a prospective study using in vivo confocal microscopy," *Invest. Ophthalmol. Vis. Sci.*, vol. 50, no. 9, pp. 4192–4198, 2009.
- [15] J. R. Hassell and D. E. Birk, "The molecular basis of corneal transparency," *Exp. Eye Res.*, vol. 91, no. 3, pp. 326–335, 2010.
- [16] D. M. Maurice, "The cornea and sclera," *eye*, vol. 1, pp. 1–158, 1984.
- [17] P. M. Pinsky, D. van der Heide, and D. Chernyak, "Computational modeling of mechanical anisotropy in the cornea and sclera," *J. Cataract Refract. Surg.*, vol. 31, no. 1, pp. 136–145, 2005.
- [18] K. M. Meek, "The cornea and sclera," in *Collagen*, Springer, 2008, pp. 359–396.
- [19] C. Boote, S. Dennis, Y. Huang, A. J. Quantock, and K. M. Meek, "Lamellar orientation in human cornea in relation to mechanical properties," *J. Struct. Biol.*, vol. 149, no. 1, pp. 1–6, 2005.
- [20] B. O. Hedbys, S. Mishima, and D. M. Maurice, "The imbibition pressure of the corneal stroma," *Exp. Eye Res.*, vol. 2, no. 2, pp. 99–IN1, 1963.
- [21] J. Ø. Hjortdal, "Regional elastic performance of the human cornea," *J. Biomech.*, vol. 29, no. 7, pp. 931–942, 1996.
- [22] A. J. Bron, "Wolff's Anatomy of the Eye and Orbit," 1997.

- [23] J. B. Randleman, D. G. Dawson, H. E. Grossniklaus, B. E. McCarey, and H. F. Edelhauser, "Depth-dependent cohesive tensile strength in human donor corneas: implications for refractive surgery.," *J. Refract. Surg. (Thorofare, NJ 1995)*, vol. 24, no. 1, pp. S85–9, 2008.
- [24] M. A. Jakus, "Studies on the cornea. II. The fine structure of Descemet's membrane," *J. Biophys. Biochem. Cytol.*, vol. 2, no. 4, pp. 243–252, 1956.
- [25] D. H. Johnson, W. M. Bourne, and R. J. Campbell, "The ultrastructure of Descemet's membrane: I. Changes with age in normal corneas," *Arch. Ophthalmol.*, vol. 100, no. 12, pp. 1942–1947, 1982.
- [26] M. Pavelka, J. Roth, M. Pavelka, and J. Roth, "Descemet's Membrane," *Funct. Ultrastruct. Atlas Tissue Biol. Pathol.*, pp. 184–185, 2010.
- [27] C. C. Danielsen, "Tensile mechanical and creep properties of Descemet's membrane and lens capsule," *Exp. Eye Res.*, vol. 79, no. 3, pp. 343–350, 2004.
- [28] A. RINGVOLD, M. DAVANGER, and E. G. OLSEN, "On the spatial organization of the cornea endothelium," *Acta Ophthalmol.*, vol. 62, no. 6, pp. 911–918, 1984.
- [29] N. C. Joyce, "Proliferative capacity of the corneal endothelium," *Prog. Retin. Eye Res.*, vol. 22, no. 3, pp. 359–389, 2003.
- [30] K. H. Carlson, W. M. Bourne, J. W. McLaren, and R. F. Brubaker, "Variations in human corneal endothelial cell morphology and permeability to fluorescein with age," *Exp. Eye Res.*, vol. 47, no. 1, pp. 27–41, 1988.
- [31] E. M. Van Buskirk, "The anatomy of the limbus.," *Eye*, no. 3 (Pt 2), pp. 101–108, 1989.
- [32] D. Meller, K. Peters, and K. Meller, "Human cornea and sclera studied by atomic force microscopy," *Cell Tissue Res.*, vol. 288, no. 1, pp. 111–118, 1997.

- [33] P. G. Watson and R. D. Young, "Scleral structure, organisation and disease. A review," *Exp. Eye Res.*, vol. 78, no. 3, pp. 609–623, 2004.
- [34] Y. Komai and T. Ushiki, "The three-dimensional organization of collagen fibrils in the human cornea and sclera.," *Invest. Ophthalmol. Vis. Sci.*, vol. 32, no. 8, pp. 2244–2258, 1991.
- [35] T. M. NEJAD, C. FOSTER, and D. GONGAL, "Finite element modelling of cornea mechanics: a review.," *Arq. Bras. Oftalmol.*, vol. 77, no. 1, 2014.
- [36] H. Hatami-Marbini and E. Etebu, "Hydration dependent biomechanical properties of the corneal stroma.," *Exp. Eye Res.*, vol. 116, pp. 47–54, Nov. 2013.
- [37] J. A. Last, S. J. Liliensiek, P. F. Nealey, and C. J. Murphy, "Determining the mechanical properties of human corneal basement membranes with atomic force microscopy," *J. Struct. Biol.*, vol. 167, no. 1, pp. 19–24, 2009.
- [38] The foundation of American academy of Ophthalmology, "History of Spectacles," *Ophthalmic heritage and museum of vision*, 2012. [Online]. Available: <http://faao.org/what/heritage/exhibits/online/spectacles/>.
- [39] G. T. Cashell, "A short history of spectacles.," *Proc. R. Soc. Med.*, vol. 64, no. 10, p. 1063, 1971.
- [40] R. M. Pearson and N. Efron, "Hundredth anniversary of August Müller's inaugural dissertation on contact lenses," *Surv. Ophthalmol.*, vol. 34, no. 2, pp. 133–141, 1989.
- [41] J. I. Barraquer, "Method for cutting lamellar grafts in frozen corneas: New orientations for refractive surgery," *Arch Soc Am Ophthalmol*, vol. 1, p. 237, 1958.

- [42] L. G. Pallikaris, M. E. Papatzanaki, E. Z. Stathi, O. Frenschok, and A. Georgiadis, "Laser in situ keratomileusis," *Lasers Surg. Med.*, vol. 10, no. 5, pp. 463–468, 1990.
- [43] R. Srinivasan, "Dynamics of the ultraviolet laser ablation of corneal tissue," in *AIP Conference Proceedings*, 1987, vol. 160, p. 703.
- [44] FDA, "List of FDA-Approved Lasers for LASIK," *US Department of Health and Human Services*, 2011. [Online]. Available: <http://www.fda.gov/MedicalDevices/ProductsandMedicalProcedures/SurgeryandLifeSupport/LASIK/ucm192109.htm>.
- [45] iLASIK, "IntraLase Femtosecond laser," *Abbott Medical Optics*. [Online]. Available: <http://www.amo-inc.com/products/refractive/ilasik/intralase-fs-laser>.
- [46] Microkeratome, "Hansatome microkeratome," *Bausch and Lomb*. [Online]. Available: <http://www.bausch.com/en>.
- [47] Y. Minami, H. Sugihara, and S. Oono, "Reconstruction of cornea in three-dimensional collagen gel matrix culture," *Invest. Ophthalmol. Vis. Sci.*, vol. 34, no. 7, pp. 2316–2324, 1993.
- [48] FDA, "What is LASIK," *United States Food and Drug Administration*, 2011. [Online]. Available: <http://www.fda.gov/MedicalDevices/ProductsandMedicalProcedures/SurgeryandLifeSupport/LASIK/ucm061358.htm>.
- [49] S. Nasir Khan, P. Shiakolas, and M. Rizwan, "An Overview on Performance Characteristics of Laser In-Situ Keratomileusis Using Lasers and Identification of Challenges," *Micro Nanosyst.*, vol. 4, no. 4, pp. 284–295, 2012.
- [50] Omar E Awad, "LASIK," *Awad Eye Center*, 2011. [Online]. Available: <http://awadeye.com/LASIK.htm>.

- [51] D. M. Wang, *LASIK Vision Correction: An Overview of Refractive Errors and Their Treatment with the Excimer Laser*. Med World Publishing, 2000.
- [52] United States FDA, "LASIK procedure," 2011. [Online]. Available: <http://www.fda.gov/MedicalDevices/ProductsandMedicalProcedures/SurgeryandLifeSupport/LASIK/default.htm>.
- [53] R. Ambrósio and S. E. Wilson, "Complications of laser in situ keratomileusis: etiology, prevention, and treatment," *J. Refract. Surg.*, vol. 17, no. 3, pp. 350–379, 2001.
- [54] M. S. El-Agha, E. W. Johnston, R. W. Bowman, H. D. Cavanagh, and J. P. McCulley, "Excimer laser treatment of spherical hyperopia: PRK or LASIK?," *Trans. Am. Ophthalmol. Soc.*, vol. 98, p. 59, 2000.
- [55] U. Vossmerbaeumer, "Application principles of excimer lasers in ophthalmology," *Med. Laser Appl.*, vol. 25, no. 4, pp. 250–257, 2010.
- [56] B. S. B. WACHLER and M. WEVILL, "Mechanical Microkeratome Versus Femtosecond Laser. Two surgeons provide a point/counterpoint debate," *Cataract Refract. Surg. TODAY Eur.*, no. January 2010, 2010.
- [57] G. Clare, T. C. B. Moore, C. Grills, A. Leccisotti, J. E. Moore, and S. Schallhorn, "Early Flap Displacement after LASIK," *Ophthalmology*, 2011.
- [58] A. M. Rosa, J. N. Murta, M. J. Quadrado, C. Tavares, C. Lobo, R. Van Velze, and A. Castanheira-Dinis, "Femtosecond laser versus mechanical microkeratomes for flap creation in laser in situ keratomileusis and effect of postoperative measurement interval on estimated femtosecond flap thickness," *J. Cataract Refract. Surg.*, vol. 35, no. 5, pp. 833–838, 2009.

- [59] G. Shemesh, G. Dotan, and I. Lipshitz, "Predictability of corneal flap thickness in laser in situ keratomileusis using three different microkeratomes.," *J. Refract. Surg. (Thorofare, NJ 1995)*, vol. 18, no. 3 Suppl, p. S347, 2002.
- [60] P. K. Vaddavalli and S. H. Yoo, "Femtosecond laser in-situ keratomileusis flap configurations," *Curr. Opin. Ophthalmol.*, vol. 22, no. 4, p. 245, 2011.
- [61] M. V Netto, R. R. Mohan, F. W. Medeiros, W. J. Dupps Jr, S. Sinha, R. R. Krueger, W. M. Stapleton, M. Rayborn, C. Suto, and S. E. Wilson, "Femtosecond laser and microkeratome corneal flaps: comparison of stromal wound healing and inflammation," *J. Refract. Surg. (Thorofare, NJ 1995)*, vol. 23, no. 7, p. 667, 2007.
- [62] T. Lim, S. Yang, M. Kim, and H. Tchah, "Comparison of the IntraLase femtosecond laser and mechanical microkeratome for laser in situ keratomileusis," *Am. J. Ophthalmol.*, vol. 141, no. 5, pp. 833–839, 2006.
- [63] C. W. Yau and H. C. Cheng, "Microkeratome blades and corneal flap thickness in LASIK," *Ophthalmic Surg Lasers Imaging*, vol. 39, pp. 471–475, 2008.
- [64] Ö. Ö. Uçakhan, "Corneal flap thickness in laser in situ keratomileusis using the summit Krumeich-Barraquer microkeratome," *J. Cataract Refract. Surg.*, vol. 28, no. 5, pp. 798–804, 2002.
- [65] M. Q. Salomão and S. E. Wilson, "Femtosecond laser in laser in situ keratomileusis," *J. Cataract Refract. Surg.*, vol. 36, no. 6, pp. 1024–1032, 2010.
- [66] K. D. Solomon, E. Donnenfeld, H. P. Sandoval, O. Al Sarraf, T. J. Kasper, M. P. Holzer, E. H. Slate, and D. T. Vroman, "Flap thickness accuracy* 1,* 2,* 3,* 4:: Comparison of 6 microkeratome models," *J. Cataract Refract. Surg.*, vol. 30, no. 5, pp. 964–977, 2004.

- [67] A. Chan, J. Ou, and E. E. Manche, "Comparison of the femtosecond laser and mechanical keratome for laser in situ keratomileusis," *Arch. Ophthalmol.*, vol. 126, no. 11, p. 1484, 2008.
- [68] M. A. Sarayba, T. S. Ignacio, D. B. Tran, and P. S. Binder, "A 60 kHz IntraLase femtosecond laser creates a smoother LASIK stromal bed surface compared to a Zyoptix XP mechanical microkeratome in human donor eyes.," *J. Refract. Surg. (Thorofare, NJ 1995)*, vol. 23, no. 4, p. 331, 2007.
- [69] C. H. Choe, C. Guss, D. C. Musch, L. M. Niziol, and R. M. Shtein, "Incidence of diffuse lamellar keratitis after LASIK with 15 KHz, 30 KHz, and 60 KHz femtosecond laser flap creation," *J. Cataract Refract. Surg.*, vol. 36, no. 11, pp. 1912–1918, 2010.
- [70] M. A. Ansari and E. Mohajerani, "Mechanisms of Laser-Tissue Interaction: I. Optical Properties of Tissue," *J. Lasers Med. Sci.*, vol. 2, no. 3, pp. 119–125, 2011.
- [71] H. K. Soong and J. B. Malta, "Femtosecond lasers in ophthalmology," *Am. J. Ophthalmol.*, vol. 147, no. 2, pp. 189–197, 2009.
- [72] N. Uppal and P. S. Shiakolas, "Micromachining characteristics of NiTi based shape memory alloy using femtosecond laser," *J. Manuf. Sci. Eng.*, vol. 130, p. 31117, 2008.
- [73] N. Uppal, S. S. PANOS, and S. Priya, "Micromachining of PZT using ultrafast femtosecond laser," *Ferroelectr. Lett.*, vol. 32, no. 3–4, pp. 67–77, 2005.
- [74] N. G. Tahzib, *Visual outcome and patient satisfaction after corneal and refractive surgery*. Universitaire Pers Maastricht, 2008.

- [75] T. Juhasz, F. H. Loesel, R. M. Kurtz, C. Horvath, J. F. Bille, and G. Mourou, "Corneal refractive surgery with femtosecond lasers," *Sel. Top. Quantum Electron. IEEE J.*, vol. 5, no. 4, pp. 902–910, 1999.
- [76] A. Vogel, P. Schweiger, A. Frieser, M. N. Asiyu, and R. Birngruber, "Intraocular Nd: YAG laser surgery: laser-tissue interaction, damage range, and reduction of collateral effects," *Quantum Electron. IEEE J.*, vol. 26, no. 12, pp. 2240–2260, 1990.
- [77] G. A. Kurtz, RM; Liu, X; Elner, VM; Squier, JA; Du, D; Mourou, "Plasma-mediated ablation in human cornea as a function of laser pulse width," *J. Refract. Surg.*, vol. 13, pp. 653–658, 1997.
- [78] Newport, "Focusing a collimated Laser Beam," *Newport Inc*, 2012. [Online]. Available: <http://www.newport.com/Focusing-and-Collimating/141191/1033/content.aspx>.
- [79] H. Sun, M. Han, M. H. Niemz, and J. F. Bille, "Femtosecond laser corneal ablation threshold: dependence on tissue depth and laser pulse width," *Lasers Surg. Med.*, vol. 39, no. 8, pp. 654–658, 2007.
- [80] T. Juhasz, G. Spooner, Z. Sacks, C. Suarez, F. Raksi, R. Zadoyan, M. Sarayba, and R. M. Kurtz, "Ophthalmic applications of ultrashort pulsed lasers," in *Commercial and Biomedical Applications of Ultrafast Lasers IV, January 27, 2004 - January 29, 2004*, vol. 5340, pp. 66–75.
- [81] N. Bloembergen, "Laser-induced electric breakdown in solids," *Quantum Electron. IEEE J.*, vol. 10, no. 3, pp. 375–386, 1974.
- [82] J. G. Fujimoto, W. Z. Lin, E. P. Ippen, C. A. Puliafito, and R. F. Steinert, "Time-resolved studies of Nd: YAG laser-induced breakdown. Plasma formation,

- acoustic wave generation, and cavitation.,” *Invest. Ophthalmol. Vis. Sci.*, vol. 26, no. 12, p. 1771, 1985.
- [83] M. H. Friedlaender, “LASIK surgery using the IntraLase femtosecond laser,” *Int. Ophthalmol. Clin.*, vol. 46, no. 3, p. 145, 2006.
- [84] M. R. Chalita, M. Xu, and R. R. Krueger, “Correlation of aberrations with visual symptoms using wavefront analysis in eyes after laser in situ keratomileusis.,” *J. Refract. Surg. (Thorofare, NJ 1995)*, vol. 19, no. 6, p. S682, 2003.
- [85] E. N. Glezer, C. B. Schaffer, N. Nishimura, and E. Mazur, “Minimally disruptive laser-induced breakdown in water,” *Opt. Lett.*, vol. 22, no. 23, pp. 1817–1819, 1997.
- [86] M. S. Habib, M. G. Speaker, and W. F. K. Schnatter, “Mass spectrometry analysis of the by-products of intrastromal photorefractive keratectomy,” *Ophthalmic Surg.*, vol. 26, no. 5, pp. 481–483, 1995.
- [87] G. Schuele, M. Rumohr, G. Huettmann, and R. Brinkmann, “RPE damage thresholds and mechanisms for laser exposure in the microsecond-to-millisecond time regimen,” *Invest. Ophthalmol. Vis. Sci.*, vol. 46, no. 2, pp. 714–719, 2005.
- [88] H. Lee, C. Alt, C. M. Pitsillides, and C. P. Lin, “Optical detection of intracellular cavitation during selective laser targeting of the retinal pigment epithelium: dependence of cell death mechanism on pulse duration,” *J. Biomed. Opt.*, vol. 12, p. 64034, 2007.
- [89] C. R. Thompson, B. S. Gerstman, S. L. Jacques, and M. E. Rogers, “Melanin granule model for laser-induced thermal damage in the retina,” *Bull. Math. Biol.*, vol. 58, no. 3, pp. 513–553, 1996.

- [90] J. Roider, N. A. Michaud, T. J. Flotte, and R. Birngruber, "Response of the retinal pigment epithelium to selective photocoagulation," *Arch. Ophthalmol.*, vol. 110, no. 12, p. 1786, 1992.
- [91] C. Winkler von Mohrenfels, R. Khoramnia, J. Salgado, C. Wullner, C. Donitzky, M. Maier, and C. P. Lohmann, "First clinical results with a new 200 kHz femtosecond laser system," *Br. J. Ophthalmol.*, Dec. 2011.
- [92] D. Basting and G. Marowsky, *Excimer laser technology*. Berlin; Springer/Praxis, c2005.
- [93] J. J. Machat, *Excimer laser refractive surgery: practice and principles*. Slack Incorporated, 1996.
- [94] Z. S. Sacks, R. M. Kurtz, T. Juhasz, G. Spooner, and G. A. MOUROUA, "Subsurface photodisruption in human sclera: wavelength dependence," *Ophthalmic surgery, lasers & imaging*, vol. 34, no. 2, pp. 104–113, 2003.
- [95] C. N. J. McGhee, H. R. Taylor, D. S. Gartry, and S. L. Trokel, *Excimer lasers in ophthalmology: principles and practice*. Martin Dunitz, 1997.
- [96] G. Balazsi, M. Mullie, L. Lasswell, P. A. Lee, and Y. J. Duh, "Laser in situ keratomileusis with a scanning excimer laser for the correction of low to moderate myopia with and without astigmatism," *J. Cataract Refract. Surg.*, vol. 27, no. 12, pp. 1942–1951, 2001.
- [97] B. Muller, T. Boeck, and C. Hartmann, "Effect of excimer laser beam delivery and beam shaping on corneal sphericity in photorefractive keratectomy," *J. Cataract Refract. Surg.*, vol. 30, no. 2, pp. 464–470, 2004.
- [98] K. M. Rocha, R. Kagan, S. D. Smith, and R. R. Krueger, "Thresholds for interface haze formation after thin-flap femtosecond laser in situ keratomileusis for myopia," *Am. J. Ophthalmol.*, vol. 147, no. 6, pp. 966–972, 2009.

- [99] F. W. Medeiros, A. Sinha-Roy, M. R. Alves, and W. J. Dupps Jr, "Biomechanical corneal changes induced by different flap thickness created by femtosecond laser," *Clinics*, vol. 66, no. 6, pp. 1067–1071, 2011.
- [100] D. S. Durrie, S. G. Slade, and J. Marshall, "Wavefront-guided excimer laser ablation using photorefractive keratectomy and sub-Bowman's keratomileusis: a contralateral eye study.," *J. Refract. Surg. (Thorofare, NJ 1995)*, vol. 24, no. 1, p. S77, 2008.
- [101] J. S. Chang, "Complications of sub-Bowman's keratomileusis with a femtosecond laser in 3009 eyes.," *J. Refract. Surg. (Thorofare, NJ 1995)*, vol. 24, no. 1, p. S97, 2008.
- [102] M. A. Sarayba, T. S. Ignacio, P. S. Binder, and D. B. Tran, "Comparative study of stromal bed quality by using mechanical, IntraLase femtosecond laser 15-and 30-kHz microkeratomes," *Cornea*, vol. 26, no. 4, p. 446, 2007.
- [103] V. M. B. Tham and R. K. Maloney, "Microkeratome complications of laser in situ keratomileusis," *Ophthalmology*, vol. 107, no. 5, pp. 920–924, 2000.
- [104] H. Ahn, J. K. Kim, C. K. Kim, G. H. Han, K. Y. Seo, E. K. Kim, and T. Kim, "Comparison of laser in situ keratomileusis flaps created by 3 femtosecond lasers and a microkeratome," *J. Cataract Refract. Surg.*, vol. 37, no. 2, pp. 349–357, 2011.
- [105] M. Wang, T. Swartz, L. Martén, H. Boerman, W. Jiang, J. Noble, and R. Solomon, "Peer reviewed literature on Epithelial Ingrowth," *Cataract Refract. Surg. TODAY*, 2007.
- [106] N. Asano-Kato, I. Toda, Y. Hori-Komai, Y. Takano, and K. Tsubota, "Epithelial ingrowth after laser in situ keratomileusis: clinical features and possible mechanisms," *Am. J. Ophthalmol.*, vol. 134, no. 6, pp. 801–807, 2002.

- [107] E. Letko, M. O. Price, and F. W. Price Jr, "Influence of original flap creation method on incidence of epithelial ingrowth after LASIK retreatment.," *J. Refract. Surg. (Thorofare, NJ 1995)*, vol. 25, no. 11, p. 1039, 2009.
- [108] G. Kamburoglu and A. Ertan, "Epithelial ingrowth after femtosecond laser-assisted in situ keratomileusis," *Cornea*, vol. 27, no. 10, p. 1122, 2008.
- [109] S. A. Melki and M. A. Fava, "Epithelial Ingrowth After LASIK," *Cornea Refract. Atlas Clin. Wisdom*, p. 211, 2011.
- [110] T. A. Mohamed, R. S. Hoffman, I. H. Fine, and M. Packer, "Post-Laser Assisted In Situ Keratomileusis Epithelial Ingrowth and Its Relation to Pretreatment Refractive Error," *Cornea*, vol. 30, no. 5, p. 550, 2011.
- [111] J. L. Güell, D. Elies, O. Gris, F. Manero, and M. Morral, "Femtosecond laser-assisted enhancements after laser in situ keratomileusis," *J. Cataract Refract. Surg.*, vol. 37, no. 11, pp. 1928–1931, 2011.
- [112] B. P. E. Institute, "Wavefront Guided Custom Excimer Laser Treatment," *University of Miami Health System*, 2012. [Online]. Available: <http://bascompalmer.org/specialties/lasik/wavefront-guided-custom-excimer-laser-treatment>.
- [113] M. Bashour, "Risk factors for epithelial erosions in laser in situ keratomileusis," *J. Cataract Refract. Surg.*, vol. 28, no. 10, pp. 1780–1788, 2002.
- [114] S. I. Mian, A. Y. Li, S. Dutta, D. C. Musch, and R. M. Shtein, "Dry eyes and corneal sensation after laser in situ keratomileusis with femtosecond laser flap creation:: Effect of hinge position, hinge angle, and flap thickness," *J. Cataract Refract. Surg.*, vol. 35, no. 12, pp. 2092–2098, 2009.

- [115] E. D. Donnenfeld, K. Solomon, H. D. Perry, S. J. Doshi, M. Ehrenhaus, R. Solomon, and S. Biser, "The effect of hinge position on corneal sensation and dry eye after LASIK," *Ophthalmology*, vol. 110, no. 5, pp. 1023–1029, 2003.
- [116] R. Ambrosio Jr, T. Tervo, and S. E. Wilson, "LASIK-associated dry eye and neurotrophic epitheliopathy: pathophysiology and strategies for prevention and treatment," *J. Refract. Surg. (Thorofare, N.J. 1995)*, vol. 24, no. 4, pp. 396–407, Apr. 2008.
- [117] M. Q. Salomão, R. Ambrósio Jr, and S. E. Wilson, "Dry eye associated with laser in situ keratomileusis: mechanical microkeratome versus femtosecond laser," *J. Cataract Refract. Surg.*, vol. 35, no. 10, pp. 1756–1760, 2009.
- [118] B. A. Nassaralla, S. D. McLeod, J. E. Boteon, and J. J. Nassaralla, "The effect of hinge position and depth plate on the rate of recovery of corneal sensation following LASIK," *Am. J. Ophthalmol.*, vol. 139, no. 1, pp. 118–124, 2005.
- [119] L. Golas and E. E. Manche, "Dry eye after laser in situ keratomileusis with femtosecond laser and mechanical keratome," *J. Cataract Refract. Surg.*, 2011.
- [120] S. V Patel, J. W. McLaren, K. M. Kittleson, and W. M. Bourne, "Subbasal nerve density and corneal sensitivity after laser in situ keratomileusis: femtosecond laser vs mechanical microkeratome," *Arch. Ophthalmol.*, vol. 128, no. 11, p. 1413, 2010.
- [121] K. D. Solomon, L. E. Fernández de Castro, H. P. Sandoval, J. M. Biber, B. Groat, K. D. Neff, M. S. Ying, J. W. French, E. D. Donnenfeld, and R. L. Lindstrom, "LASIK world literature review: quality of life and patient satisfaction," *Ophthalmology*, vol. 116, no. 4, pp. 691–701, 2009.
- [122] F. E. C. M. Corp., "LASIK report," Cleveland, Ohio, 2010.
- [123] "Comprehensive report on the global refractive surgery market," 2011.

- [124] "Humanitarian Use Devices," *U.S. Food and Drug Administration*, 2004. [Online]. Available:
<http://www.accessdata.fda.gov/scripts/cdrh/cfdocs/cfHDE/HDEInformation.cfm>.
[Accessed: 26-Aug-2014].
- [125] T. Nomura, M. P. Powers, J. L. Katz, and C. Saito, "Finite element analysis of a transmandibular implant," *J. Biomed. Mater. Res. Part B Appl. Biomater.*, vol. 80, no. 2, pp. 370–376, 2007.
- [126] M. Sevimay, A. Usumez, and G. Eskitascioglu, "The influence of various occlusal materials on stresses transferred to implant-supported prostheses and supporting bone: A three-dimensional finite-element study," *J. Biomed. Mater. Res. Part B Appl. Biomater.*, vol. 73, no. 1, pp. 140–147, 2005.
- [127] T. Kitagawa, Y. Tanimoto, M. Odaki, K. Nemoto, and M. Aida, "Influence of implant/abutment joint designs on abutment screw loosening in a dental implant system," *J. Biomed. Mater. Res. Part B Appl. Biomater.*, vol. 75, no. 2, pp. 457–463, 2005.
- [128] I. Y. Lee, H. B. Skinner, and J. H. Keyak, "Effects of variation of prosthesis size on cement stress at the tip of a femoral implant," *J. Biomed. Mater. Res.*, vol. 28, no. 9, pp. 1055–1060, 1994.
- [129] R. Sorrentino, D. Apicella, C. Riccio, E. Gherlone, F. Zarone, R. Aversa, F. Garcia-Godoy, M. Ferrari, and A. Apicella, "Nonlinear visco-elastic finite element analysis of different porcelain veneers configuration," *J. Biomed. Mater. Res. Part B Appl. Biomater.*, vol. 91, no. 2, pp. 727–736, 2009.
- [130] C. Li, Y. Wang, and J. Mason, "The effects of curing history on residual stresses in bone cement during hip arthroplasty," *J. Biomed. Mater. Res. Part B Appl. Biomater.*, vol. 70, no. 1, pp. 30–36, 2004.

- [131] H. Alexander, J. L. Ricci, and G. J. Hrico, "Mechanical basis for bone retention around dental implants," *J. Biomed. Mater. Res. Part B Appl. Biomater.*, vol. 88, no. 2, pp. 306–311, 2009.
- [132] R. P. Vito and P. H. Carnell, "Finite element based mechanical models of the cornea for pressure and indenter loading.," *Refract. Corneal Surg.*, vol. 8, no. 2, pp. 146–151, 1991.
- [133] M. Bercovier, K. Hanna, and F. Jouve, "An analysis of refractive surgery by the finite element method," in *Computational Mechanics' 86*, Springer, 1986, pp. 823–828.
- [134] A. Gefen, R. Shalom, D. Elad, and Y. Mandel, "Biomechanical analysis of the keratoconic cornea," *J. Mech. Behav. Biomed. Mater.*, vol. 2, no. 3, pp. 224–236, 2009.
- [135] K. A. Buzard, "Introduction to biomechanics of the cornea.," *Refract. Corneal Surg.*, vol. 8, no. 2, pp. 127–138, 1991.
- [136] M. R. Bryant and P. J. McDonnell, "Constitutive laws for biomechanical modeling of refractive surgery," *J. Biomech. Eng.*, vol. 118, no. 4, pp. 473–481, 1996.
- [137] Z. Han, X. Sui, D. Zhou, C. Zhou, and Q. Ren, "Biomechanical and refractive behaviors of keratoconic cornea based on three-dimensional anisotropic hyperelastic models.," *J. Refract. Surg. (Thorofare, NJ 1995)*, vol. 29, no. 4, pp. 282–290, 2013.
- [138] G. J. Orssengo and D. C. Pye, "Determination of the true intraocular pressure and modulus of elasticity of the human cornea in vivo," *Bull. Math. Biol.*, vol. 61, no. 3, pp. 551–572, 1999.

- [139] K. Anderson, A. El-Sheikh, and T. Newson, "Application of structural analysis to the mechanical behaviour of the cornea," *J. R. Soc. Interface*, vol. 1, no. 1, pp. 3–15, 2004.
- [140] M. A. Lago, M. J. Rupérez, F. Martínez-Martínez, C. Monserrat, E. Larra, J. L. Güell, and C. Peris-Martínez, "A new methodology for the in vivo estimation of the elastic constants that characterize the patient-specific biomechanical behavior of the human cornea," *J. Biomech.*, vol. 48, no. 1, pp. 38–43, 2015.
- [141] B. L. Boyce, R. E. Jones, T. D. Nguyen, and J. M. Grazier, "Stress-controlled viscoelastic tensile response of bovine cornea," *J. Biomech.*, vol. 40, no. 11, pp. 2367–2376, 2007.
- [142] T. D. Nguyen, R. E. Jones, and B. L. Boyce, "A nonlinear anisotropic viscoelastic model for the tensile behavior of the corneal stroma.," *J. Biomech. Eng.*, vol. 130, no. 4, p. 041020, Aug. 2008.
- [143] T. D. Nguyen and B. L. Boyce, "An inverse finite element method for determining the anisotropic properties of the cornea.," *Biomech. Model. Mechanobiol.*, vol. 10, no. 3, pp. 323–37, Jun. 2011.
- [144] A. Elsheikh, D. Wang, P. Rama, M. Campanelli, and D. Garway-Heath, "Experimental assessment of human corneal hysteresis," *Curr. Eye Res.*, vol. 33, no. 3, pp. 205–213, 2008.
- [145] P. M. Pinsky, D. V. Datye, and T. A. Silvestrini, "Numerical-Simulation of Topographical Alterations in the Cornea After ICR (R)(Intrastromal Corneal Ring)," in *Investigative Ophthalmology & Visual Science*, 1995, vol. 36, no. 4, pp. S309–S309.

- [146] S. Kling and S. Marcos, "Finite-element modeling of intrastromal ring segment implantation into a hyperelastic cornea," *Invest. Ophthalmol. Vis. Sci.*, vol. 54, no. 1, pp. 881–889, 2013.
- [147] K. Anderson, A. El-Sheikh, and T. Newson, "FEA of the biomechanics of porcine corneas.," *Struct. Eng.*, vol. 82, no. 12, pp. 20–25, 2004.
- [148] E. Uchio, S. Ohno, J. Kudoh, K. Aoki, and L. T. Kisielwicz, "Simulation model of an eyeball based on finite element analysis on a supercomputer," *Br. J. Ophthalmol.*, vol. 83, no. 10, pp. 1106–1111, 1999.
- [149] A. Elsheikh and D. Alhasso, "Mechanical anisotropy of porcine cornea and correlation with stromal microstructure.," *Exp. Eye Res.*, vol. 88, no. 6, pp. 1084–91, Jun. 2009.
- [150] A. Elsheikh, "Finite element modeling of corneal biomechanical behavior (vol 26, pg 289, 2010)," *J. Refract. Surg.*, vol. 28, no. 4, p. 245, 2012.
- [151] P. M. Pinsky and D. V. Datye, "A microstructurally-based finite element model of the incised human cornea," *J. Biomech.*, vol. 24, no. 10, pp. 907–922, 1991.
- [152] H. Gross, W. Singer, M. Totzeck, F. Blechinger, B. Ahtner, B. Dörband, and H. Müller, *Handbook of optical systems*, vol. 1. Wiley Online Library, 2005.
- [153] S. Khan, P. Shiakolas, and V. Mootha, "Descemet's Stripping Automated Endothelial Keratoplasty (DSAEK) Tissue Insertion Devices: A Review," *J. ophthalmic Vis. Res.*, 2015.
- [154] A. Elsheikh, D. Alhasso, and P. Rama, "Assessment of the epithelium's contribution to corneal biomechanics," *Exp. Eye Res.*, vol. 86, no. 2, pp. 445–451, 2008.

- [155] H. Hatami-Marbini and E. Etebu, "A new method to determine rate-dependent material parameters of corneal extracellular matrix," *Ann. Biomed. Eng.*, vol. 41, no. 11, pp. 2399–2408, 2013.
- [156] A. Elsheikh and D. Wang, "Numerical modelling of corneal biomechanical behaviour," *Comput. Methods Biomech. Biomed. Engin.*, vol. 10, no. 2, pp. 85–95, 2007.
- [157] A. Elsheikh, "Finite element modeling of corneal biomechanical behavior," *J. Refract. Surg.*, vol. 26, no. 4, p. 289, 2010.
- [158] R. W. Ogden, "Non-linear elastic deformations," *Eng. Anal.*, vol. 1, no. 2, p. 119, 1984.
- [159] S.-Y. Woo, A. S. Kobayashi, W. A. Schlegel, and C. Lawrence, "Nonlinear material properties of intact cornea and sclera," *Exp. Eye Res.*, vol. 14, no. 1, pp. 29–39, 1972.
- [160] Wolfram, "Radius of Curvature," *Wolfram Mathworld*, 2014. [Online]. Available: <http://mathworld.wolfram.com/RadiusofCurvature.html>.
- [161] A. Daxer, "Corneal intrastromal implantation surgery for the treatment of moderate and high myopia," *J. Cataract Refract. Surg.*, vol. 34, no. 2, pp. 194–198, 2008.
- [162] Dioptex, "Myoring by Dioptex," 2014. [Online]. Available: http://www.dioptex.com/fileadmin/daten_dioptex/pdf/MYORING.pdf.
- [163] T. E. Burriss, P. C. Baker, C. T. Ayer, B. E. Loomas, M. L. Mathis, and T. A. Silvestrini, "Flattening of central corneal curvature with intrastromal corneal rings of increasing thickness: an eye-bank eye study," *J. Cataract Refract. Surg.*, vol. 19, pp. 182–187, 1993.

- [164] A. Daxer, "MyoRing for central and noncentral keratoconus," *J Kerat Ect Cor Dis*, vol. 2, pp. 117–119, 2012.
- [165] P. Albert Daxer, MD, "Intracorneal ring: A good alternative to LASIK?," *Ophthalmol. Times Eur.*, vol. 3, no. 8, 2007.
- [166] M. Jabbarvand, H. Hashemi, M. Mohammadpour, H. Khojasteh, M. Khodaparast, and H. Hashemian, "Implantation of a Complete Intrastromal Corneal Ring at 2 Different Stromal Depths in Keratoconus," *Cornea*, vol. 33, no. 2, pp. 141–144, 2014.
- [167] D. Smerdon, "Anatomy of the eye and orbit," *Curr. Anaesth. Crit. Care*, vol. 11, no. 6, pp. 286–292, 2000.
- [168] S. J. Tuft and D. J. Coster, "The corneal endothelium," *Eye*, vol. 4, no. 3, pp. 389–424, 1990.
- [169] D. H. Geroski, M. Matsuda, R. W. Yee, and H. F. Edelhauser, "Pump function of the human corneal endothelium," *Ophthalmology*, vol. 92, pp. 759–763, 1985.
- [170] A. Laule, M. K. Cable, C. E. Hoffman, and C. Hanna, "Endothelial cell population changes of human cornea during life," *Arch. Ophthalmol.*, vol. 96, no. 11, p. 2031, 1978.
- [171] R. S. Wilson and M. J. Roper-Hall, "Effect of age on the endothelial cell count in the normal eye.," *Br. J. Ophthalmol.*, vol. 66, no. 8, p. 513, 1982.
- [172] M. O. Price and F. W. Price Jr, "Endothelial cell loss after Descemet stripping with endothelial keratoplasty: influencing factors and 2-year trend," *Ophthalmology*, vol. 115, no. 5, pp. 857–865, 2008.
- [173] A. Anshu, M. O. Price, D. T. H. Tan, and F. W. Price Jr, "Endothelial keratoplasty: a revolution in evolution," *Surv. Ophthalmol.*, vol. 57, no. 3, pp. 236–252, 2012.
- [174] "2012 Eye Banking statistical report," 2012.

- [175] Mayo clinic, "Full-thickness cornea transplant." [Online]. Available: <http://www.mayoclinic.com/health/medical/IM03700>.
- [176] Medical eye center, "Partial Thickness Transplants," *Center, Medical eye*. [Online]. Available: <http://www.medicaleyecenter.com/eye-care-education/about-corneal-transplantation/>.
- [177] D. Alberto and R. Garello, "Corneal Sublayers Thickness Estimation Obtained by High-Resolution FD-OCT," *Int. J. Biomed. Imaging*, vol. 2013, 2013.
- [178] C. Boimer, K. Lee, L. Sharpen, R. Shehadeh Mashour, and A. R. Slomovic, "Evolving surgical techniques of and indications for corneal transplantation in Ontario from 2000 to 2009," *Can. J. Ophthalmol. Can. d'Ophthalmologie*, vol. 46, no. 4, pp. 360–366, 2011.
- [179] J. K. Lee and A. M. Hwang, "Descemetâ s Stripping Automated Endothelial Keratoplasty â A Review," 2009.
- [180] J. L. Clements, C. S. Bouchard, W. B. Lee, S. P. Dunn, M. J. Mannis, J. J. Reidy, T. John, S. B. Hannush, K. M. Goins, and M. D. Wagoner, "Retrospective review of graft dislocation rate associated with Descemet stripping automated endothelial keratoplasty after primary failed penetrating keratoplasty," *Cornea*, vol. 30, no. 4, pp. 414–418, 2011.
- [181] R. W. Thompson Jr, M. O. Price, P. J. Bowers, and F. W. Price Jr, "Long-term graft survival after penetrating keratoplasty," *Ophthalmology*, vol. 110, no. 7, pp. 1396–1402, 2003.
- [182] N. A. Afshari, M. S. Gorovoy, S. H. Yoo, T. Kim, A. N. Carlson, G. O. D. Rosenwasser, N. B. Griffin, B. W. McCuen II, C. A. Toth, and F. W. Price Jr, "Dislocation of the donor graft to the posterior segment in Descemet stripping

- automated endothelial keratoplasty,” *Am. J. Ophthalmol.*, vol. 153, no. 4, pp. 638–642, 2012.
- [183] M. O. Price, K. M. Fairchild, D. A. Price, and F. W. Price Jr, “Descemet’s stripping endothelial keratoplasty: five-year graft survival and endothelial cell loss,” *Ophthalmology*, vol. 118, no. 4, pp. 725–729, 2011.
- [184] E. S. Chen, M. A. Terry, N. Shamie, K. L. Hoar, and D. J. Friend, “Descemet-stripping automated endothelial keratoplasty: six-month results in a prospective study of 100 eyes,” *Cornea*, vol. 27, no. 5, pp. 514–520, 2008.
- [185] I. Bahar, I. Kaiserman, E. Levinger, W. Sansanayudh, A. R. Slomovic, and D. S. Rootman, “Retrospective contralateral study comparing descemet stripping automated endothelial keratoplasty with penetrating keratoplasty,” *Cornea*, vol. 28, no. 5, pp. 485–488, 2009.
- [186] S. B. Koenig and D. J. Covert, “Early results of small-incision Descemet’s stripping and automated endothelial keratoplasty,” *Ophthalmology*, vol. 114, no. 2, pp. 221–226, 2007.
- [187] T. Ide, S. H. Yoo, J. M. Goldman, V. Perez, and T. P. O’Brien, “Descemet-stripping automated endothelial keratoplasty: effect of inserting forceps on DSAEK donor tissue viability by using an in vitro delivery model and vital dye assay,” *Cornea*, vol. 26, no. 9, pp. 1079–1081, 2007.
- [188] M. Ang, J. S. Mehta, F. Lim, S. Bose, H. M. Htoon, and D. Tan, “Endothelial cell loss and graft survival after Descemet’s stripping automated endothelial keratoplasty and penetrating keratoplasty,” *Ophthalmology*, 2012.
- [189] S. Bose, M. Ang, J. S. Mehta, D. T. Tan, and E. Finkelstein, “Cost-Effectiveness of Descemet’s Stripping Endothelial Keratoplasty versus Penetrating Keratoplasty,” *Ophthalmology*, 2012.

- [190] S. S. Prabhu, R. Kaakeh, A. Sugar, D. G. Smith, and R. M. Shtein, "Comparative Cost-Effectiveness Analysis of Descemet Stripping Automated Endothelial Keratoplasty Versus Penetrating Keratoplasty in the United States," *Am. J. Ophthalmol.*, 2012.
- [191] M. A. Terry, H. A. Saad, N. Shamie, and A. K. Shah, "Peripheral endothelial cell damage after trephination of donor tissue," *Cornea*, vol. 28, no. 10, pp. 1149–1152, 2009.
- [192] A. Hong, M. C. Caldwell, A. N. Kuo, and N. A. Afshari, "Air bubble-associated endothelial trauma in Descemet stripping automated endothelial keratoplasty," *Am. J. Ophthalmol.*, vol. 148, no. 2, pp. 256–259, 2009.
- [193] F. W. Price Jr and M. O. Price, "Descemet's stripping with endothelial keratoplasty in 200 eyes: early challenges and techniques to enhance donor adherence," *J. Cataract Refract. Surg.*, vol. 32, no. 3, pp. 411–418, 2006.
- [194] H. Alkatan, A. Al-Rajhi, A. Al-Shehri, and A. Khairi, "Histopathological findings of failed grafts following Descemet's stripping automated endothelial keratoplasty (DSAEK)," *Saudi J. Ophthalmol.*, vol. 26, no. 1, pp. 79–85, 2012.
- [195] T. Ide, "Descemet's stripping automated endothelial keratoplasty injecting device," *Expert Rev. Ophthalmol.*, vol. 4, no. 1, pp. 5–9, 2009.
- [196] E. S. Chen, M. A. Terry, N. Shamie, K. L. Hoar, P. M. Phillips, and D. J. Friend, "Endothelial keratoplasty: vision, endothelial survival, and complications in a comparative case series of fellows vs attending surgeons," *Am. J. Ophthalmol.*, vol. 148, no. 1, pp. 26–31, 2009.
- [197] M. A. Terry, N. Shamie, M. D. Straiko, D. J. Friend, and D. Davis-Boozer, "Endothelial keratoplasty: the relationship between donor tissue storage time and donor endothelial survival," *Ophthalmology*, vol. 118, no. 1, pp. 36–40, 2011.

- [198] M. Busin, P. R. Bhatt, and V. Scorcia, "A modified technique for Descemet membrane stripping automated endothelial keratoplasty to minimize endothelial cell loss," *Arch. Ophthalmol.*, vol. 126, no. 8, p. 1133, 2008.
- [199] I. Bahar, I. Kaiserman, W. Sansanayudh, E. Levinger, and D. S. Rootman, "Busin guide vs forceps for the insertion of the donor lenticule in Descemet stripping automated endothelial keratoplasty," *Am. J. Ophthalmol.*, vol. 147, no. 2, pp. 220–226, 2009.
- [200] W.-B. Khor, J. S. Mehta, and D. T.-H. Tan, "Descemet stripping automated endothelial keratoplasty with a graft insertion device: surgical technique and early clinical results," *Am. J. Ophthalmol.*, vol. 151, no. 2, pp. 223–232, 2011.
- [201] N. B. Griffin and K. A. Walter, "A Safe and Convenient Method of Inserting and Controlling Donor Tissue During Endothelial Keratoplasty," 2011.
- [202] H. Yokogawa, A. Kobayashi, and K. Sugiyama, "Clinical evaluation of a new donor graft inserter for Descemet's stripping automated endothelial keratoplasty," *Ophthalmic Surg. Lasers Imaging*, vol. 43, no. 1, p. 50, 2012.
- [203] J. B. Foster, K. R. Swan, R. A. Vasan, M. A. Greven, and K. A. Walter, "Small-incision Descemet stripping automated endothelial keratoplasty: a comparison of small-incision tissue injector and forceps techniques," *Cornea*, vol. 31, no. 1, pp. 42–47, 2012.
- [204] D. Tan, "Special DSAEK techniques for Asian eyes," in *DSEK: What You Need to Know About Endothelial Keratoplasty*, SLACK Incorporated, 2009.
- [205] "Kobayashi-Busin DSAEK Glide," 2013. [Online]. Available: <http://www.asico.com/product/kobayashi-busin-dsaek-glide/>. [Accessed: 15-Jul-2013].

- [206] V. Gangwani, A. Obi, and E. J. Hollick, "A prospective study comparing EndoGlide and Busin glide insertion techniques in descemet stripping endothelial keratoplasty," *Am. J. Ophthalmol.*, vol. 153, no. 1, pp. 38–43, 2012.
- [207] U. de Sanctis, V. Aragno, L. Brusasco, F. Damiani, and F. Grignolo, "Pull-Through Insertion Technique for Descemet Stripping Automated Endothelial Keratoplasty (DSAEK): Graft Survival and Endothelial Cell Loss after 1 Year in 100 Eyes," *J Transpl. Technol Res S*, vol. 2, pp. 991–2161, 2011.
- [208] M. A. Terry, H. A. Saad, N. Shamie, E. S. Chen, P. M. Phillips, D. J. Friend, J. D. Holiman, and C. Stoeger, "Endothelial keratoplasty: the influence of insertion techniques and incision size on donor endothelial survival," *Cornea*, vol. 28, no. 1, pp. 24–31, 2009.
- [209] C. Macaluso, "J3760.1 DSEK/DSAEK endothelial graft inserter," 2011. [Online]. Available: <http://www.janach.it/newsdett.aspx?n=2836>.
- [210] C. Macaluso, "Closed-chamber pulling-injection system for donor graft insertion in endothelial keratoplasty," *J. Cataract Refract. Surg.*, vol. 34, no. 3, pp. 353–356, 2008.
- [211] C. Macaluso, "Communication by S N Khan [electronic mail], Acquiring image of Macaluso injector, UTA," 06-20-2013. .
- [212] D. Tan, "Endoglide DSAEK insertion and procedure," 2009. [Online]. Available: <http://www.angioedupro.com/Sharpoin/?seek=394>.
- [213] FDA-USA, "FDA approval of Neusidl corneal inserter by Fischer surgical." [Online]. Available: <http://www.accessdata.fda.gov/scripts/cdrh/cfdocs/cfpmn/pm n.cfm?ID=36541>.
- [214] F. Surgical, "NCI spatula by Fischer surgical." [Online]. Available: <http://www.fischersurgical.com/NCI Animation Video 3-31-09.wmv>.

- [215] S. B. Hannush, A. Aldave, and H. D. Perry, "Discover the Advantages of Endothelial Keratoplasty," *Ophthalmol. Manag.*, vol. 16, no. 1, pp. 48–53, 2012.
- [216] M. A. Terry, M. D. Straiko, J. M. Goshe, N. Shamie, A. Shah, A. A. Alqudah, and D. Davis-Boozer, "Endothelial Keratoplasty: Prospective, Randomized, Masked Clinical Trial Comparing an Injector With Forceps for Tissue Insertion," *Am. J. Ophthalmol.*, 2013.
- [217] Keramed, "Endoinjector." [Online]. Available: <http://keramed.com/endoinjector.html>.
- [218] FDA-USA, "FDA approval of endoserter by ocular systems." [Online]. Available: <http://www.accessdata.fda.gov/scripts/cdrh/cfdocs/cfpcd/classification.cfm?ID=3982>.
- [219] O. Systems, "Endoserter by ocular systems." [Online]. Available: <http://us.ocularsystemsinc.com/physicians/the-endoserter/>.
- [220] J. S. Mehta, Y. M. Por, R. Poh, R. W. Beuerman, and D. Tan, "Comparison of donor insertion techniques for descemet stripping automated endothelial keratoplasty," *Arch. Ophthalmol.*, vol. 126, no. 10, pp. 1383–1388, 2008.
- [221] A. N. Kuo, T. M. Harvey, and N. A. Afshari, "Novel delivery method to reduce endothelial injury in Descemet stripping automated endothelial keratoplasty," *Am. J. Ophthalmol.*, vol. 145, no. 1, pp. 91–96, 2008.
- [222] S. Khan and P. S. Shiakolas, "An overview on performance characteristics of laser in-situ keratomileusis using lasers and identification of challenges," *Micro Nanosyst.*, 2012.
- [223] R. A. B. Crabb, E. P. Chau, D. M. Decoteau, and A. Hubel, "Microstructural characteristics of extracellular matrix produced by stromal fibroblasts," *Ann. Biomed. Eng.*, vol. 34, no. 10, pp. 1615–1627, 2006.

- [224] D. P. Piñero and N. Alcón, "In vivo characterization of corneal biomechanics," *J. Cataract Refract. Surg.*, vol. 40, no. 6, pp. 870–887, 2014.
- [225] H. Hatami-Marbini and A. Rahithemi, "Evaluation of hydration effects on tensile properties of bovine corneas," *J. Cataract Refract. Surg.*, 2015.
- [226] M. Ahearn, Y. Yang, K. Y. Then, and K.-K. Liu, "An indentation technique to characterize the mechanical and viscoelastic properties of human and porcine corneas," *Ann. Biomed. Eng.*, vol. 35, no. 9, pp. 1608–1616, 2007.
- [227] H. Hatami-Marbini, "Hydration Dependent Viscoelastic Tensile Behavior of Cornea," *Ann. Biomed. Eng.*, vol. 42, no. 8, pp. 1740–1748, 2014.
- [228] J. Dias, V. F. Diakonis, V. P. Kankariya, S. H. Yoo, and N. M. Ziebarth, "Anterior and posterior corneal stroma elasticity after corneal collagen crosslinking treatment.," *Exp. Eye Res.*, vol. 116, pp. 58–62, Nov. 2013.
- [229] V. V. Vasiliev and E. Morozov, *Mechanics and analysis of composite materials*. Elsevier, 2001.
- [230] A. Pandolfi and F. Manganiello, "A model for the human cornea: constitutive formulation and numerical analysis," *Biomech. Model. Mechanobiol.*, vol. 5, no. 4, pp. 237–246, 2006.
- [231] S. J. Tuft and D. J. Coster, "The corneal endothelium.," *Eye (Lond)*, vol. 4 (Pt 3), pp. 389–424, Jan. 1990.
- [232] K.-D. Chen, Y.-S. Li, M. Kim, S. Li, S. Yuan, S. Chien, and J. Y. J. Shyy, "Mechanotransduction in response to shear stress roles of receptor tyrosine kinases, integrins, and Shc," *J. Biol. Chem.*, vol. 274, no. 26, pp. 18393–18400, 1999.

- [233] M. M. Moore, J. Goldman, A. R. Patel, S. Chien, and S. Q. Liu, "Role of tensile stress and strain in the induction of cell death in experimental vein grafts," *J. Biomech.*, vol. 34, no. 3, pp. 289–297, 2001.
- [234] N. C. Joyce, "Corneal Endothelial Cells," *Schepens Eye Research Institute*. [Online]. Available: <http://www.schepens.harvard.edu/researchstory/nancy-c-joyce-phd/research-story.html>. [Accessed: 03-Apr-2014].
- [235] S. T. Fontana and R. F. Brubaker, "Volume and depth of the anterior chamber in the normal aging human eye," *Arch. Ophthalmol.*, vol. 98, no. 10, pp. 1803–1808, 1980.
- [236] V. Bhardwaj and G. P. Rajeshbhai, "Axial length, anterior chamber depth-a study in different age groups and refractive errors," *J. Clin. diagnostic Res. JCDR*, vol. 7, no. 10, p. 2211, 2013.
- [237] M. Haghighi Abyaneh, "A hybrid approach to determining cornea mechanical properties using a combination of inverse finite element analysis and experimental techniques." Loughborough University, 2014.
- [238] J. Ø. Hjortdal, "On the biomechanical properties of the cornea with particular reference to refractive surgery.," *Acta Ophthalmol. Scand. Suppl.*, no. 225, p. 1, 1998.
- [239] T. K. Tonge, B. J. Muriene, B. Coudrillier, S. Alexander, W. Rothkopf, and T. D. Nguyen, "Minimal Preconditioning Effects Observed for Inflation Tests of Planar Tissues," *J. Biomech. Eng.*, vol. 135, no. 11, p. 114502, 2013.
- [240] V. Triacca, L. Spinelli, and A. Pandolfi, "Mechanical Characterization of Porcine Corneas."
- [241] P. H. Carnell and R. P. Vito, "A model for estimating corneal stiffness using an indenter," *J. Biomech. Eng.*, vol. 114, no. 4, pp. 549–552, 1992.

- [242] S. Khan and P. Shiakolas, "Finite element analysis of Descemet's stripping automated endothelial keratoplasty (DSAEK) surgery allograft to predict endothelial cell loss (Under Review)," *J. Cataract Refract. Surg.*, 2015.
- [243] S. Ramanujan, "Ramanujan's collected works," *Chelsea, New York*, vol. 52, 1962.

Biographical Information

Salman N Khan received his bachelor's degree in Mechatronics and Control Engineering in 2009 from The University of Engineering and Technology, Lahore. After graduation he worked in the process automation industry for a year before joining UTA as a BS to PhD student in 2010. During his academic career he has received numerous honors. He was awarded the Enhanced graduate teaching assistantship and doctoral fellowship on admission to UTA and maintained it throughout graduate school. He was the recipient of the prestigious Dr. Sharmin Sughra Malik Engineering Scholarship at UTA (2015), Graduate Dean's Dissertation Fellowship (2014) and I-engage Mentoring Fellowship (2014) among others. He was also the recipient of an academic distinction by the University of Cambridge in 2004. His research interests include biomechanics, bioinstrumentation, applied solid mechanics, computational mechanics and computer aided design/analysis. He likes to apply fundamental mechanical engineering principles in the study of biomedical ailments and the design of procedures or devices to alleviate these ailments. In future, he intends to continue his research after joining an educational/research institute.